X chromosome status:
a gatekeeper of germ cells meiotic entry

Jacqueline Severino

TESI DOCTORAL UPF / 2020

Thesis Supervisor
Dr. Bernhard Payer

Centre for Genomic Regulation (CRG)
Gene Regulation, Stem Cells and Cancer Program

Universitat Pompeu Fabra (UPF)
Department of Experimental and Health Sciences

ACKNOWLEDGEMENTS

Faró in modo che le persone che mi hanno aiutata lo sappiano. Se non lo sanno giá.

ABSTRACT

X chromosome reactivation in female mouse germ cells is essential for the transmission of one active X chromosome to the progeny. However, despite its key role in development, the mechanistic details and kinetics still remain elusive, as previous studies were restricted by a scarcity of cells *in vivo* and a lack of adequate *in vitro* systems. Here, I present the characterization of X-chromosome dynamics during germ cell formation through the use of a tailor-made *in vitro* system, which facilitates accurate profiling of X-chromosome activity. We recapitulate X-inactivation starting in epiblast-like cells (EpiLCs) and follow its dynamics in the progression to primordial germ cell-like cells (PGCLCs), followed by X-reactivation in germ cells upon meiotic entry. We show that PGCLCs undergoing X-inactivation can enter meiosis more efficiently, whilst PGCLCs bypassing X-inactivation and therefore also lacking subsequent X-reactivation, show a reduced meiotic potential. We conclude that tracing the X chromosome status during germ cell formation facilitates the dissection of the relationship between X chromosome dynamics and proper germline fate acquisition.

RESUMEN

En las hembras de ratón, la reactivación del cromosoma X en las células germinales es esencial para la transmisión de un cromosoma X activo a la descendencia. Sin embargo, a pesar del papel crucial del cromosoma X durante el desarrollo, el mecanismo y la dinámica de su reactivación siguen siendo difíciles de alcanzar, ya que los estudios realizados anteriormente estaban restringidos por la escasez de células *in vivo* y la falta de sistemas *in vitro* adecuados. En este estudio he desarrollado un sistema que me permite seguir y caracterizar de manera detallada la actividad del cromosoma X durante la formación de las células germinales femeninas. Empezando por células similares a las células del epiblasto y diferenciandolas hacia células parecidas a células germinales primordiales (PGCLCs), hemos conseguido recapitular la inactivación del cromosoma X. A continuación hemos observado la reactivación del cromosoma X a medida que las células germinales primordiales entran en meiosis. Mostramos que las PGCLCs que se someten a inactivación del cromosoma X pueden entrar en meiosis forma más eficiente, mientras que las PGCLCs que no logran inactivar el cromosoma X, con la consiguiente falta de su posterior reactivación, muestran un menor potencial para entrar en meiosis. Concluimos que el seguimiento del estado del cromosoma X durante la formación de las células germinales nos permitió analizar la relación entre la dinámica del cromosoma X y la correcta especificación y desarrollo de la línea germinal.

TABLE OF CONTENTS

INTRODUCTION

Early mouse embryonic development

Germline life cycle

The generation of a new individual in mammals starts with the fertilization of a very specialized cell, the egg, by another highly specialized cell, the sperm. This results in the formation of a totipotent zygote, that will commence consecutive divisions and give rise to a structure of approximately 16 cells: the morula. Here, differential developmental factors will drive the differentiation of an outer layer of cells that will become the trophectoderm (TE) and an inner group of cells that will become the pluripotent inner cell mass (ICM) of the developing blastocyst. In mouse, at embryonic day (E) ~E4.5, a segment of the ICM cells will commit to a ground-state of pluripotency, forming the epiblast. Upon implantation (~E6.5) cells of the epiblast commence a series of transformations that narrow their differentiation potential committing to a primed-state of pluripotency (Weinberger et al. 2016; Nichols and Smith 2009). From the primed epiblast, at ~E7.25, a cluster of approximately 40 cells (Chiquoine 1954; Ginsburg, Snow, and McLaren 1990) becomes identifiable as primordial germ cells (PGCs). These are the unipotent precursors of gametes, that will continue to specify and will develop into either sperm or the egg depending on the sex of the newly generated embryo. This cycle is what ensures the survival of the specis and the perpetuation of genetic and epigenetic information from one generation to the next.

Development of germ cells *in vivo*

Primordial germ cell specification and migration

Germ cell fate is induced at the postimplantation epiblast. Here, PGC precursors start emerging in response to extrinsic signals, mostly bone morphogenetic proteins (BMPs) BMP4 and BMP8b derived from the extra-embryonic ectoderm (ExE). At ~E5.5-5.75, BMP4 activates, via the SMAD signal transduction pathway, key germline transcription factors such as *Blimp1* and *Prdm14* in a small group of epiblast cells (Vincent et al. 2005; Ohinata et al. 2005; Yamaji et al. 2008). Another layer of control is played by

BMP8b signaling, which counteracts the inhibitory signals for germline specification from the anterior visceral endoderm (AVE). Taken together, the expression of specific transcription factors together with the BMP8b signaling, distinguishes PGC precursors from the surrounding cells in the epiblast (Ohinata et al. 2009). However, the question of why only a small cluster of epiblast cells is responsive to those signals and which other signals may be involved in germline specification remains largely unknown.

At ~E7.5 a cluster of ~40 founder cells starts dividing. Each of these cells individually migrates anteriorly along the developing hindgut endoderm into the dorsal mesentery. The migration towards the future gonad is directed by the interaction between chemokine somatic lineage stromal cell-derived factor 1 (SDF1), expressed by somatic lineage, and the PGC receptor CXCR4 (Molyneaux et al. 2003; Richardson and Lehmann 2010; Ara et al. 2003). Another interaction known to be involved in PGCs proliferation/survival and motility occurs between c-KIT and its ligand Stem Cell Factor (SCF), expressed by the somatic cells throughout the migration (Gu et al. 2009). Around 1,000 PGCs will colonize the recently formed bipotential embryonic gonad. Here, PGCs will continue to proliferate, modify their morphology and adhesion properties (De Felici, Dolci, and Pesce 1992; Donovan et al. 1986; García-Castro et al. 1997).

Figure Intro1. Germ cell development *in vivo* and its recapitulation *in vitro*
(a) Top: illustration of the main stage of development of the germ cell lineage. ICM, inner cell mass; Epi, epiblast; PGCs, primordial germ cell, UGR, urogenital ridge; XCR, X chromosome reactivation; XCI, X chromosome inactivation. **(b)** Key developmental events associated with mouse germ cell development. **(c)** Expression of key genes during mouse development. **(d)** Schematic of the original *in vitro* systems allowing gametogenesis. ESCs in 2i are induced into EpiLCs for 2 days. EpiLCs are then induced into PGCLCs either by cytokines or via transcription factor overexpression.

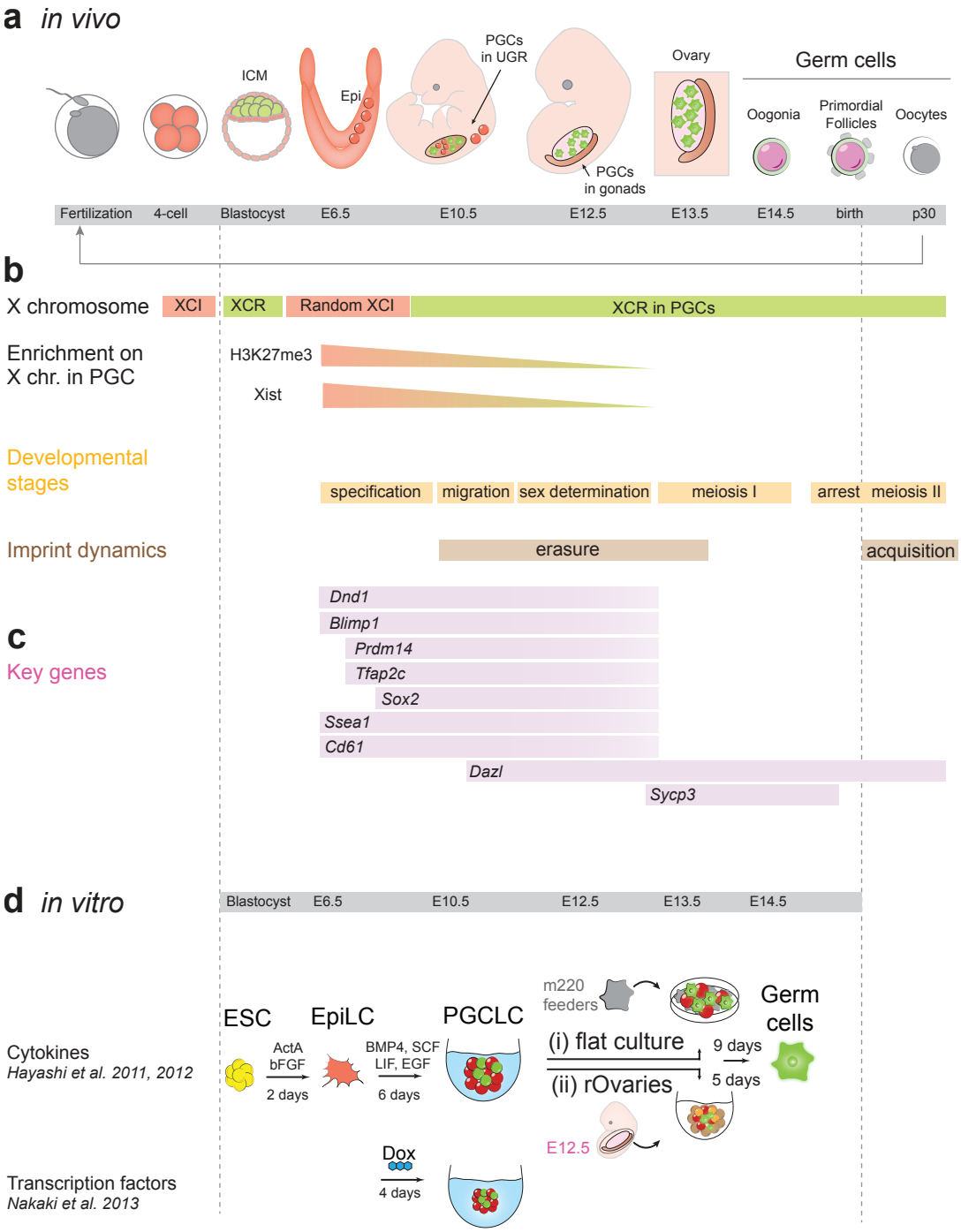
a in vivo
ICM
Epi
PGCs in UGR
PGCs in gonads
Ovary
Germ cells
Oogonia
Primordial Follicles
Oocytes
Fertilization
4-cell
Blastocyst
E6.5
E10.5
E12.5
E13.5
E14.5
birth
p30
b
X chromosome
XCI
XCR
Random XCI
XCR in PGCs
Enrichment on X chr. in PGC
H3K27me3
Xist
Developmental stages
specification
migration
sex determination
meiosis I
arrest
meiosis II
Imprint dynamics
erasure
acquisition
c
Key genes
Dnd1
Blimp1
Prdm14
Tfap2c
Sox2
Ssea1
Cd61
Dazl
Sycp3
d in vitro
Blastocyst
E6.5
E10.5
E12.5
E13.5
E14.5
ESC
EpiLC
PGCLC
ActA
bFGF
2 days
BMP4, SCF
LIF, EGF
6 days
Cytokines
Hayashi et al. 2011, 2012
Dox
4 days
Transcription factors
Nakaki et al. 2013
m220 feeders
(i) flat culture
9 days
(ii) rOvaries
5 days
E12.5
Germ cells

Sex differentiation

Between ~E10.5 and ~E11.5, the bipotential gonad will start to differentiate into either a male (testis) or a female (ovary) gonad. This decision depends on the activation of the Y chromosome linked gene *Sry*. In males, *Sry* expression in the supporting cells (Koopman et al. 1991; Gubbay et al. 1990) will initiate a feedback loop leading to the differentiation of male gonadal somatic cells into Sertoli cells. In a female embryo, the absence of the *Sry* gene allows *Wnt4* and *Rspo1* to be expressed, creating a signaling cascade that counteracts the expression of the male feedback loop leading to the commitment of female somatic cells into the granulosa lineage (Heikkilä et al. 2005; Kim et al. 2006; Schmidt et al. 2004; Parma et al. 2006). The signals emanating from the gonadal niche will establish a sex specific fate in PGCs (Adams and McLaren 2002; Best et al. 2008), which will respond by changing their transcriptional activity in a sex-specific fashion (Jameson et al. 2012). Studies from past years, proposed that the sexual fate of germ cells could be independent of the sex chromosome composition, rather being under the influence of the gonadal milieu. For example, ovarian somatic cells can drive meiotic entry in XY germ cells when exposed to the female gonadal signaling niche (Byskov and Saxén 1976). XY germ cells can take the oogenic path when placed in XX-XY chimeric mice (Evans, Ford, and Lyon 1977). A contrasting view was that both XX and XY germ cells would bear an intrinsic clock mechanism that would allow the entry into meiosis also when incorrectly migrated into the mesonephros (the primordium of the kidney) or the adrenal glands at E13.5 (A. McLaren 1995). In female, the opposing theories were resolved thanks to the observations of an asynchronous and directional order of meiotic initiation correlating with a specular wave of pluripotency loss which seemed to clash with the idea of intrinsic clock and rather support the idea of a meiotic inducer.

Meiotic entry in female germ cells

Once the female program has been set in the bipotential ovary, PGCs start a series of morphological and transcriptional changes to mature into oogonia, which are germ cells that have entered meiosis. Between E10 - E11, PGCs lose their migratory potential and between E12.5 - E13.5 mitotic proliferation ends and PGCs access a pre-meiotic stage. The entry into meiosis is triggered by increased levels of retinoic acid (RA) synthesized by aldehyde dehydrogenases (*Aldh1a1/a2/a3*). While *Aldh1a1* is found in the gonad

Aldh1a2 and *Aldh1a3* are located in the tubules of the mesonephros and diffuse RA into the gonads. In females, RA accumulates in the gonad due to the absence of the RA degrading enzyme cytochrome CYP26B1 (P450, family 26, subfamily b, polypeptide 1) (Josephine Bowles et al. 2006; Koubova et al. 2006; Menke and Page 2002) and triggers the expression of transcription factor stimulated by retinoic acid, gene 8 (*Stra8*), which is a key meiotic regulator (Josephine Bowles et al. 2010; K. Ohta et al. 2010; Tedesco et al. 2013; Spiller, Koopman, and Bowles 2017). A link between chromatin composition and *Stra8* activation was also supported by *in vivo* studies from (Yokobayashi et al. 2013). The authors show a level of control of sexual differentiation and timing of meiotic entry played by Polycomb repressive complex 1 (PRC1), which modulates PGCs response to RA. *Stra8* also regulates *Dazl* expression, which in turn regulates translation of *Sycp3* mRNA (Reynolds et al. 2007; Y. Lin et al. 2008). At ~E13.5, approximately 6,000 oogonia per gonad are found; by ~E15.5, the number of germ cells that have entered meiosis reaches a peak of 15,000 cells per ovary, however around the time of birth, most germ cells will undergo apoptosis (Findlay et al. 2015).

Prophase I: Cellular and chromosomal organization

Prophase I refers to the initial sequence of molecular and cellular events happening during meiosis, both in males and females. It is the longest and most complex phase of meiosis, during which the correct segregation of paternal and maternal homologous chromosomes (homologues) secures the formation of haploid gametes. Among the key events taking place during prophase I, homologous recombination is what ensures genetic exchange between homologues, leading to the transmission of newly formed allelic combinations to the progeny. Prophase I progression can be divided into five substages according to chromosome morphology and the status of pairing and synapsis: leptotene, zygotene, pachytene, diplotene and finally diakinesis.

Briefly, at the **leptotene** stage meiotic recombination starts, defined by the formation of programmed double-strand breaks (DSBs) on chromosomal DNA by SPO11 (Keeney, Giroux, and Kleckner 1997), generating crossover or non-crossover events by the end of pachytene (Allers and Lichten 2001; Hunter and Kleckner 2001; Börner, Kleckner, and Hunter 2004). When transitioning to **zygotene**, homologues stably pair (migrate into close proximity and recognize the homology) via RAD51 and DMC1, shown to promote homologous interactions between kilobase-long stretches of DNA (Eggler,

Inman, and Cox 2002; Sung et al. 2003). Subsequently, the synaptonemal complex (SC) is installed between the now paired homologues, called bivalents. This is a tripartite structure consisting of two lateral elements that connect to chromatin, linked in the middle by a central region of transverse filaments. At this stage, synapsis takes place, cementing the bivalents via the SC. Chromosomal ends cluster and attach to a few defined regions of the nuclear membrane, forming the so-called “bouquet stage”. Once the SC is completely assembled, germ cells reach **pachytene** stage and meiotic recombination between homologues is completed. At the **diplotene** stage, the SC disassembles and chiasmata regions can be observed, holding together the homologues. Lastly, during **diakinesis**, the chromosomes go through a final condensation round. After prophase I ends, meiosis II starts. It resembles a mitotic division, with the exception that the chromosomal number has been reduced by half. Thereofere, the products of meiosis II will be four haploid cells, containing a single copy of each chromosome. From those four cells, only one functional oocyte will be obtained. The other three haploid cells will be squeezed out from the oocyte as polar bodies.

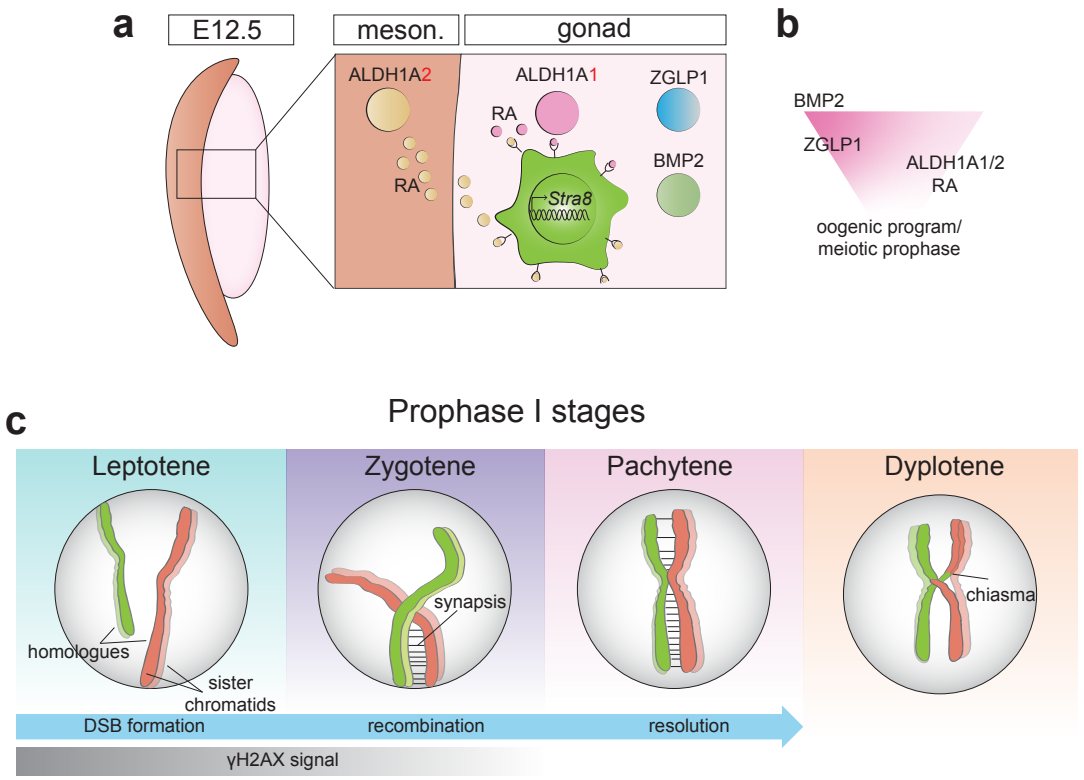

Figure Intro2. Meiotic prophase I inducing factors and chromosomal organization
(a) E12.5 Mesonephros with gonad. Retinoic acid is produced by ALDH1A2 in the mesonephros and by ALDH1A1 in the gonad. Retinoic acid binds to its receptor and induces expression of *Stra8*. **(b)** Signaling cascade driving oogenic program (BMP2 / ZGLP1 pathway) and meiotic initiation via *Stra8* expression. RA, retinoic acid **(c)** Chromosome organization during meiotic prophase I is illustrated with two pairs of homologous chromosomes (red and green), each split into two sister chromatids (red and light red, green and light green). Panel sizes do not reflect duration of the stages. DSB, double strand break.

Genome-wide epigenetic reprogramming of *in vivo* PGCs

Epigenetic reprogramming in mice takes place during early embryo development in the ICM of the blastocyst and PGCs. On the one hand, differentiated cells in an organism acquire an epigenetic signature that instructs gene expression, inherited mitotically and referred to as “cellular memory”. On the other hand, the germline genome needs to be kept in a more “flexible” state since it represents the only genome that will be used for species propagation. Therefore, from the early specification stages, the PGCs' genome must be equipped with the tools necessary to ensure the essential reprogrammable state. Although most of the epigenetic reprogramming in PGCs occurs while they are migrating, a portion of the changes takes place before and simultaneously to their specification (Gu et al. 2009; Guibert, Forne, and Weber 2012).

In PGCs, the major event in genome resetting is genome-wide DNA demethylation with consequent erasure of sex-specific imprints, demethylation of transposons/repetitive elements, the re-acquisition of the pluripotency-associated gene network (Yabuta et al. 2006) and, in females, the reactivation of the inactivate X chromosome (Monk, Boubelik, and Lehnert 1987; Kafri et al. 1992; Szabo and Mann 1995; Petra Hajkova et al. 2002; Kohda et al. 2002; Lane et al. 2003; Popp et al. 2010; Guibert, Forne, and Weber 2012; Saitou, Kagiwada, and Kurimoto 2012). DNA methylation analysis of male and female E13.5 PGCs, considered the endpoint of methylation erasure, showed that the levels of methylated CpG dinucleotides are extremely low in both sexes, lower than those of methylation-deficient ESCs. Importantly, female PGCs show even lower DNA methylation levels than male PGCs and similarly *in vitro* female ESCs have lower methylation than male ESCs (Popp et al. 2010). This significantly lower level of genome methylation in the sole two cell types that have reactivated the X chromosome might be attributable to having two active X chromosomes (Zvetkova et al. 2005). When specifically assessing different genomic elements (promoter, exons, introns, transposons families etc.) of E13.5 PGCs, long terminal repeat (LTR) retrotransposons showed the highest resistance to DNA demethylation. The methylation state of the promoters of LTR regions might be subjected to transgenerational epigenetic inheritance in the female gamete (reviewed in (Daxinger and Whitelaw 2012)). On the contrary, the major loss of methylation was observed for repeats in genic and intergenic regions, followed by exons and lastly promoters (Guibert, Forne, and Weber 2012; Popp et al. 2010).

However, despite being a key event in the reprogramming of the germ cell lineage, the underlying mechanisms behind genome-wide DNA demethylation at control elements in PGCs have been a long-standing subject of debate: Is DNA demethylation an active process happening fast and enzymatically or rather a slow and passive process resulting from a failure of perpetuating methylation patterns that would otherwise be transmitted by mitotic inheritance? (reviewed in (Ooi and Bestor 2008; S. C. Wu and Zhang 2010)).

Several putative pathways have been postulated to be involved in the **active** mechanism of DNA demethylation: i) It might involve two deaminases, AID and APOBEC1, that create a T:G mismatch, targeted by thymine DNA glycosylase (TDG) for the base-excision mismatch repair (BER) pathway (Morgan et al. 2004), as in plants (Gehring et al. 2006). However, the two deaminases are lowly expressed in PGCs (P. Hajkova et al. 2010) and the KO mice for AID are fertile (Popp et al. 2010) suggesting that their role in PGCs development is likely to be minimal. ii) More recent studies showed that ten-eleven translocation (TET) dioxygenases TET1 and TET2 expressed in PGCs (P. Hajkova et al. 2010) catalyze the modification of 5mC to 5-hydroxymethylcytosine (5hmC) (Tahiliani et al. 2009), successively into 5-formylcytosine (5fC) and into 5-carboxylcytosine (5caC) and that could be converted into a C during DNA replication in PGCs to then be fixed by the BER pathway (Ito et al. 2011; He et al. 2011). Another role for TET1 during PGC maturation was reported by (Hill et al. 2018) where TET1 was shown to be responsible for maintaining but not driving DNA demethylation, by assisting the removal of PRC1-mediated gene silencing. However, despite the models supporting active DNA demethylation being the prevailing view, the connection between DNA demethylation and an enzyme catalyzing it, remains only a hypothesis.

In contrast, other groups recently showed a **passive** mechanism as the primary mode of DNA demethylation in PGCs (Kagiwada et al. 2013; Saitou, Kagiwada, and Kurimoto 2012). In line with previous work (Seki et al. 2005; Yabuta et al. 2006; Kurimoto et al. 2008) it was shown that key genes implicated in both maintenance and *de novo* DNA methylation are repressed between E9.5 and E13.5 in PGCs: DNMT3A/3B, in conjunction with DNMT3L which lacks methyltransferase activity but enhances the activity of DNMT3a, are *de novo* methyltransferases. These proteins are lowly expressed until E12.5. In contrast, the maintenance enzyme DNMT1 is expressed in

PGCs, however, this fails to be recruited into regions where DNA methylation maintenance is required due to the lack of expression of the recruiting factor UHRF (ubiquitin-like with PHD and ring finger domain 1) (Bostick et al. 2007; Sharif et al. 2007). In (Kagiwada et al. 2013) the authors measured methyltransferase expression from E9.5 to E13.5 PGCs, assessed cell division rate, imprint erasure dynamics, chromatin composition and ultimately demonstrated that upon specification, PGCs are incapable to provide for both their *de novo* and maintenance DNA methylation.

Similar to DNA demethylation, reprogramming of histone modifications marks occurs during the PGCs migration period in a progressive, cell-by-cell manner. From ~E7.75 to ~E8.75, a genome-wide reduction of histone H3 lysine 9 dimethylation (H3K9me2) takes place, possibly due to competition with H3K9ac or due to downregulation of H3K9 methyltransferase GLP (EHMT1) from the G9a–GLP complex (Seki et al. 2007). It follows an upregulation of H3 lysine 27 trimethylation (H3K27me3) together with its catalysing enzyme EZH2. Additionally, there is an increase of histone H3 lysine 4 methylation (H3K4me2 and H3K4me3) as well as other active promoter marks, such as H3K9ac and symmetrical methylation of arginine 3 on histones H4 and H2A (H2A/H4R3me2s) (Ancelin et al. 2006). To investigate whether in this developmental window transcription would be hyper-activated due to the decrease of multiple repressive marks, RNA polymerase II (PolII) activity was measured (Seki et al. 2007). Surprisingly, it was shown that PolII transcription is transiently silenced during epigenetic reprogramming. This transcriptional repression was then gradually released later on, simultaneously with the exit from the G2 phase, in which 60% of PGCs were arrested to then resume a rapid proliferation similar to ESCs.

Once the reprogramming is finalized, PGCs have acquired a necessary and exclusive epigenetic state, with genome-wide DNA demethylation and depletion of both activating and repressive histone marks. Future work will be needed to finalize the debate whether genome-wide DNA demethylation in PGCs is controlled by an active, passive or a combination of both mechanisms and the interplay between DNA demethylation and histone modifications reprogramming.

In vitro systems to study germ cells development

Germ cells are the only cell type capable of generating a new organism, allowing the continuation of mammalian species, representing the key players of genetic diversity

and evolution. The uniqueness of germ cells has brought many researchers to study the mechanisms driving their development. However, the difficulty in accessing *in vivo* germ cells has been a limiting factor and has therefore led to the establishment of *in vitro* culture systems to generate germ cells. Those systems allow the study of the fundamental principles of germ cell development in a systematic fashion. Consequently they represent a very powerful addition in the field of germ cells research.

The first attempt to study oocyte development *in vitro*, was reported in 1971 (Odor and Blandau 1971). 16 dpp fetuses mouse ovaries were dissociated and cultured for 45 days on rose chambers with medium containing horse serum. The experiment resulted in an efficient formation of laminar follicles and oocyte growth, but very inefficient meiotic completion, only one oocyte showed first meiotic metaphase spindle. Due to its low capacity for meiotic induction, this system was replaced in the 2000's by numerous systems completely *in vitro (Eguizabal et al. 2009; Katsuhiko Hayashi and Surani 2009)*. Most of the trials to generate *in vitro* germ cells intended to follow the *in vivo* differentiation timeline, starting from ESCs, EpiSCs (epiblast stem cells), iPSCs (induced pluripotent stem cells) or EGCs (embryonic like germ cells). The first study successful in the generation of mouse oocyte-like cells used ESCs as starting material and was reliant on cell spontaneous differentiation, without the addition of any growth factors or cytokines (Hübner et al. 2003). The quality of the generated oocyte-like cells was assessed by measuring the expression of oocyte specific markers and the diameter of the cells, which resulted to be in the size range of *in vivo* oocytes (between 60 - 70 μm (Eppig, Wigglesworth, and O'Brien 1992)). The two systems presented above, share the commonality of being based on a spontaneous/indirect differentiation approach, followed by the selection of a very lowly abundant population of germ-like cells. Moreover, a common pitfall in those studies was the lack of the ultimate functional test of the obtained germ-like cells, that is live offspring delivery.

Current protocols for primordial germ cell-like cell (PGCLC) induction

Cytokine based induction of primordial germ cell-like cells

The first two studies that achieved the generation of both male and female PGC-like cells both from mouse ESCs and iPSCs used a cocktail of defined growth factors and cytokines (Katsuhiko Hayashi et al. 2011, 2012). It is known from *in vivo* studies (Katsuhiko Hayashi et al. 2002) that only the postimplantation epiblast has the capacity

to respond to BMPs, PGC inducing factors. Therefore the published protocols commence with the induction of pluripotent ESCs (or iPSCs), maintained in a naive state, into epiblast-like cells (EpiLC) via addition of basic fibroblast growth factor (bFGF) and activin A, which are reported to drive the differentiation into epiblast stem cells (Tesar et al. 2007; Brons et al. 2007; Guo et al. 2009). After 2 days of EpiLC induction, cells are aggregated in a PGC induction media composed of BMP4, LIF, SCF and epidermal growth factor (EGF). BMP4 alone is sufficient for PGCLC induction. It activates T (BRACHYURY) via WNT3 and regulates expression of key germline genes such as *Prdm14*, *Blimp1* and *Tfap2c* (Lawson et al. 1999; Tam and Snow 1981; Aramaki et al. 2013). LIF, SCF and EGF are added to increase the efficiency of PGCLC generation, mostly by reducing cell death *in vitro*. The functionality of the resulting PGCLCs was assessed by transplantation assays into host seminiferous tubules (for male PGCLCs) or ovaries (for female PGCLCs). A more recent study (Hikabe et al. 2016) reported the reconstitution of the entire female germ line, both from ESCs and iPSCs. Over a culture period of 45 days, the key events of germ cell development were recapitulated: specification, differentiation into primary oocytes and maturation into MII oocytes. Upon *in vitro* fertilization embryos were obtained and transferred into surrogate mothers, giving rise to pregnancy and live offspring. Additionally, pluripotent stem cells were re-derived from the embryos obtained from *in vitro* generated oocytes. This is the first study in which the full germline cycle was reproduced i*n vitro*. It is important to notice, however, that the percentage of embryos that reached full-term development was low (13 pups were born out of 1997 2-cell stage transferred embryos). Further studies will be required to elucidate why such a low percentage of transferred embryos can successfully develop and give rise to live offspring.

Transcription factor based induction of primordial germ cell-like cells

In addition to cytokine-based PGCLC induction, the Saitou lab also showed functional PGCLC induction by simultaneous overexpression of three transcription factors (TFs) key for PGC specification *in vivo*: *Blimp1*, *Prdm14* and *Tfap2c*. Similarly to the cytokine system, only when the TFs were overexpressed in EpiLCs, and not in ESCs, could the germ cell fate be induced. Interestingly, PGCLC induction via TF overexpression bypasses the transient upregulation of mesodermal genes such as *Hoxa1*, *Hoxb1* and

T (also known as *brachyury*), showing that the mesodermal program characteristic during PGC specification by cytokines is dispensable (Nakaki et al. 2013).
The results presented in this PhD thesis will describe a before unavailable female version of the transcription factor inducible cell line.

PRDM14: launching the germ cell lineage

PRDM14, a PR domain-containing transcriptional regulator member of the *Prdm* family, is a key germ cell gene (Grabole et al. 2013; Kurimoto et al. 2008; Yamaji et al. 2008). A mutation in *Prdm14* resulted in PGCs carrying aberrant epigenetic patterns such as persistent H3K9me2 mark and lack of genome-wide H3K27me3 deposition. The resulting PGCs died shortly after specification, indicating that PRDM14 is important for setting up the epigenetic landscape of early germ cells (Petra Hajkova et al. 2008; P. Hajkova et al. 2010; Yamaji et al. 2008; Seki et al. 2007; Mallol, Guirola, and Payer 2019). *In vitro*, the overexpression of PRDM14 alone was sufficient in inducing PGCLCs. However the efficiency was lower than when combined with the overexpression of Tcfap2c and Blimp1, indicating that PRDM14 is found upstream of the other 2 TFs. Indeed it has already been demonstrated *in vivo* that PRDM14 is driving the expression of many other PGC genes such as *Dppa3*, *Sox2* and *Blimp1* (Grabole et al. 2013; Magnúsdóttir et al. 2012, 2013; Yamaji et al. 2008).

BLIMP1: regulator of PGC specification

Prdm1 encodes for BLIMP1, a PR domain zinc-finger protein crucial for PGC specification (K. Hayashi, de Sousa Lopes, and Surani 2007; Ohinata et al. 2005; Vincent et al. 2005; Chang, Cattoretti, and Calame 2002). BLIMP1 expression *in vivo* initiates at ~E6.25 in a few cells in the proximal epiblast, defining the onset of PGC differentiation. A mutated form of BLIMP1 can still give rise to PGCs however these cells aberrantly express genes belonging to the somatic programme, failing to induce PGCs specific genes such as *Tcfap2c* (Ohinata et al. 2005).

TCFAP2C: required for PGC maintenance

Tcfap2c encodes for AP2γ and is a crucial early PGC differentiation gene and direct target of BLIMP1 (Kurimoto et al. 2008; Magnúsdóttir et al. 2013; Weber et al. 2010). Although PGCs carrying a mutation in the *Tcfap2c* gene are known to cause early PGC loss, those cells still remain to be fully characterized. However, it has been proposed

that AP2γ might have a role in repressing genes connected to the somatic/mesodermal programme, such as *Hoxb1* (Weber et al. 2010).
Thus, BLIMP1, PRDM14 and AP2γ create an interdependent network for PGC specification and maintenance.

Other *in vitro* systems for PGCLC induction

The cytokine BMP4, or the overexpression of a tripartite network of germ cell specific transcription factors, has been reported to be necessary for epiblast differentiation into the germ cell lineage (Lawson et al. 1999; Magnúsdóttir et al. 2013; Nakaki et al. 2013; Ohinata et al. 2005; Vincent et al. 2005; Yamaji et al. 2008; Weber et al. 2010).
Contradictorily, it has also been shown that the sole overexpression at physiological (meaning similar to ESCs) or higher levels of the pluripotency factor *Nanog* can induce PGCLCs from EpiLCs, independently of BMP4-SMAD signalling (Murakami et al. 2016). This phenotype is explained by a genomic and epigenomic resetting phase during the transition from ESCs to EpiLC, during which NANOG binds and activates enhancers of *Blimp1* (which in turn activates *Tfap2c*) and *Prdm14*. The authors confirm that the Nanog-induced germ cells obtained have a normal PGCLC transcriptional landscape and are not cells that have re-acquired a ESCs state.
BMP4 signaling is the cytokine that induces a germ cell program rather than a somatic program in the differentiating cells of the epiblast. During this lineage segregation time window, the downregulation of the transcription factor OTX2, preceding the PGC specification program, has been shown to play a key role both *in vivo* and *in vitro* PGC specification (Zhang et al. 2018). In fact, knock-out experiments of *Otx2* show that PGCLCs can be obtained, and in a more efficient manner, even in the complete absence of the BMP4-SMAD signaling and absence of BLIMP1. Therefore OTX2 acts upstream of the PGC factors cascade, hindering germ cell fate entry, ensuring a correct balance of germline and soma.
Those systems show the importance of considering the role of transcription factors in a context-dependent manner, allowing for flexible fate determination scenarios. However, no transplantation functional experiments have been performed with the germ cells generated in those two studies, leaving unanswered questions about the maturation phase of those germ cells.

Pluripotency maintenance in PGCs

In the developing postimplantation embryo, during PGCs specification, the expression of certain core pluripotency factors such as *Oct4* and *Nanog* is retained/regained (Kurimoto et al. 2008) in PGCs. In fact, when *ex vivo* derived PGCs are put in culture, they have been shown to either die after a few rounds of cell divisions (Dolci et al. 1991; Matsui et al. 1991; Pesce et al. 1993; Kawase et al. 1996) or to be able to de-differentiate into pluripotent Embryonic Germ Cells (EGCs) with the ability to form chimeras. The defined medium in which PGCs are kept to induce the de-differentiation contains SCF, bFGF and LIF (Matsui, Zsebo, and Hogan 1992; Labosky, Barlow, and Hogan 1994; Resnick et al. 1992; Stewart, Gadi, and Bhatt 1994). The role of those cytokines is to repristinate or maintain a stable pluripotency network: bFGF represses BLIMP1, allowing the expression of *Klf4* and *c-Myc*; leukemia inhibitory factor (LIF) activates STAT3 (another important pluripotency factor) and finally the inactivation of the p53 pathway enhances the de-differentiation (Kimura 2003; Kimura et al. 2008). A more efficient culture method to derive EGCs is by the combinatorial treatment using bFGF and SCF together with MEK and Gsk3b pathways inhibitors (2i conditions), with a ratio of derivation of ~10% (Leitch et al. 2010). Therefore, is the activation of multiple signaling pathways and subsequent transcription factors modulations that orchestrate the transition from PGCs to EGCs. Overall, ESCs and EGCs are almost indistinguishable. They share a very similar transcriptional profile and DNA methylation levels and EGCs can be derived with intact imprints (Leitch et al. 2013), differently to what was previously postulated (Tada et al. 1998).

Current protocols for PGCLC maturation

Between E9.5 and E12.5, *in vivo* PGCs have a highly proliferative capacity, increasing their numbers 100-fold (Tam and Snow 1981). The efforts in defining the conditions for a long-term proliferation in culture of PGCLCs have been trying to both mimic the *in vivo* situation and to define the molecules and cytokines that stimulate their survival/proliferation.

3D Reconstituted ovaries (rOvaries) aggregation system

The development of a culture system in which *in vitro* derived immature female germ cells could further develop into oocyte has been approached by studying available

ovarian organ cultures and looking at previous works from Morohaku et *al.* (Morohaku et al. 2016; Morohaku, Hirao, and Obata 2017), which defined successful conditions for *ex vivo* culture of fetal ovaries and consequent production of functional oocytes. Useful strategies were imported from those experiments and applied to a newly developed system that allows full maturation of *in vitro* derived PGCLCs (Katsuhiko Hayashi et al. 2017) in a 3D environment similar to the *in vivo* situation. The procedure is laborious, spanning over ~2 months, and requires the aggregation of PGCLCs with somatic cells of embryonic ovaries. This culture system has been shown to promote PGCLC maturation into a state equivalent to E12.5, with advanced germline and meiotic genes being expressed (e.g. *Dazl, Ddx4, Mael, Piwil2, Stra8, Spo11, Sycp3* etc.). Moreover, this system allows PGCLCs to differentiate into meiotic oocytes. Important technical bottlenecks of this system are the limited number of gonadal somatic cells obtained per embryo, the low developmental potency of the resulting mature oocytes (11/316 oocytes gave rise to pups) and the remaining endogenous germ cells within the gonadal somatic cell suspension. Therefore, the use of germ cells-specific reporters will have to be implemented to be able to distinguish the endogenous vs. *in vitro* derived PGCLCs . Due to the current limitations reported above, refining the culture conditions for *in vitro* oocyte generation will be tedious and it might be challenging to apply it to the human system in the near future.

2D expansion system on stromal feeder cells with defined chemicals

To overcome the limitations of the 3D maturation system reported above and to find out new mechanisms involved in the sex determination of germ cells, a completely *in vitro* system that allows the proliferation and maturation of PGCLCs has been developed (H. Ohta et al. 2017; Miyauchi et al. 2017). Ohta et al. have performed a screen to identify which combination of chemicals could stimulate and sustain the proliferation of *in vitro* derived PGCLCs. As a result, two cAMP signaling activators were identified: forskolin and rolipram. When provided simultaneously to the culture medium, PGCLCs proliferation increased ~20 fold. Moreover the PGCLCs were expanded on top of immortalized m220 stromal cells, which have been engineered to express a membrane bound form of mSCF, a cytokine known to support the survival of PGCs (Dolci et al. 1991; Majumdar et al. 1994). Focusing on the female germ line development, the system has been used to identify key players of meiotic entry *in vitro*. Briefly, Ohta and colleagues reported that retinoic acid (RA) alone is not sufficient for meiotic entry and

only when provided in combination with the cytokine BMP2, PGCLCs could robustly be induced into prophase I oocytes. In a more recent study (Nagaoka et al. 2020), this 2D expansion system allowed the identification of a BMP2 downstream effector, Zinc Finger GATA Like Protein 1 (ZGLP1), which is an essential factor for the oogenic program and meiotic entry. When overexpressed, ZGLP1 alone can induce the maturation of PGCLCs into fetal oocytes. Therefore, this 2D culture system has proven to be very useful for the mechanistic investigation of mammalian oogenic fate determination. However, no functional experiments have been performed with the female oocytes generated.

X chromosome reactivation in female PGCs

X status during embryogenesis

Sex determination in mammals is defined by karyotype complement, with females being XX and males being XY. To balance X-linked genes dosage differences between males and females, the X chromosome is turned on and off at precise developmental stages. From the early 2-cell stage until mid-blastocyst, the X chromosome inherited from the spermatocyte is inactivated in all cells (imprinted XCI) (Huynh and Lee 2003; Okamoto et al. 2004). By the late-blastocyst stage, exclusively the epiblast cells of the inner cell mass (ICM) will undergo X chromosome reactivation (XCR) (Mak et al. 2004; Marks et al. 2012; Barakat and Gribnau 2012), while the extraembryonic tissues will maintain the imprinted XCI (Takagi and Sasaki 1975). This first round of XCI/XCR is necessary to allow 24 hours later a second round of XCI in the epiblast cells which will silence randomly either the paternal or the maternal X chromosome. From the epiblast, a small subset of cells starts to differentiate into germ cells. At this point, a second round of XCR initiates in primordial germ cells (PGCs) (Sugimoto and Abe 2007) to allow for the transmission of an active X chromosome onto the next generation.

The XCI/XCR *in vivo* dynamics can be modelled and followed *in vitro* by differentiating embryonic stem cells (ESCs) and inducing pluripotent stem cells (iPSC) reprogramming (Panning and Jaenisch 1996) or via primordial germ cell-like cells (PGCLCs) formation (Katsuhiko Hayashi et al. 2012). In this thesis, I will model the XCI/XCR dynamics in the PGCLCs system.

X chromosome epigenetic reprogramming of *in vivo* PGCs

In both male and female PGCs, various events of genome-wide epigenetic reprogramming take place. In females only, before sex-specific differentiation is initiated, the inactive X chromosome is reactivated, resulting in two transcriptionally active X chromosomes (Reviewed in (Ohhata and Wutz 2013; Monk and McLaren 1981)). Similarly to genome-wide epigenetic reprogramming, the timing for X-reactivation in PGCs is still under debate/has been debated over the last years. Initial studies have shown that X-reactivation occurs very fast in a short time window; once PGCs have already colonized the developing ovary (E10.5-E12) but before meiotic initiation takes place (E13.5) (Kratzer and Chapman 1981; Monk and McLaren 1981; Tam, Zhou, and Tan 1994; Nesterova et al. 2002). Furthermore, X-reactivation has been shown to be accompanied by a rapid wave of DNA demethylation (Petra Hajkova et al. 2002). On the contrary, more recent studies (Sugimoto and Abe 2007) have shown X-reactivation to already begin in nascent E7.0 PGCs and spanning over a developmental window of over 7 days, taking place in a gradual manner and probably involving passive steps.The transcription of X-linked genes and X status in the latest studies was assessed using whole-mount RNA fluorescence in situ hybridization (FISH) and single-cell PCR combined with germ cells markers. On the one hand, those techniques allowed cell to cell resolution and represented an improved analysis compared to previous studies, on the other hand, still lacked the depth of sequencing approaches. Despite the limited literature and lack of knowledge on X-reactivation in PGCs, it is known that the following events are part of the process:

Repression of *Xist* RNA

The coating of the long noncoding Xist is a characteristic feature of the inactive X chromosome. Therefore, a possible way to define if an X chromosome is active or inactive is by analyzing Xist expression. From ~E7.0 until ~E10.5, a substantial number of PGCs (~30%) starts to downregulate *Xist*, transcribe negligible levels of its antisense RNA *Tsix*, and concomitantly re-express the pluripotency marker *Nanog* (Yamaguchi et al. 2005; Sugimoto and Abe 2007). To identify the beginning of *Xist* downregulation, whole-mount embryos were analyzed by RNA FISH combined with immunofluorescence (IF) for stage-specific PGC markers. At E7.0, ~20% of PGCs showed a small or faint Xist signal and unexpectedly, ~10% were already Xist negative.

At ~E8.5, 16.5% of PGCs appeared to be Xist-negative and by E10, the percentage increased to 48.2%. By E12.5, almost all PGCs had lost the Xist signal (Sugimoto and Abe 2007). The mechanisms behind Xist removal in PGCs have not been shown in any studies but the results presented in (Sugimoto and Abe 2007) hint towards a *Tsix*-independent mechanism. Moreover, it still remains to be clarified whether *Xist* repression is even necessary for X-reactivation in PGCs.

Reactivation of X-linked genes

Evaluating the biallelic expression of X-linked genes represents another way to measure X-reactivation. The presence of SNPs between the hybrid strain *Mus musculus molossinus* x *M. m. domesticus* combined with single-cell RT-PCR on 10 X-linked genes, has allowed to demonstrate that X-reactivation in PGCs, at a gene expression level, occurs in a gradual fashion (Sugimoto and Abe 2007). By ~E10.5 *Xist* becomes completely undetectable and 3 genes (*Np15*, *Fgd1*, and *Pdha1*) start to show biallelic expression. At E12.5, 5 genes were expressed biallelically in more than half of the PGCs analyzed (*Np15*, *Fgd1*, *Pdha1*, *Hprt* and *Fmr1*). However, 2 X-linked genes (*G6pd* and *Rex3*) were still showing monoallelic expression even at ~E14.5, when most of the cells have already initiated meiosis (Anne McLaren 2003). McLaren and colleagues showed how that the maintenance of an inactive status of X-linked genes does not require Xist RNA in normal embryonic development *in vivo*. A later study (Chuva de Sousa Lopes et al. 2008) published similar observations. The authors also followed the expression of a few X-linked genes by RT-PCR between E9.5 and E13.5. They observed a pattern of X-reactivation emanating from the centromere towards the X-inactivation center, the region where the *Xist* gene is located. For example, genes such as *Rhox4b* (closer to the centromere) were already biallelic at E9.5, *Hprt* at E11.5 (where the X-reporter transgene used by Chuva de Sousa Lopes and colleagues was located) and *Fmr1* and *Zfx (*closer to the X inactivation center) only later at E13.5 (Chuva de Sousa Lopes et al. 2008). However, a complete characterization of X-reactivation dynamics considering X-linked gene expression as a readout is still missing, given the overall low number of genes analyzed (~10) until now. Therefore, so far any conclusion in terms of X-reactivation following gene expression should be taken carefully.

Loss of H3K27me3 accumulation on the X chromosome

In migrating PGCs a genome-wide increase of H3K27me3 can be observed. On the contrary, the reactivating X chromosome undergoes a gradual reduction of H3K27me3, a mark of the inactive X chromosome (Plath 2003; Silva et al. 2003). This step by step removal of H3K27me3 has been shown to follow PRDM14 expression dynamics during the progressive PGCs migration along the gonad (Mallol, Guirola, and Payer 2019). It has been reported in ESCs that *Xist* grants polycomb recruitment on the X chromosome, which in turn catalyzes the deposition of the H3K27me3 mark. (Plath 2003; Kohlmaier et al. 2004). Therefore, the loss of H3K27me3 in PGCs could be explained as a consequence of *Xist* downregulation. X-reactivation has also been shown to take place in *in vitro* PGCLCs aggregated with somatic gonadal cells, recapitulating a developmental stage similar to E9.5 PGCs. However, X-reactivation was assessed solely by H3K27me3 immunostaining, showing merely the loss of H3K27me3 accumulation on the X chromosome (Katsuhiko Hayashi et al. 2012).

Exposure to female urogenital niche signaling

As reported above, female PGCs start X chromosome reactivation while migrating towards the urogenital ridge (UGR), the primordium of the kidney and gonad. However, a more active transcription of X-linked genes only starts once PGCs enter the UGR. Therefore it was hypothesized that signals coming from the UGR niche could play a role in X-reactivation (Chuva de Sousa Lopes et al. 2008). Authors performed co-culture experiments of E9.5 and E11.5 X inactive PGCs alone or with E11.5 female somatic gonadal cells for 48h and reported that the percentage of X reactivated PGCs increased significantly in the presence of the female environment. Summarizing, the authors not only proved that signals deriving from the female urogenital ridge tissues seem to stimulate the reactivation of the silenced X-linked GFP transgene (Hadjantonakis et al. 1998) on the X chromosome in PGCs, but also that as early as E9.5, PGCs are competent to respond to these signals. Despite the advances in the knowledge of X-reactivation in PGCs, a precise molecular mechanism and a detailed characterization about the timing of events remains elusive.

PROJECT AIMS

The goal of this project is to investigate the impact of X-inactivation/X-reactivation dynamics on female mouse germ cell development. The central hypothesis states that during germ cell maturation, X-inactivation followed by X-reactivation is essential to allow entry into meiosis, required for the generation of haploid gametes. In order to test the central hypothesis, we have set four specific aims:

1. **Establish an *in vitro* model allowing the recapitulation of X-inactivation / X-reactivation.**

   While various methodologies have already been reported to allow the *in vitro* generation of germ cells, the X chromosome has been poorly characterized during this process. We will therefore develop a tailor-made system to achieve germ cell formation while tracing X-chromosome dynamics *in vitro*.
2. **Understand the dependencies between X chromosome status and early germ cell fate acquisition.**

   The pluripotent landscape has been previously reported to be influenced by the intrinsic chromosomal composition. Thus, the X-status can be part of the factors dictating a certain cell fate. To investigate the possibility of X-activity playing a role in early germ cell formation, we will analyze and compare the transcriptional landscape of X-active and X-inactive PGCLCs.
3. **Investigate the necessity of X-reactivation and the biological consequences upon its failure especially affecting meiotic entry and germ cell development.**

   We will use the two existing systems reported to stimulate meiotic entry. We aim to profile the impact of X-reactivation, or lack thereof, by immunostainings, identifying different meiotic stages.
4. **Identify factors implicated at the interphase between X-reactivation and meiosis.**

   We will apply combinatorial signaling niches and quantify X-reactivation and meiosis by immunostainings.

RESULTS

Establishing an *in vitro* system to generate X inactive PGCLCs

In this study, I have established an *in vitro* culture system that permits to follow the X chromosome status throughout ESC differentiation towards PGCLCs, as well as to isolate X inactive PGCLCs. Therefore it provides an opportunity to dissect the relationship between X chromosome dynamics and germ cell development. Specifically, such a system allows to study the timing and kinetics of X inactivation/reactivation during germ cell development in a highly controlled manner. Furthermore, this *in vitro* system allows to overcome one of the main limitations of *ex vivo* systems: the restricted amount of available material. Few studies have monitored the X status during *in vitro* PGCLC differentiation (see introduction), and mostly assessed the activity of the X-chromosome using imaging techniques or small scale gene expression analysis. The study presented here is the first report to carefully monitor the X status during germ cell specification combining imaging, FACS and allele-specific RNA-sequencing.

XRep: a tailor made female PGCLC-inducible X reporter line

As previously mentioned, the timing of X chromosome reactivation in the developing female germline represented a difficult question to answer, and thus gave rise to contradictory results (Monk and McLaren 1981; Tam, Zhou, and Tan 1994; Nesterova et al. 2002; Gartler, Rivest, and Cole 1980). Indeed, due to technical difficulties and the limited material available *ex vivo,* a comprehensive assessment of the X-chromosome status during germ cell development was absent in the field. To overcome the limited amount of materiale available and to allow the traceability of the X chromosome, we engineered a reporter ESC line to generate *in vitro* germ cells, following mostly published protocols (Katsuhiko Hayashi et al. 2012; Nakaki et al. 2013). The newly tailor-made ESC line carried the following features: (i) a hybrid background to distinguish sequencing reads from the two X chromosomes thanks to the single nucleotide polymorphisms existing between the two genetically distant species *Mus musculus musculus* (mus) and *Mus musculus castaneus* (cas) occurring on average

every 300 bp (Marks et al. 2015) (ii) a truncation of the long noncoding *Tsix* on the X^{mus} which forces a non-random X inactivation of the X^{mus} upon cell differentiation (Luikenhuis, Wutz, and Jaenisch 2001) (iii) a GFP and a tdTomato reporter integrated in the *Hprt* locus of X^{mus} and X^{cas} respectively to monitor the activity of X chromosomes at single cell resolution (Bauer et al. 2020) (vi) the integration of previously published vectors (Nakaki et al. 2013) to allow the controlled overexpression of three key germline transcription factors: *Blimp1*, *Prdm14* and *Tfap2c* (Vincent et al. 2005; Ohinata et al. 2005; Yamaji et al. 2008; Weber et al. 2010).

Given that the first three cell line manipulations were performed previously to the start of this study, in depth description of the results will focus only on the addition of the inducible transcription factors into the previously existing female cell line.

Cytokines-based induction impairs X-inactivation during PGCLC generation

To study X-reactivation in PGCLCs we first need to identify the culture conditions that will ensure the generation of PGCLCLs carrying an inactive X chromosome. To reconstitute X inactive PGCLCs differentiation in culture from ESCs, passing through the EpiLCs stage, we tested what is considered as the gold-standard protocol for PGCLC induction (Katsuhiko Hayashi and Saitou 2013). Our first attempts to generate X inactive PGCLC were carried out using a modification of the dual color reporter ESC line, bearing solely an XGFP reporter on the X^{mus}. The reason for that was to have access to more fluorescent channels to perform putative image analysis using multiple markers when assessing the quality of the PGCLC generated. We applied the cytokine induction protocol which, briefly, consists of a 2-day EpiLCs differentiation followed by culturing floating aggregates of those for 6 days in a medium containing BMP4, SCF, LIF and EGF (see methods). Using the standard protocol with the single X reporter cell line, we obtained ~8% of PGCLCs, identified by measuring two endogenous surface proteins known to be expressed in early stages of PGCLC specification: the pluripotency marker SSEA1 and integrin-beta3 (CD61) (Katsuhiko Hayashi et al. 2011). The percentage of PGCLCs obtained was in line with the reported efficiencies as well as the levels of expression of the surface markers (Katsuhiko Hayashi and Saitou 2013). However, as indicated by the levels of XGFP in the double positive population SSEA1+/CD61+ of PGCLCs, the X^{mus} chromosome was still active, indicating that during the differentiation from ESCs to EpiLCs and finally into PGCLCs, the expected X inactivation did not occur. To better understand the nature of the generated X active

PGCLCs and whether the XGFP reporter was recapitulating faithfully the lack of X linked gene inactivation and *Xist* expression, we isolated PGCLCs and measured gene expression of a few selected marker genes by quantitative RT-PCR (qPCR). We observed that pluripotency genes that were expected to stay down regulated during the transition from EpiLCs to PGCLC, such as *Klf4*, still displayed comparable expression levels to ESCs, while early PGC signature genes such as *Dnd1,* were not upregulated compared to EpiLCs. Together with low *Xist* expression, we concluded that the obtained PGCLCs had an X active status and a phenotype resembling the pluripotent starting population of ESCs.

Therefore, following this strategy we encountered two main difficulties: i) lack of a distinctive PGCLCs gene expression pattern, and ii) lack of an inactive X chromosome in the early PGCLCs obtained. To overcome those problems we decided to change strategy and engineer a transcription factor-inducible ESC line. This new line would allow us to i) force the expression of PGCLC signature genes (*Blimp1*, *Prdm14*, *Tfap2c*), boosting the PGCLC efficiency ii) bypass the addition of cytokines, impacting the X-inactivation phenotype iii) take advantage of a dual color reporter cell line (Bauer et al. 2020) to monitor a putative X-loss phenotype.

Transcription factors-based induction allows efficient generation of X-inactive PGCLCs

An alternative published protocol based on the overexpression of key germ cell line transcription factors (*Blimp1*, *Prdm14* and *Tfap2c*) was successful in generating PGCLCs (Nakaki et al. 2013). However, this overexpression system was available only in male cells. We therefore faced the necessity to engineer the overexpression of *Blimp1*, *Prdm1*4 and *Tfap2c* in our female dual color X reporter ESC line. We first transfected a selected ESC clone to insert homozygously the reverse tetracycline transactivator (rtTA) under the control of the constitutively active *Rosa26* promoter (Hochedlinger et al. 2005). As shown in (Fig S1c), out of the 6 transfected clones only one displayed a homozygous integration in the Rosa26 locus (clone 9). We additionally confirmed the expression of the *rTTA* gene by qPCR. The selected clone was then transfected with *piggyBac* transposon-based vectors (Nakaki et al. 2013) expressing the transcription factors (TFs) *Blimp1*, *Prdm14* and *Tfap2c* under the control of doxycycline (dox) regulatory elements. Clones were selected according to the following criteria: (i) carrying all three TFs transgenes (ii) showing expression upon dox

treatment of the three TFs comparable to the published levels, preferably with high *Prdm14* levels (iii) showing approximately 20 random transposon insertions. Therefore, we selected two clones, A11 and E9, that carried both the desired number of insertions assessed by southern blot (Fig. Sd) and levels of expression of the transcription factor, measured by qPCR, comparable to the original publication (Nakaki et al. 2013).

To ensure that the endogenous levels of the cassette genes (*Tfap2c, Blimp1*, *Prdm14*) would still be detectable upon their overexpression, we measured their expression by qPCR. The dox-induced TFs could be differentiated from the endogenous thanks to the presence of specific tag sequences. We analyzed the effects of dox treatment on TFs expression over a time course of 5 days, extracting the RNA from a whole body, without FACS sorting for PGCLCs surface markers. We observed a peak for all of the exogenous TFs after 24h, followed by a decrease in expression. Similarly, the endogenous TFs started to be expressed after 24h but, differently from the exogenous, gradually increased in expression (*Blimp1*, *Prdm14*) or maintained the same levels (*Tfap2c*) (Fig. Sf). To control for the leakiness of the system, we performed a PGCLCs induction without doxycycline, and as expected, we did not observe upregulation of PGCLCs-specific cell surface markers SSEA1 and CD61 (Fig. Sg). Next, we set up the TF induction protocol following the standard timing reported in (Nakaki et al. 2013): 2 days of EpiLC induction and 4 days of PGCLC induction. Surprisingly, we did not observe PGCLC induction from day 2 EpiLCs, as shown in Fig. Sg by the absence of SSEA1 and CD61 surface markers. Considering that female germ cells are known to develop at a slower rate compared to males (Mittwoch 1993), we extended EpiLC differentiation until day 4, maintaining PGCLC differentiation 4 days long. With this strategy, we successfully generated bodies containing ~50% of PGCLCs as indicated by SSEA1 and CD61 expression. Moreover, ~60% of the PGCLCs were showing a downregulation of the GFP reporter (Fig. Sd), indicating X chromosome inactivation. This result showed not only that PGCLCs could be induced from a later EpiLC day (day 4), to the contrary of what had been reported (Katsuhiko Hayashi et al. 2011), but also that PGCLCs induced via the overexpression of TFs could give rise to X inactive PGCLCs, as shown by the downregulation of the XGFP reporter. Before, epigenetic profiling of X-inactivation in PGCLCs was only shown by immunostaining for H3K27me3, showing accumulation on the X chromosome upon aggregation of EpiLCs (Katsuhiko Hayashi et al. 2012). To test whether the PGCLC induction efficiency and XGFP downregulation could be increased, we overexpressed *Blimp1*, *Prdm14* and

Tfap2c for 5 days instead of 4. At PGCLC d5, we found ~60% of the cell population to be double positive for PGCLC surface markers and up to 90% downregulation of the XGFP reporter. To assess the quality of our PGCLCs, we stained cryosections of PGCLC bodies at d5 of induction for SOX2 and TFAP2C, both germ-line specific transcription factors. We observed, as expected, that more than 50% of the PGCLC d5 body was double positive for SOX2 and AP2γ, confirming PGCLC cell identity. Overall, the modifications applied to the original protocol led to an efficiency increase in the generation of PGCLCs and the establishment of the physiological X inactivation status observed during female epiblast development in the vast majority of PGCLCs.

Figure S1. Generation of the *XRep* cell line and set up of the PGCLC induction system.
(a) Representative FACS analysis of PGCLC d6 induced from EpiLC d2 using cytokines. FACS gating strategy for PGCLCs according to germ cells specific surface markers SSEA1 and CD61. Out of the double positive SSEA1+ CD61+, cells were gated for X-activity according to XGFP and FCS. Numbers indicate the percentage of gates cells. **(b)** Expression of the indicated genes measured by qRT-PCR in the Single Color cell line. For each gene, the delta Ct from the average Ct values of the housekeeping gene *Arbp* is shown. Each point represents the mean value of three technical replicates. **(c)** Top panel: *rtTA* expression measured by qRT-PCR. Values are normalized against *Gapdh* expression. Error bars indicate SD (n = 3 wells per clone). Bottom panel: Southern blot analysis showing the *rtTA* integration in the *Rosa26* locus. Genomic DNA was digested with EcoRV. Expected fragment sizes: WT (wild-type) = 11.5kb, targeted = 5.2kb. Selected homozygous clone is indicated by a red outline. WT, parental cell line; undig., undigested gDNA. **(d)** Southern blot analysis showing the copy number of the integrated *piggyBac* transposon vectors in each *XRep* transfectant. Genomic DNA was digested with BamHI. A fragment of the *ß-galactosidase* reporter, included in all 3 transcription factor vectors, downstream of BamHI site, was used as a probe. Expected fragment size: 1.6 kb. Selected clones are indicated by a red outline. Estimated copy number for the selected clones is indicated in brackets.
(e) qRT-PCR of cassette specific transcripts of *Avi-Blimp1*, *3xFLAG-Prdm14*, and *V5-Ap2g*. Values were normalized against *Arbp* expression. Error bars indicate SD (n = 3 technical replicates). **(f)** Expression levels measured by qRT-PCR of the exogenous (magenta) and endogenous (blue) *Blimp1*, *Prdm14* and *Tfap2c* transcripts from whole unsorted EpiLC aggregates induced with Dox along the 5 days of induction. For each gene, values are normalized against *Arbp* expression in EpiLCs. The line shows the mean value of two independent experiments, with three technical replicates. **(g)** FACS analysis of PGCLCs d4, induced with Dox from either EpiLC d2 or EpiLC d4. FACS gating strategy for PGCLCs according to surface germ cell markers SSEA1 and CD61. Gating strategy for X-activity according to XGFP and XTomato. Shown are contour plots on live cells. Numbers indicate the percentage of gated cells. **(h)** FACS analysis of *XRep* induction without Dox in PGCLC d5 from EpiLC d4. The number indicates the gated germ cells.

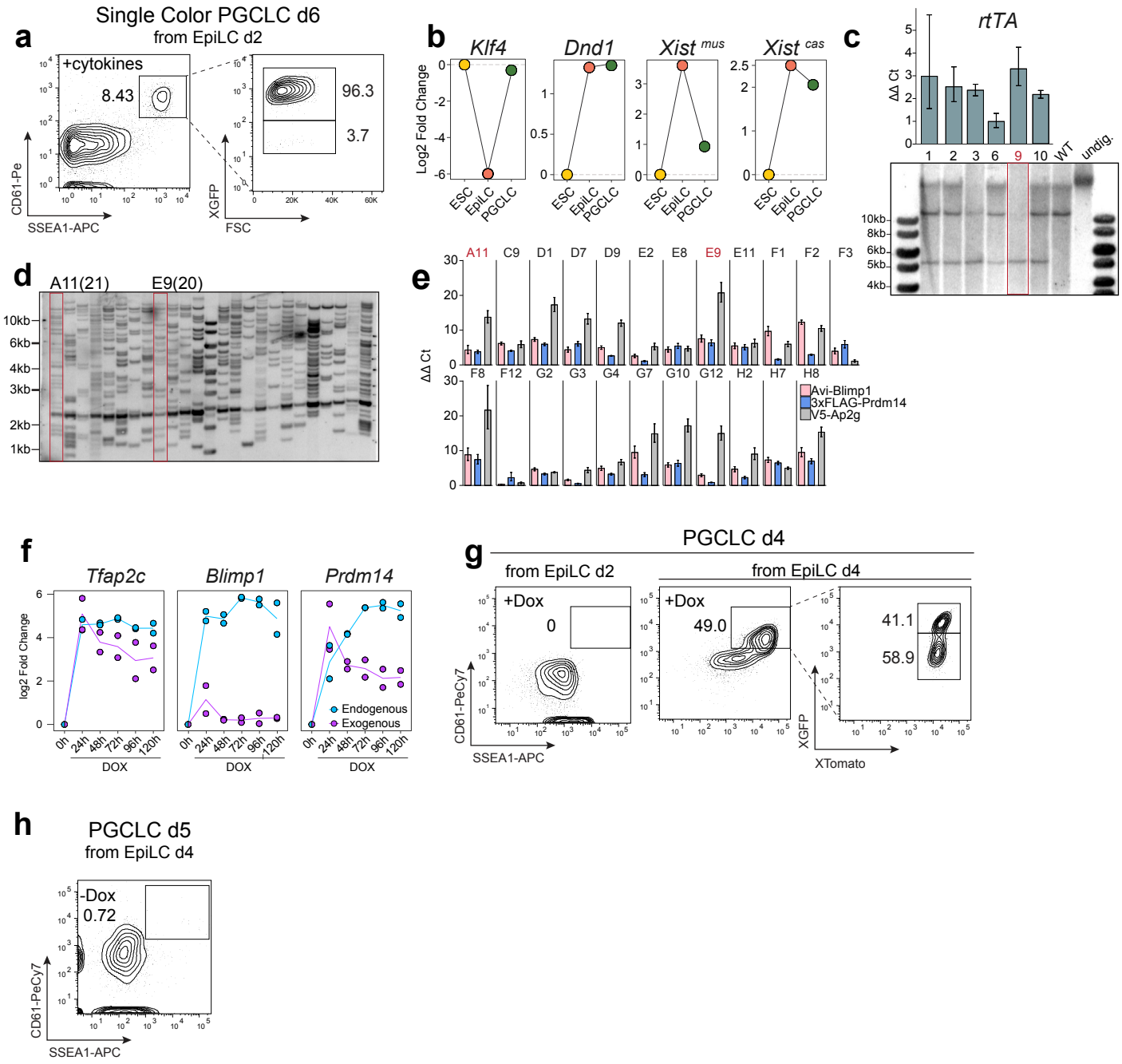
a
Single Color PGCLC d6
from EpiLC d2
+cytokines
8.43
96.3
3.7
CD61-Pe
SSEA1-APC
XGFP
FSC
b
Klf4
Dnd1
Xist mus
Xist cas
Log2 Fold Change
ESC
EpiLC
PGCLC
c
rtTA
ΔΔ Ct
1 2 3 6 9 10 WT undig.
10kb
8kb
6kb
5kb
4kb
d
A11(21)
E9(20)
10kb
6kb
4kb
3kb
2kb
1kb
e
A11 C9 D1 D7 D9 E2 E8 E9 E11 F1 F2 F3
F8 F12 G2 G3 G4 G7 G10 G12 H2 H7 H8
ΔΔ Ct
Avi-Blimp1
3xFLAG-Prdm14
V5-Ap2g
f
Tfap2c
Blimp1
Prdm14
log2 Fold Change
Endogenous
Exogenous
0h 24h 48h 72h 96h 120h
DOX
g
PGCLC d4
from EpiLC d2
from EpiLC d4
+Dox
0
49.0
41.1
58.9
CD61-PeCy7
SSEA1-APC
XGFP
XTomato
h
PGCLC d5
from EpiLC d4
-Dox
0.72
CD61-PeCy7
SSEA1-APC

Distinct populations revealed by tracing the X-status

The dynamics of X chromosome activity during the transition from EpiLCs to PGCLCs still remain elusive. PGCLC induction in our *Xrep* cell line revealed two clearly distinct populations of PGCLCs in terms of X chromosome status: a small population of PGCLCs carrying two active X chromosomes (XGFP+, ~10%) and a major population that underwent X chromosome inactivation (XGFP-,~90%) (Fig. 1e). First, we wondered whether XGFP+ PGCLCs were the result of (i) a failure to inactivate the X chromosome during EpiLCs - PGCLC differentiation (ii) or spurious X-reactivation during the 5 days of PGCLCs induction. To test our first hypothesis, we assessed the percentage of X chromosome inactivation within our EpiLCs population. We applied Immuno-RNA FISH to visualize at single-cell resolution the two major X inactivation markers: H3K27me3 spot and Xist RNA cloud. We observed an H3K27me3 mark and Xist RNA cloud in almost all EpiLCs (~80%), indicating an epigenetic X inactivation phenotype (Fig. 1f). However, despite the presence of the two main X inactivation marks, the fluorescence levels of the XGFP reporter in EpiLCs were still high, yet lower than the levels of XGFP in ESCs (Fig. 1e). To further understand the heterogeneity of EpiLCs at the level of X-status and whether there may be a fraction of cells displaying a delay in differentiation and consequently in X-inactivation, we sorted EpiLC XGFP high and XGFP low, extracted RNA from each population and measured the expression of a few selected genes by qPCR. We analyzed *Rex1 (Zfp42)*, which is a canonical naive pluripotency gene (Rogers, Hosler, and Gudas 1991) together with the *de novo* DNA methylases *Dnmt3b* and *Dnmt3l* (Reik, Dean, and Walter 2001) reported to be signature genes of EpiLC differentiation. We observed that XGFP high EpiLCs displayed higher levels of *Rex1* as well as lower levels of *Dnmt3b*, suggesting a delayed differentiation of these cells and unexpectedly higher levels of *Dnmt3l* which usually follows the trend of *Dnmt3b*. At the allelic level, we analyzed the expression of *Xist* and 3 X-linked genes using primer pairs designed specifically to amplify either the X^{mus} or the X^{cas} allele. While Xist expression levels were similar between EpiLC XGFP high and EpiLCs XGFP low, we observed that X-linked genes *Amot*, *Prdx4* and *Prkx* were exclusively repressed in the EpiLCs XGFP low, indicating that this EpiLC population had initiated X-inactivation (Fig. 1i).

To asses our second hypothesis, whether PGCLCs XGFP+ could arise due to spurious reactivation of PGCLCs during the induction time course, we separately induced

PGCLCs from XGFP high and XGFP low EpiLCs and monitored XGFP levels in the SSEA1+/CD61+ PGCLC population. We started analyzing XGFP levels by flow cytometry from PGCLCs at d2 of induction as early PGCLCs at d1 do not express SSEA1 nor CD61 yet. We noticed that in the PGCLC population originating from EpiLCs sorted XGFP high, XGFP levels remained high, around 10^4 of fluorescence intensity, over the 5 days of induction. In contrast, in PGCLCs originating from EpiLCs sorted XGFP low, levels of XGFP decreased over time until the majority of PGCLCs (~80%) was XGFP- (Fig. 1j). These results suggest that EpiLC d4 consist of two distinct populations. On the one hand, an XGFP high population that shows a delay in the downregulation of the pluripotency factor *Rex1* and concomitantly a delay in X-inactivation, while still allowing the acquisition of PGCLCs cell surface markers in the TF overexpression system. On the other hand, an EpiLCs XGFP low population that give rise to PGCLCs that continue to undergo X-inactivation.

Differences in cell cycle profiles during PGCLC induction

Our data suggests that PGCLCs XGFP+ originate from a subpopulation of EpiLCs that fails to X-inactivate and displays features resembling ESCs. Therefore we set out to investigate whether PGCLCs XGFP+ present additional pluripotency features such as a distinctive cell cycle profile. Cell cycle analysis revealed that the majority of XGFP+ PGCLCs (>~65%) were in S phase and showed a short G1 phase, typical of ESCs. In contrast, the cell cycle of PGCLCs XGFP- was observed to be slower, with fewer cells in S phase (~44%) and longer G1 phase (Fig. 1k). These findings further suggest that PGCLCs XGFP+ exists as a distinct population with PGCLC surface markers and a cell cycle profile highly similar to pluripotent ESCs.

Figure 1. A tailor-made system to trace X-chromosome inactivation and reactivation dynamics during PGCLC induction reveals two distinct PGCLC populations.
(a) Schematic representation of the features implemented in the *XRep* cell line: A hybrid background in which cells carry one X chromosome from *M.m musculus* (X^{mus}) and one from *M.m castaneus* (X^{cas}). The X^{mus} carries a GFP reporter and the X^{cas} carries a tdTomato reporter. The cell line carries an *rtTA* under the control of the *Rosa26* locus and *piggyBac* transposon-based vectors with doxycycline (Dox) -responsive promoters driving the expression of *Prdm14*, *Blimp1*, *Tfap2c*. **(b)** Overview of the culture system. Stages of PGCLC induction are shown. Green and red bars at the bottom represent the X^{mus} and X^{cas} activity status, respectively. **(c)** FACS analysis of primordial germ cells specific surface markers CD61 and SSEA1 in ESCs, EpiLCs d4 and PGCLCs d5. Numbers indicate the percentages of gates cells. **(d)** Immunostaining of PGCLCs d5 cryosections for SOX2 (magenta) and TFAP2C (cyan). **(e)** FACS analysis of XGFP and XTomato reporters from bulk ESCs, bulk EpiLCs and double positive CD61+/SSEA1+ PGCLCs. Numbers indicate the percentages of gated cells. **(f)** Immunolabeling with antibody against H3K27me3 (green) combined with Xist RNA-FISH (red). Images show a representative group of cells showing Xist RNA coating and H3K27me3 enrichment on the X^{mus}. Barplot indicates the percentage of cells having both Xist RNA coating and H3K27me3 accumulation, cells with Xist only or H3K27me3 only. Below the graph, the total cell number analysed is indicated. Scale bar, 10 μm. **(g)** FACS plots of EpiLCs d4, showing a representative contour plot with colored boxes indicating percentages of populations defined GFP high (light green rectangle) and GFP low (darker green rectangle). Numbers indicate the percentages of sorted cells. **(h)** Quantitative RT-PCR (qRT-PCR) in EpiLCs d4 sorted GFP high (light green) and GFP low (dark green) for the indicated genes. Each point represents the mean of two separate inductions for each biological replicate (clones A11 and E9). Dashed line at 0 indicates ESCs expression. Log2 fold change relative to ESCs is shown. **(i)** qRT-PCR in EpiLC d4 sorted GFP high (light green) and GFP low (dark green) for the indicated X-linked genes. Each point represents the mean of two separate inductions for each biological replicate (clones A11 and E9). Dashed lines at 0.5 indicate biallelic expression. **(j)** Histograms showing XGFP distribution during PGCLC induction from EpiLCs sorted GFP high and GFP low. Numbers indicate the percentage of gated cells according to the XGFP status (red = GFP negative, green = GFP positive). **(k)** Representative histograms for the cell cycle analysis by FACS of the indicated cell types. Cells in G1, S and G2/M phase are shown along with the percentage of each population.

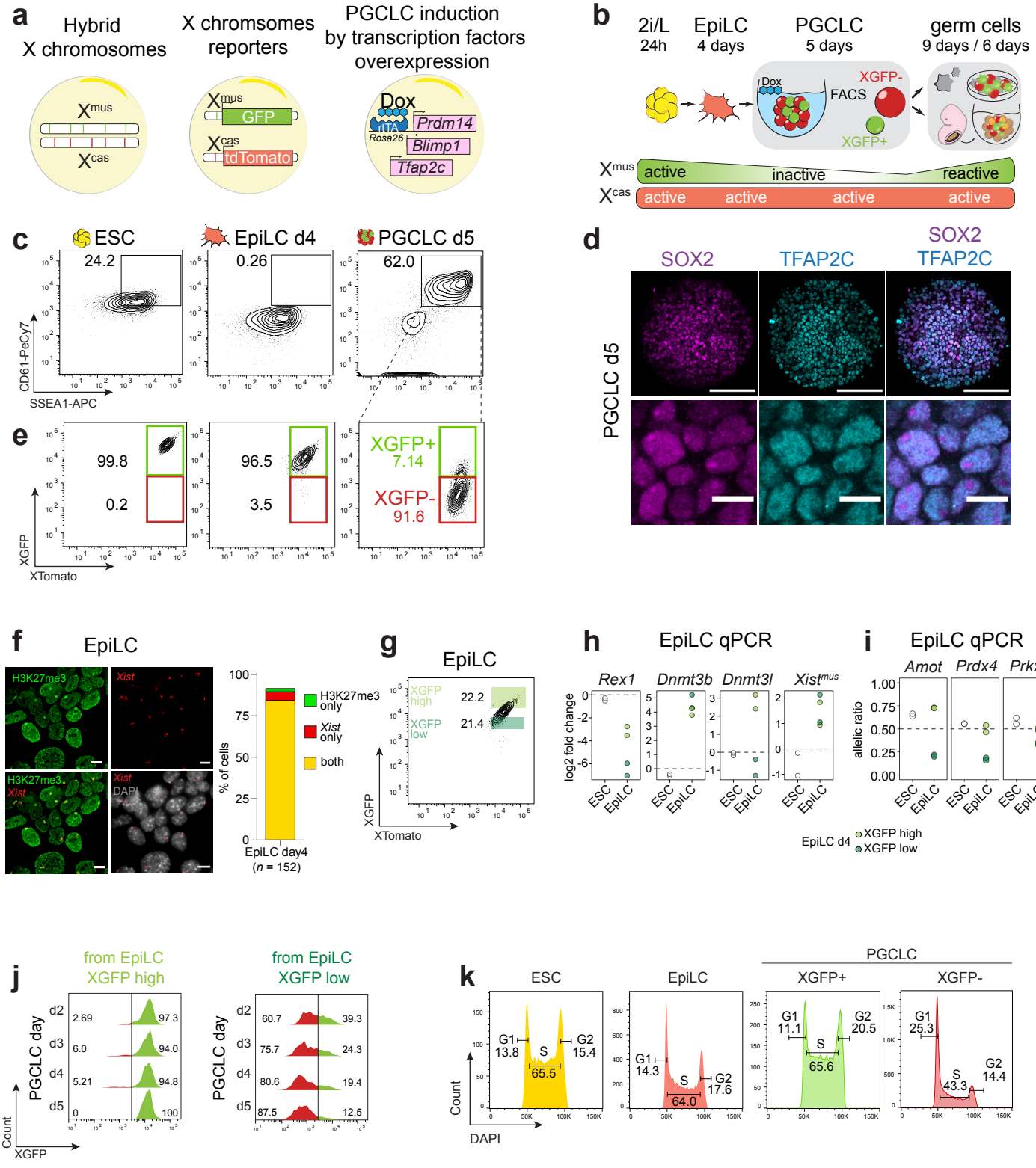
a
Hybrid X chromosomes
X chromsomes reporters
PGCLC induction by transcription factors overexpression
Xmus
Xcas
GFP
tdTomato
Dox
rtTA
Rosa26
Prdm14
Blimp1
Tfap2c
b
2i/L 24h
EpiLC 4 days
PGCLC 5 days
germ cells 9 days / 6 days
Dox
FACS
XGFP-
XGFP+
Xmus active inactive reactive
Xcas active active active active
c
ESC
EpiLC d4
PGCLC d5
24.2
0.26
62.0
CD61-PeCy7
SSEA1-APC
d
SOX2
TFAP2C
SOX2 TFAP2C
PGCLC d5
e
99.8
0.2
96.5
3.5
XGFP+ 7.14
XGFP- 91.6
XGFP
XTomato
f
EpiLC
H3K27me3
Xist
DAPI
% of cells
H3K27me3 only
Xist only
both
EpiLC day4 (n = 152)
g
EpiLC
XGFP high
XGFP low
22.2
21.4
XGFP
XTomato
h
EpiLC qPCR
Rex1
Dnmt3b
Dnmt3l
Xistmus
log2 fold change
ESC
EpiLC
i
EpiLC qPCR
Amot
Prdx4
Prkx
allelic ratio
EpiLC d4
XGFP high
XGFP low
j
from EpiLC XGFP high
from EpiLC XGFP low
PGCLC day
d2
d3
d4
d5
2.69
97.3
6.0
94.0
5.21
94.8
0
100
60.7
39.3
75.7
24.3
80.6
19.4
87.5
12.5
Count
XGFP
k
ESC
EpiLC
PGCLC
XGFP+
XGFP-
G1 13.8
S
65.5
G2 15.4
G1 14.3
S
64.0
G2 17.6
G1 11.1
S
65.6
G2 20.5
G1 25.3
S 43.3
G2 14.4
Count
DAPI

Transcriptional changes during PGCLC induction

Thanks to the set up of the *in vitro* system we could maximize the number of X inactive PGCLCs to conduct RNA-seq experiments. To gain insights into the transcriptional changes taking place during PGCLCs differentiation, naive ESCs, primed d4 EpiLCs, d5 PGCLCs XGFP+ and d5 PGCLCs XGFP- were sampled in two technical replicates (inductions performed at different times) and two biological replicates (two different clones, A11 and E9 induced in parallel) and their total RNA extracted and analyzed by RNA-seq. Firstly, Principal component analysis (PCA) of the expression profiles revealed high coherence between the technical and biological replicates. Secondly, PCA revealed a cell differentiation trajectory along the PC2 corresponding to a separation of X-active and and X-inactive samples suggesting PC2 as the component reflecting the X-status (Fig. 2a). We were then interested in identifying possible marker genes dictating the trajectory of our samples. We visualized the 10 genes influencing positively the PC1 and three out of ten were located on the X chromosome (Fig. 2b). To exclude the possibility that the clustering of our samples was merely due to the influence of the X chromosome, we repeated the PCA while eliminating X chromosome-linked genes from the analysis. We observed a similar clustering of samples with minimal changes in component variances (Fig. 2c).

Despite PGCLCs XGFP- and XGFP+ sharing the same surface markers identified by FACS, in our PCA the two populations clustered separately, irrespective of the X status, indicating distinct cell identities. This finding was further supported by the analysis of early and late germ cells genes. We found early germ cells genes expressed at quite similar levels between PGCLCs XGFP- and XGFP+ while late germ cell genes such as *Dazl* and *Ddx4* were expressed much higher in the PGCLCs XGFP+. Moreover, it has been previously reported that PGCLCs and ESCs share many pluripotency genes. Therefore we measure core pluripotency gene expression and found that PGCLCs XGFP+ shared similar expression levels of *Nanog*, *Zfp42*, *Esrrb* and *Nr0b1* with ESCs, while other pluripotency genes such as *Fgf4, Tbx3,* and *Klf4* were exclusively expressed in ESCs. We also examined the expression of epiblast marker genes such as *Fgf5* and the DNA methylation machinery genes *Dnmt3b*, *Dnmt3a* and confirmed their expression in our EpiLCs (Fig. 2d).

After having observed that the PGCLCs XGFP+ expressed late germ cells genes and PGCLCs XGFP- early germ cells genes, we wanted to investigate what would be their

transcriptional equivalent *in vivo*. We therefore compared our RNA-seq dataset to published datasets of *in vivo* female PGCs from the following timepoints: E9.5, E10.5, E11.5 and E12.5 (Nagaoka et al. 2020). Clustering of samples revealed that PC1 seemed to clearly define the *in vivo* developmental timing component. Notably, PGCLCs XGFP- clustered closest to E9.5 - E10.5 *in vivo* samples, whereas PGCLCs XGFP+ more closely to E10.5 and E11.5, indicating a slightly more advanced transcriptional landscape of the latter. In summary, the comparison to *in vivo* data allowed us to collectively confirm that the TFs overexpression in our system allowed to recreate an *in vivo* PGC-like transcriptome (Fig. 2e).

To further describe the differences between PGCLCs XGFP+ and PGCLCs XGFP-, we performed differential gene expression analysis. We could identify 2464 upregulated and 2384 downregulated genes in the PGCLCs XGFP- (14% genes). Among the genes upregulated in the PGCLCs XGFP- we found early germ cells genes, the imprinted gene *H19* and *Xist*. In contrast, in PGCLCs XGFP+ we found late germ cell genes *Ddx4* and *Dazl* and naive pluripotency genes such as *Zfp42* (Fig. 2f). Functional annotation of upregulated genes in PGCLC XGFP- revealed enrichment for different classes of genes including those involved in the urogenital system development, MAPK regulation and WNT signaling, while genes upregulated in PGCLCs GFP+ were enriched for response to LIF signaling and meiotic entry (Fig. 2g).

Figure 2. Gene expression analysis confirms proper PGCLC induction
(a) PCA of gene expression of the top 500 most variable genes in the indicated cell types. PGCLCs were sorted by SSEA1 and CD61 and further divided into XGFP+ and XGFP-. Axes indicate the variance. Arrow indicates hypothetical trajectory. Shapes indicate the clone (A11 = square, E9 = rhombus) **(b)** Plot showing the 10 top genes contributing positively negatively to the first principal component shown in (a). Genes in blue are located on the X chromosome. **(c)** PCA of gene expression of the top 500 most variable genes excluding X chromosomal genes, in the indicated cell types.. Axes indicate the variance. Arrow indicates hypothetical trajectory. Shapes indicate the clones (A11 = square, E9 = rhombus) **(d)** Heatmap of gene expression of 33 manually selected genes belonging to the category reported in the boxes. **(e)** PCA of gene expression compared to *in vivo* samples, taken from Nagaoka et al. 2020, showing the top 500 most variable genes. Shape indicates the clone (A11 = square, E9 = rhombus, circle = Nagaoka et al.) **(f)** MAplot of differential gene expression changes between PGCLC XGFP- and PGCLC XGFP+ as determined by RNA-seq. Log2-mean expression (log2-normalized counts from DESeq2) on the x axis and the log2-fold change on the y axis. Significantly upregulated and downregulated genes are highlighted in red and green respectively. False Discovery Rate (FDR) < 0.001. Non-significant genes between 0 and absolute 0.2 were removed for easier plot visualization. **(g)** Selected GO terms enriched in PGCLC XGFP- and XGFP+.

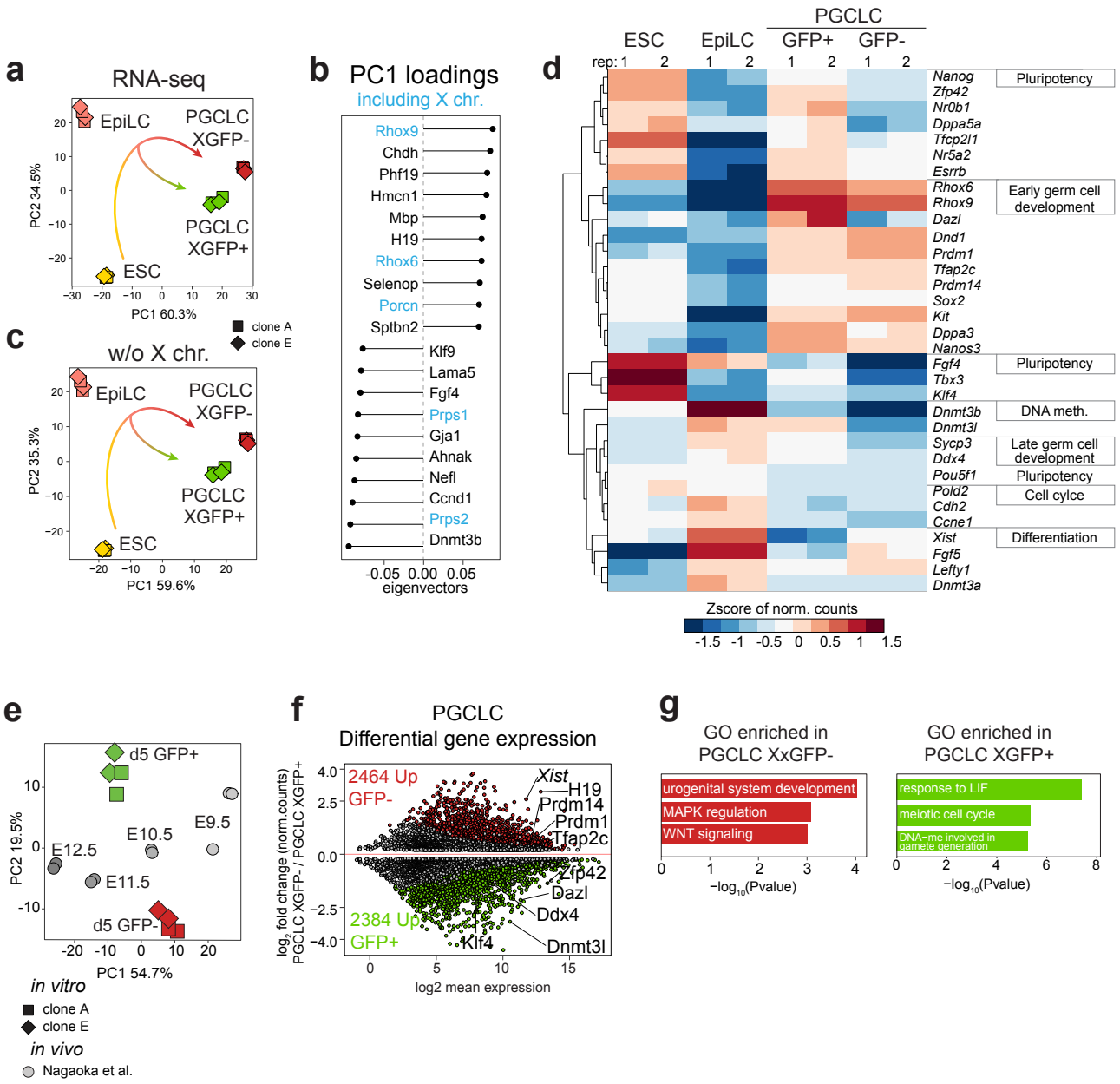
a
RNA-seq
EpiLC
PGCLC XGFP-
PGCLC XGFP+
ESC
PC2 34.5%
PC1 60.3%
clone A
clone E
b
PC1 loadings
including X chr.
Rhox9
Chdh
Phf19
Hmcn1
Mbp
H19
Rhox6
Selenop
Porcn
Sptbn2
Klf9
Lama5
Fgf4
Prps1
Gja1
Ahnak
Nefl
Ccnd1
Prps2
Dnmt3b
-0.05 0.00 0.05
eigenvectors
c
w/o X chr.
PC2 35.3%
PC1 59.6%
d
ESC
EpiLC
PGCLC
GFP+
GFP-
rep: 1 2 1 2 1 2 1 2
Nanog
Zfp42
Nr0b1
Dppa5a
Tfcp2l1
Nr5a2
Esrrb
Pluripotency
Rhox6
Rhox9
Dazl
Dnd1
Prdm1
Tfap2c
Prdm14
Sox2
Kit
Dppa3
Nanos3
Early germ cell development
Fgf4
Tbx3
Klf4
Pluripotency
Dnmt3b
Dnmt3l
DNA meth.
Sycp3
Ddx4
Late germ cell development
Pou5f1
Pluripotency
Pold2
Cdh2
Ccne1
Cell cylce
Xist
Fgf5
Lefty1
Dnmt3a
Differentiation
Zscore of norm. counts
-1.5 -1 -0.5 0 0.5 1 1.5
e
d5 GFP+
E9.5
E10.5
E12.5
E11.5
d5 GFP-
PC2 19.5%
PC1 54.7%
in vitro
clone A
clone E
in vivo
Nagaoka et al.
f
PGCLC
Differential gene expression
2464 Up
GFP-
2384 Up
GFP+
Xist
H19
Prdm14
Prdm1
Tfap2c
Zfp42
Dazl
Ddx4
Klf4
Dnmt3l
log2 fold change (norm.counts)
PGCLC XGFP- / PGCLC XGFP+
log2 mean expression
g
GO enriched in
PGCLC XxGFP-
urogenital system development
MAPK regulation
WNT signaling
−log10(Pvalue)
GO enriched in
PGCLC XGFP+
response to LIF
meiotic cell cycle
DNA−me involved in gamete generation
−log10(Pvalue)

Gradual X-inactivation throughout PGCLC induction

Allele-specific X-inactivation analysis

A prominent epigenetic feature during mouse early development is the establishment and maintenance of X-inactivation in the epiblast after implantation (Payer 2016). X-inactivation represents a powerful model to study the formation of facultative heterochromatin where multiple layers of chromatin modifications act together to enable stable transcriptional silencing. Thanks to our cell line harboring a completely hybrid X chromosome (as well as chromosome 13), we can utilize allele-specific RNA-seq to describe chromosome-wide gene expression dynamics of X-linked genes during X-inactivation. We utilized an in-house customized pipeline to measure the transcripts from the X^{mus} and X^{cas} allele and calculated an allelic ratio (see methods). To define a trajectory from X active to X inactive during the PGCLC specification time course, we performed PCA of the allelic ratio of our samples with additional Neural Progenitor Cell samples from (Bauer et al. 2020) to include in the analysis a cell type reported to be fully X inactive. We observed a clear clustering of the samples according to the X activity status on the PC1 with ESCs bearing two active X chromosomes clustering the furthest away from NPCs, bearing a fully inactivated X chromosome. Of notice, we observed that EpiLCs were at an intermediate position (Fig. 3a).

To have an overview of the distribution of the allelic ratio of X-linked genes that passed our quality control criteria (see RNA-seq analysis methods), we plotted the allelic ratio of ESCs and defined a range of biallelic genes (allelic expression ratio >0.3 and <0.7), resulting in 294 genes (Fig. 3b). The definition of this window of biallelically expressed genes will help avoid a skewing of the X-inactivation analysis and the future downstream analysis of X-reactivation. Once we selected the 294 biallelically expressed genes, we needed to establish a threshold of X-inactivation to be able to distinguish genes undergoing X-inactivation from non-inactivating genes. We therefore plotted the distribution of the allelic ratio of the previously selected 294 genes, this time in the NPCs samples (Fig. 3c). The reasoning behind choosing NPCs was to set the X-inactivation threshold using a sample with complete X-inactivation, as the allele specific PCA indicated that PGCLC XGFP- harbor an incomplete X-inactivation phenotype compared to NPCs. We decided to establish an X-inactivation cutoff at 0.135, representing the allelic ratio value corresponding to the first dip in the genes

distribution. Genes with allelic ratio < 0.135 were considered to have fully undergone X-inactivation, while genes with an allelic ratio > 0.135 were considered to still be active.

To understand the extent of X-inactivation in terms of number of inactive genes across our samples, we plotted the allelic ratio of all our selected genes. As expected, ESCs did not show inactive genes and only 5 genes in the PGCLC XGFP+ (*Mbnl3*, *Bex4*, *Tsc22d3*, *Tceal8*, *Timm8a1*) were inactivated. On the other hand, EpiLCs showed 63 inactive genes and PGCLCs GFP- showed 198 genes out of 294 being inactive. These results indicated that X inactivation at the gene level is initiated in EpiLCs and reinforced only later during PGCLCs (Fig. 3d). This is in line with published genome-wide *in vivo* data which reports that E6.5 post implantation epiblast cells are a mixture of cells that have and have not completed X-inactivation, pointing to significant asynchrony in X-inactivation among epiblast cells (Cheng et al. 2019).

It has been previously reported that Xist RNA upregulation and spreading is a key event in the initiation of X-inactivation (Borsani et al. 1991; Brockdorff et al. 1991; Penny et al. 1996). We therefore wanted to assess whether the upregulation of *Xist* expression would reflect the initiation of X chromosome inactivation and to which degree it would accompany PGCLCs differentiation. We observed high levels of *Xist* expression in EpiLCs, reaching levels comparable to those of X inactive control samples NPCs. Interestingly, PGCLC XGFP-, despite displaying the lowest XGFP reporter intensity, showed a decrease in levels of *Xist* expression, which might be explained by the dox induced overexpression of the TF *Prdm14*, a known repressor of *Xist* (Payer et al. 2013) (Fig. 3e).

Figure 3. Characterization of X-inactivation dynamics during PGCLC induction.
(a) PCA of X chromosome allelic ratio (see methods) for 334 X-linked genes. Axes indicate the variance. Shapes indicate the clones (A11 = square, E9 = rhombus, circle = neural progenitors cells (NPC) from Bauer et al.) **(b)** Distribution of the allelic ratio in ESCs. Dashed lines indicate a biallelic expression window from 0.3 to 0.7 **(c)** Distribution of the allelic ratio in NPCs. Dashed line represents allelic ratio of 0.135 used as a threshold for X-inactivation. Genes below the threshold are considered X-inactive. **(d)** Boxplots of allelic ratio (n = 294). Upper dashed line indicates the biallelic ratio of 0.5, lower dashed line indicates X-inactivation threshold of 0.13. **(e)** $Xist^{mus}$ expression (see methods). NPCs from Bauer et al. Barplot indicates the mean value. **(f)** Circos plot showing allelic ratio for selected X-linked genes (n = 295). Outer (1), middle (2) and inner (3) circles represent ESCs, EpiLCs and PGCLC XGFP-, respectively. Dotted box highlights clusters of genes active in all three time points, solid box highlights clusters of genes already undergoing X-inactivation in EpiLCs. (**g**-**i**) Violin plots quantifying **(g)** gene density, **(h)** linear distance from the transcription start site (TSS) of the *Xist* gene to the TSS of the other X-linked genes. **(i)** X^{mus} gene expression levels in ESCs. Solid black line indicates the median. *P* values from a two-sided Mann-Whitney U test are shown. On the right, Pearson correlation coefficient (r) was calculated to indicate the correlation between ESC expression and EpiLC (salmon dots) or PGCLC (red dots). **(j)** Boxplots for allelic ratio of X-linked genes contained in A and B compartment as defined in ESC in Bauer et al.. Dashed lines indicate biallelic ratio and X-inactivation threshold, respectively. *P*values from a two-sided Mann-Whitney U test are shown. The upper, centre, and lower line of the boxplots indicate 75%, 50%, and 25% quantile, respectively. Whiskers extend to the most extreme data point within 1.5-times the interquartile range.

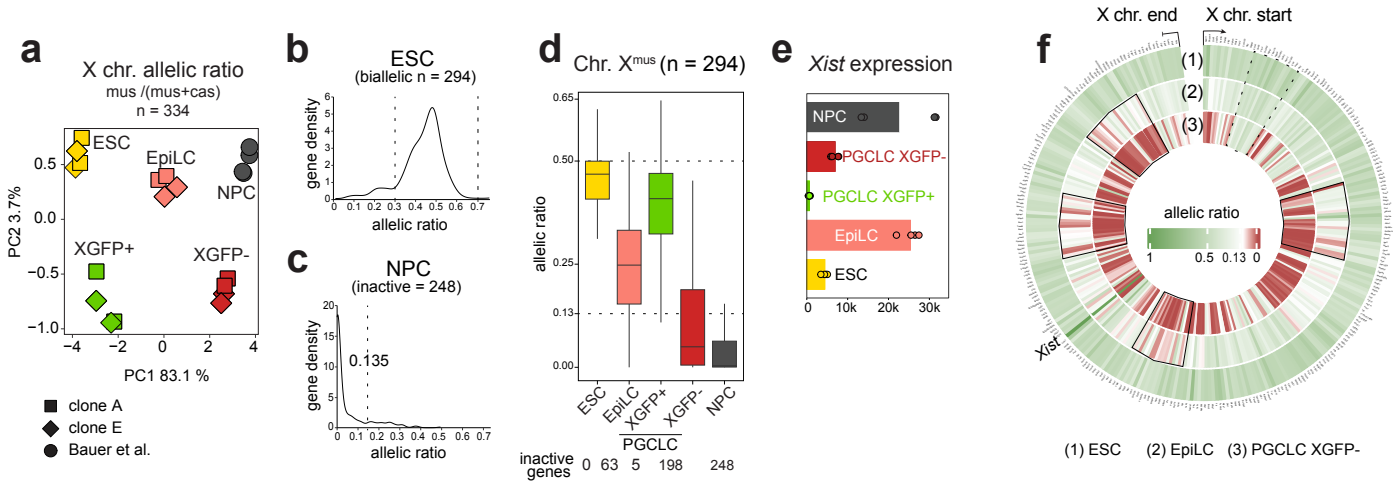
a
X chr. allelic ratio
mus /(mus+cas)
n = 334
ESC
EpiLC
NPC
XGFP+
XGFP-
PC2 3.7%
PC1 83.1 %
clone A
clone E
Bauer et al.
b
ESC
(biallelic n = 294)
gene density
allelic ratio
c
NPC
(inactive = 248)
0.135
d
Chr. Xmus (n = 294)
allelic ratio
inactive genes
0 63 5 198 248
PGCLC
e
Xist expression
PGCLC XGFP-
PGCLC XGFP+
f
X chr. end
X chr. start
allelic ratio
Xist
(1) ESC (2) EpiLC (3) PGCLC XGFP-

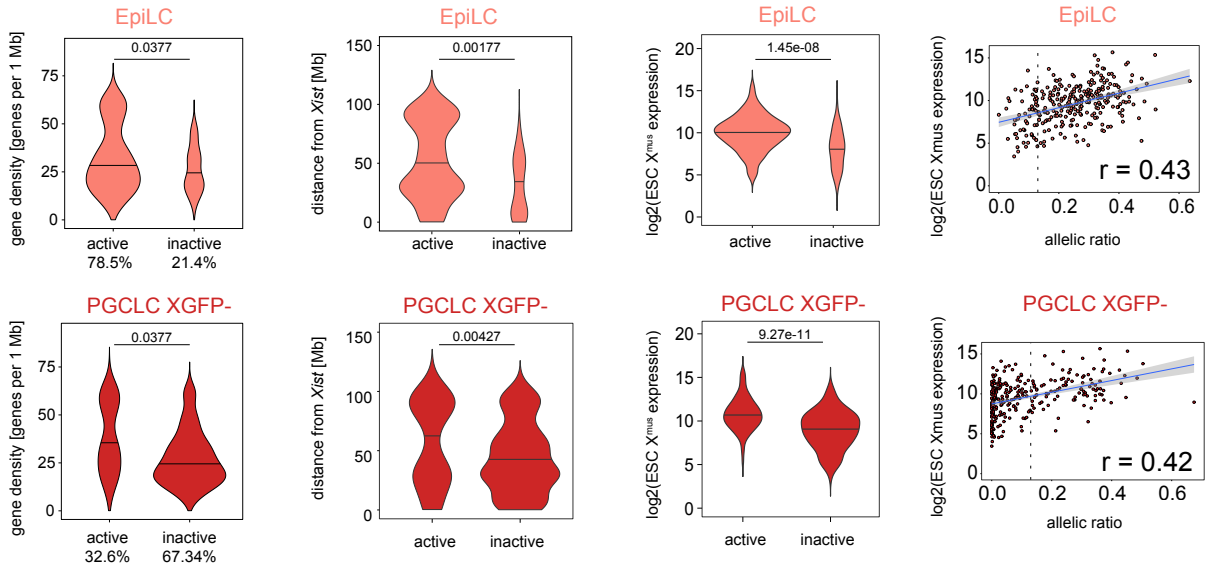
g
Gene density
EpiLC
gene density [genes per 1 Mb]
0.0377
active
inactive
78.5%
21.4%
PGCLC XGFP-
0.0377
32.6%
67.34%
h
Linear distance from Xist
EpiLC
distance from Xist [Mb]
0.00177
PGCLC XGFP-
0.00427
i
ESC expression
EpiLC
log2(ESC Xmus expression)
1.45e-08
r = 0.43
allelic ratio
PGCLC XGFP-
9.27e-11
r = 0.42

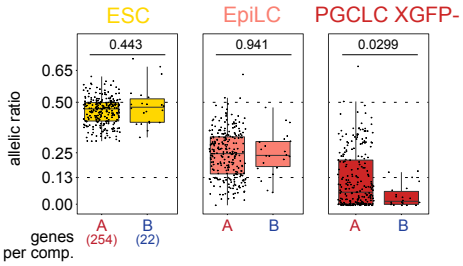
j
ESC A B compartments
ESC
EpiLC
PGCLC XGFP-
allelic ratio
0.443
0.941
0.0299
genes per comp.
A (254)
B (22)

Features associated with X-inactivation in EpiLCs and PGCLCs XGFP-

Previous studies have demonstrated the association of various genomic, epigenomic and three-dimensional genome architecture features to X-inactivation kinetics (Engreitz et al. 2013; Simon et al. 2013; Marks et al. 2015; Borensztein et al. 2017; L. B. de A. e. Sousa et al. 2019; Żylicz et al. 2019). We were also interested in finding out putative features that would possibly predict in our system the preference of certain genes to undergo X-inactivation or not. As the inactive genes in EpiLCs maintained an inactive state in PGCLCs XGFP- (except *Mageel*), we wanted to assess whether genes to be inactivated first clustered together or were located randomly along the X chromosome. We generated a heatmap of the allelic ratio and ordered genes according to their location on the X chromosome. We observed that the first genes to be inactivated were not completely interspersed along the X chromosome but rather clustered in a few restricted regions.

Since we observed that EpiLCs X-inactivation initiated within clusters of genes in close proximity, we wanted to know whether differences in gene density could explain X-inactivation timing. While we observed a trend for early inactivating genes to be located in gene poor regions, a considerable number of inactive genes in PGCLCs were found in gene rich regions as well, excluding gene density as a sole determining factor for X-inactivation kinetics (Fig. 3g).

As the inactive X chromosome is coated by Xist and it has been previously shown that Xist initially binds to chromatin sites in close proximity that can be distal to its endogenous locus (Simon et al. 2013; Engreitz et al. 2013), we wanted to assess whether the linear distance from the *Xist* locus could be a defining feature of X-inactivation. We calculated the distance from *Xist* TSS and we found a slight correlation of inactive genes being situated significantly closer to *Xist*, compared to active genes. However, inactive genes in PGCLCs XGFP- were also found far away from *Xist*, discarding the linear distance from *Xist* as the main component driving X-inactivation (Fig. 3h).

We next set out to investigate whether the starting levels of X^{mus} gene expression in ESCs, could be a possible feature influencing the timing of X-inactivation. We found a significant correlation between genes having a higher ESC X^{mus} expression and the persistence of an active X-status (Fig.3i). We then calculated the Pearson correlation and found a significant positive correlation between the expression in ESC and the

allelic ratio, suggesting that the silencing process might take longer if a gene is highly expressed (Fig. 3i).

After having analyzed major linear genomic aspects that were reported to be influential in predetermining X-inactivation choice, we set out to assess whether the 3D architecture could explain X-inactivation kinetics observed in our system. It is known that chromosomes are spatially segregated into two compartments: a euchromatic gene dense A compartment and an heterochromatic gene poor B compartment (Lieberman-Aiden et al. 2009). Furthermore, it has been reported that Xist RNA spreads initially through the A compartment where the *Xist* locus itself is located (Wang et al. 2018). We therefore incorporated recently published Hi-C datasets from the same parental cell line (Bauer et al. 2020) to assess how compartmentalization might influence X-inactivation kinetics. We could not detect a significantly higher X-inactive status in the A compartment compared to the B compartment, suggesting that the 3D organization of the X chromosome does not impact the inactivation dynamics (Fig. 3j). Of important note, the A compartment is considerably more gene dense than B. Therefore, the scarce number of genes localized in the B compartment makes it difficult to draw conclusions.

Taken together, our results indicate that we could not identify a unique feature dictating X-inactivation, besides the ESCs X^{mus} expression, in neither EpiLCs nor in PGCLCs suggesting that our phenotype might be the result of a combination of multiple traits.

Exploring the kinetics of X-reactivation and meiosis in PGCLCs

Up to date, the investigation of X-linked gene activity at the scale of the entire X chromosome during PGCs differentiation has been quite scarce. Several questions remain open (i) what was the X-status preceding X-reactivation, was it partly or fully inactivated? (ii) how does X-reactivation occur genome-wide? (iii) is X-reactivation linked with germ cell maturation and meiotic entry? Shedding light on those open questions will be fundamental for understanding the extent of the plasticity of X-reactivation in PGCs.

In our previous analysis, we have observed that *in vitro* derived PGCLCs exist either with two active X-chromosomes (PGCLCs XGFP+) or with one inactivated X-chromosome (PGCLCs XGFP-). We wanted to assess whether X-inactivation undergone by the PGCLCs XGFP- was necessary for germ cell maturation and finally if the X-reactivation status and the developmental stage could be related.

To determine the X-reactivation kinetics during *in vitro* PGCLC reprogramming we combined an adapted version of the *in vitro* reconstituted Ovary (rOvary) protocol (Katsuhiko Hayashi and Saitou 2013) with the novel single cell RNA-seq protocol Smart-seq v5 (unpublished). Briefly, we aggregated *in vitro* derived PGCLCs (both XGFP+ and XGFP-) for 6 days with somatic cells isolated from E13.5 female embryonic gonads + mesonephros in order to mimic the urogenital environment and then we sorted single cells and performed scRNA-seq. We obtained as total output, 391 million reads, meaning an average of 740 k reads per cell (data not available yet).

As shown in Fig. 4b, both PGCLCs XGFP- and PGCLCs XGFP+ could aggregate with E13.5 somatic gonadal cells and, in the case of PGCLCs XGFP-, cells reactivated the XGFP transgene. Of notice, the rOvary obtained from PGCLCs XGFP+ was slightly bigger in size and contained more Xtomato+ cells, indicating a higher proliferation rate of PGCLCs XGFP+ compared to the PGCLCs XGFP-.

As our aggregation protocol is a variation of previously published ones, we first wanted to confirm that our *in vitro* derived PGCLCs could mature and enter meiosis upon aggregation, as reported in the original protocols. Therefore, after the formation of the rOvary at d5, we performed immunostaining of cryosections and stained for the advanced germ cell marker DAZL, for the meiotic marker SYCP3 and XGFP. We noticed that the rOvary from PGCLC XGFP- contained the expected DAZL+/SYCP3+/GFP+ cells and few DAZL+/SYCP3+/XGFP- cells. In contrary, the

rOvary derived from PGCLCs XGFP+ contained only 2 meiotic cells, suggesting a severe impairment of PGCLCs XGFP+ to enter meiosis (Fig. 3c).

Having ascertained by immunostaining that our rOvaries have the ability to properly develop, we generated a dataset composed of the following single-cells. Derived from the PGCLC XGFP- rOvary, we collected the following populations: (1) XTomato+/XGFP+: X-reactivated, 144 cells (2) XTomato+/XGFP~:X-intermediate, 144 cells (3) XTomato/XGFP+:X-constitutively-inactive, 136 cells. From the PGCLC XGFP+ rOvary we collected: (4) XTomato+/XGFP+: X-constitutively-active, 188 cells. As control for the downstream allelic analysis we sorted 24 single ESCs. We observed that in the PGCLCs XGFP- rOvary, the majority of the cells belonged to the category "X-constitutively-inactive" (~40%), indicating that almost half of the PGCLCs did not undergo X-reactivation, while ~20% of germ cells belonged to the "X-reactivated" category and 18% to the "X-intermediate" category. For the PGCLC XGFP+ rOvary, as expected, we found ~86% of the germ cells stayed active (Fig. 3d).

By examining single PGCLCs from the different categories, representing pseudo developmental time points (Fig. 3e), we will be able to define candidate early X-reactivated genes and late X-reactivating genes. Their kinetics of reactivation will be eventually compared to the behaviour during X-reactivation in the ICM and will be correlated with important genetic and epigenetic features (ex. genomic location, local epigenetic landscapes, 3D architectural traits). Currently, the bioinformatic analysis of the samples is ongoing.

Figure 4. Set up of Single-cell RNA-seq of maturing germ cells using the rOvary system
(a) Schematic illustration of the single-cell RNA-seq experiment and the isolated populations during germ cell maturation in rOvaries. The first 24h of culture are indicated as d0. rOvary = reconstituted Ovary, d = day of rOvary culture, X react. = X-reactivated, X interm. = X-intermediate, X const. active = X constitutively active, X const. inactive = X constitutively active. **(b)** Imaging of XGFP and XTomato X-reporters in rOvary d5 aggregated with E13.5 goandal and mesonephric cells. Scale bars = 50µm. BF = bright field. **(c)** Expression of DAZL (red), SYCP3 (cyan) and XGFP (green) in rOvaries cryosections. Cells were counterstained with DAPI (gray). White dashed lines indicate XGFP- cells in SYCP3+ cells. Scale bars = 10 µm. **(d)** FACS gating strategy for single-cell sorted XTomato+ cells against XGFP intensities. Numbers indicate the percentage of gated cells over the total population. Numbers in brackets indicate the percentage of gated cells over the XTomato+ population. **(e)** Schematic representation of an anticipated result from the dimensionality reduction of the to be obtained scRNA-seq dataset.

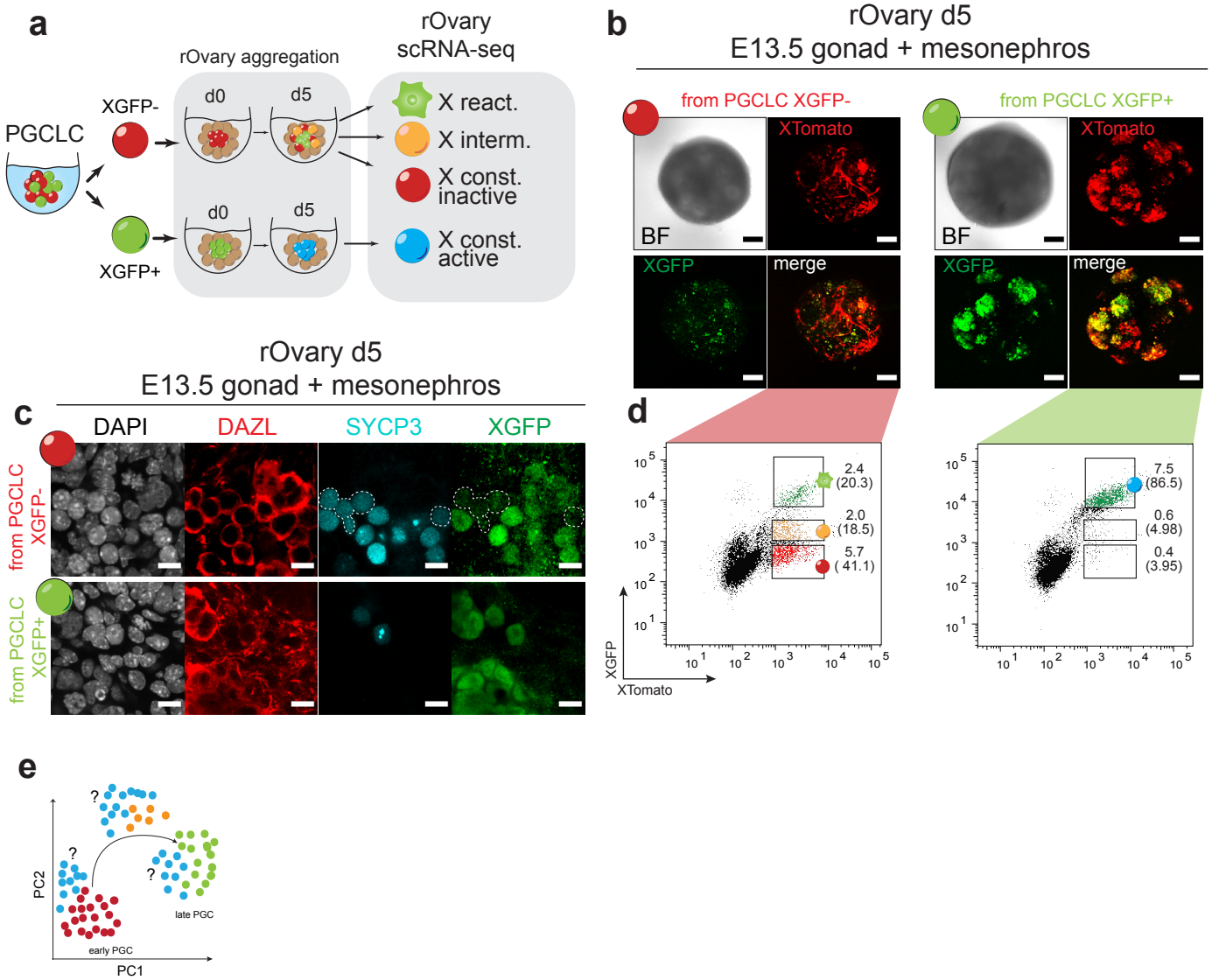
a
rOvary aggregation
rOvary scRNA-seq
PGCLC
XGFP-
XGFP+
d0
d5
d0
d5
X react.
X interm.
X const. inactive
X const. active
b
rOvary d5
E13.5 gonad + mesonephros
from PGCLC XGFP-
from PGCLC XGFP+
XTomato
XTomato
BF
BF
XGFP
merge
XGFP
merge
c
rOvary d5
E13.5 gonad + mesonephros
DAPI
DAZL
SYCP3
XGFP
from PGCLC XGFP-
from PGCLC XGFP+
d
2.4 (20.3)
2.0 (18.5)
5.7 (41.1)
7.5 (86.5)
0.6 (4.98)
0.4 (3.95)
XGFP
XTomato
e
PC2
PC1
early PGC
late PGC
?
?
?

Low competency of X-active PGCLCs to enter meiosis

Due to the scarcity of *in vivo* material and the lack of appropriate *in vitro* systems, a detailed study on the interplay between X chromosome status and primordial germ cells developmental competence is still lacking. Nevertheless, the recent advances in germ cell culture reported a 2D system completely *in vitro* to expand PGCLCs and complete prophase I of meiosis via the addition of signaling molecules BMP2 and retinoic acid (H. Ohta et al. 2017; Miyauchi, Ohta, and Saitou 2018). We utilized this recently published protocol in combination with our tailor made *XRep* cell line in order to clarify the following observations: (i) confirm our previous observation by immunostainings of rOvaries showing that PGCLCs XGFP- were able to enter meiosis more efficiently than PGCLCs XGFP+ and (ii) identify the timing of X-reactivation.

To confirm our first observation, we cultured PGCLCs XGFP+ and PGCLCs XGFP- separately, on m220 feeders (see methods) to monitor differences in proliferation. As we previously observed, after 5 days of culture, PGCLCs XGFP+ had a proliferative advantage and expanded in big, flat colonies, while PGCLCs XGFP- formed smaller colonies (Fig. 5b). However, despite the higher proliferation rate, the absolute numbers of SYCP3+ cells counted every 48h after meiotic induction were significantly higher in the expanding PGCLCs XGFP- (Fig. 5b). These results support our previous observation in the rOvary system.

The precise coordination and timing between X-reactivation and meiotic prophase I still remains elusive. We, therefore, set out to determine whether meiotic germ cells would also already show X-reactivation. We again expanded and induced meiosis from PGCLCs XGFP+ and PGCLCs XGFP-. The resulting few meiotic cells originating from PGCLCs XGFP+ were, as expected, still 100% XGFP+ indicating that the X stayed active. The meiotic SYCP3+ cells originating from PGCLCs XGFP- were also almost 100% GFP+ indicating X-reactivation. These results suggest that X-reactivation occurs concomitantly with meiotic entry (Fig. 5e).

After having concluded that meiotic entry was possible, but with clear different efficiencies, for both germ cells originating from PGCLCs XGFP+ which stayed active during meiosis initiation and PGCLCs XGFP-, that X-reactivated while entering meiosis, we wondered whether the extent of prophase I progression would be different. We prepared chromosomal spreads from expansion culture c9 and stained for SYCP3, characterized by a distinctive shape according to the prophase stage. Moreover, to

help the correct recognition of the different phases, we stained for the double strand breaks marker phosphorylated form of histone variant H2AX (gammaH2AX) (Mahadevaiah et al. 2001). While the zygotene and pachytene stages were easily identifiable, the former characterized by the typical 40 unpaired chromosome homologues and the presence of gammaH2AX and the latter by 20 paired homologous and the disappearance of gammaH2AX, we struggled to identify cells at the diplotene stage, due to the more unstructured aspect of chromosomes undergoing crossover (Fig. 5f). Moreover, this experiment was performed only once and very few cells appeared to be in the pachytene stage (Fig. 5g). To conclude, we could not answer the question about meiotic progression due to the lack of both replication of the experiment and expertise in prophase I phase recognition.

Until today, the m220 expansion protocol has only allowed the maturation of germ cells until prophase I. Only one protocol has successfully shown the development of *in vitro* PGCLCs beyond prophaseI and into primary follicles (Katsuhiko Hayashi and Saitou 2013). This protocol requires the aggregation with *ex vivo* derived somatic gonadal cells forming a rOvary followed by the culture of the rOvary onto a transwell to allow *in vitro* differentiation (IVDi) of PGCLCs. Once we observed that PGCLCs XGFP- could enter meiosis more efficiently than the XGFP+ and could finish prophase I, we wanted to confirm whether those cells could continue the developmental route and generate primary oocytes. To test this, we collaborated with the Hayashi lab (Kyushu University), who kindly sent isolated somatic gonadal cells. We were able to perform 1 single IVDi tissue with slight modifications of the protocol: (i) to measure the extent of X-reactivation in a more physiological niche, without external cues, no retinoic acid was added to the IVDi culture (ii) the IVDi tissue was cultured for 11 days instead of 21 days, to avoid the risk of cell death considering that the following step required for secondary follicle maturation would have been extremely delicate and challenging. We then stained the entire whole-mount tissue for DAZL, XGFP and SYCP3 to identify X-reactivating (XGFP+), meiotic (SYCP3+), mature germ cells (DAZL+) and quantified the number of prophase I cells and the number of those that reached the primordial oocyte stage. We obtained ~36 SYCP3+ primordial oocytes per tissue and ~200 SYCP3+ prophase I germ cells. When assessing XGFP staining, as previously observed in the m220 expansion system, the majority of SYCP3+ cells were also XGFP+. However, to our surprise, the localization of the XGFP protein in the primordial

oocytes while still detectable, seemed to have been relocalized from the nucleus to the cytoplasm (Fig. 5h).

Figure 5. Interplay between X-reactivation and meiotic entry using m220 system
(a) Schematic representation of the PGCLC expansion system on m220 feeders. c = m220 culture day. Orange arrow indicates the meiotic induction period. **(b)** Imaging of XTomato reporter in the indicated samples. Figures indicate representative images of the experiment. Scale bars = 1000 μm. **(c)** Representative images for the expression of XGFP (green) and SYCP3 (red) in germ cells at c5, c7 and c9 coming from the indicated PGCLC conditions. Cells were counterstained with DAPI (gray). Scale bars = 10 μm. **(d)** Number of SYCP3+ cells per m220 culture day originating from the indicated PGCLC conditions. Each white dot represents an independent experiment (n=3). Y axis is in square root scale. *P* values shown are from a two-sided Mann-Whitney U test. n.s. = not significant. **(e)** Percentage of XGFP+ cells among SYCP3+ cells at the indicated m220 culture day, originating from the indicated PGCLC conditions. Green lines represent X-reactivation. Each white dot is an independent experiment (n=3). **(f)** Representative images showing the substages of meiotic prophase I in c9 cultured germ cells from the indicated PGCLC conditions. C9 germ cells were spread and immunostained for SYCP3 (red), and γH2AX (gray). A question mark (?) indicates the non-identifiable stages. Scale bar = 10 μm. **(g)** Percentages of meiotic stages at culture day c9, from the indicated PGCLC conditions. L, leptotene; Z, zygotene; P, pachytene; D, diplotene. (n=1). **(h)** Immunofluorescence images of GFP (green), SYCP3 (red), DAZL (yellow) and DAPI at Agg11 of IVDi tissue. IVDi = in vitro differentiation. White squares indicate the positions of zoomed-in section shown below. Top panel scale bar = 100 μm. Lower panel scale bar = 10 μm. (n=1). Quantification shown on the right.

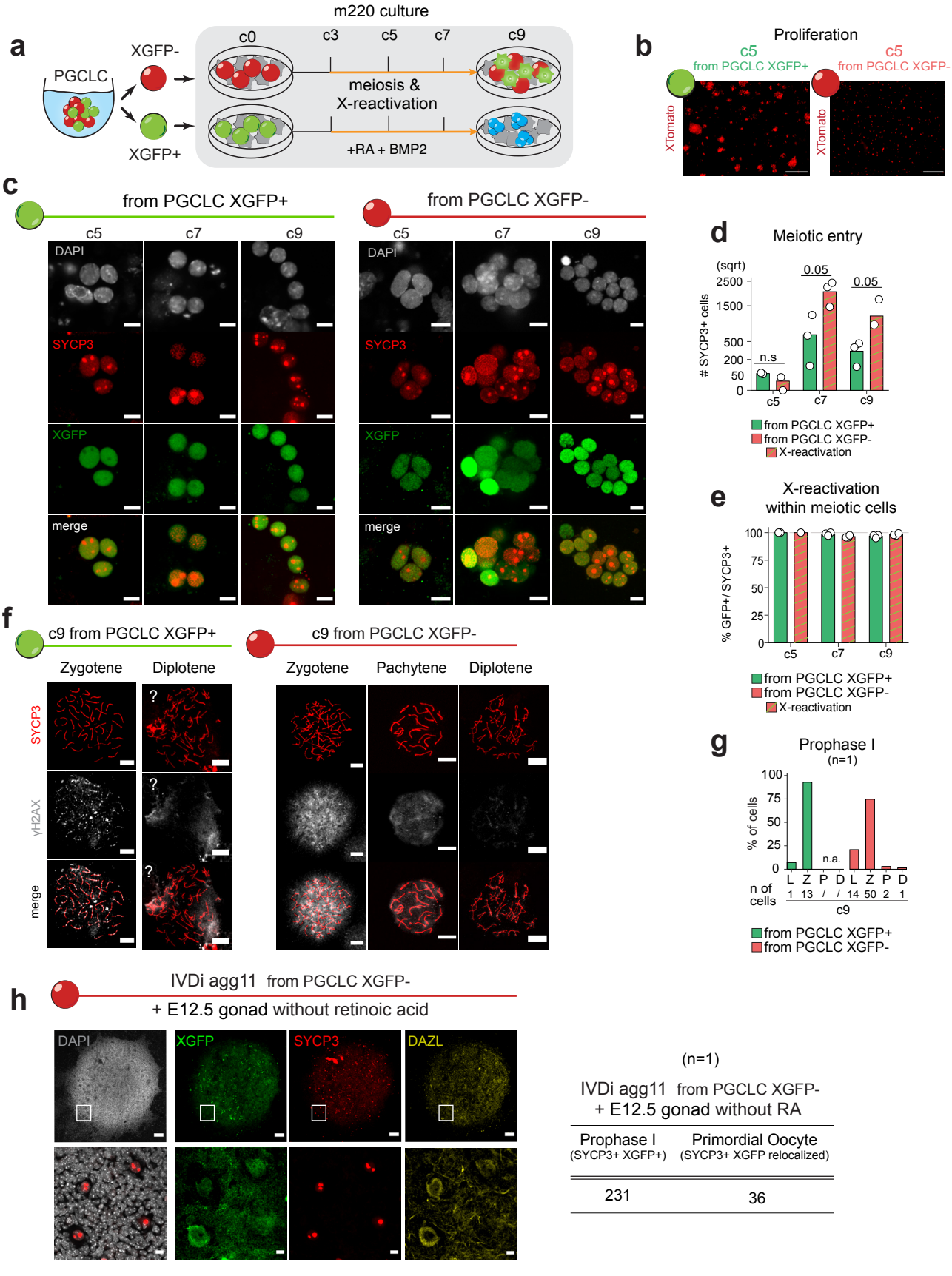

(n=1)

IVDi agg11 from PGCLC XGFP-
+ E12.5 gonad without RA

Prophase I (SYCP3+ XGFP+)	Primordial Oocyte (SYCP3+ XGFP relocalized)
231	36

Signalling pathways involved in X-reactivation and meiosis

After the specification of germ cell fate, *in vivo* PGCs migrate towards the gonads and differentiate in a sex-dependent manner in response to signals from the somatic niche (see Introduction). As presented in the results above, the signals between germ cells and the surrounding somatic cells are, to date, known to be necessary for the complete development of *in vitro* PGCLCs into oocytes. However, the difficulty in analyzing the complex interactions between germ cells and somatic gonadal cells have impaired the investigation of which signals and mechanisms are driving two prominent events in germ cells development: epigenetic reprogramming regulating X-reactivation and meiotic entry.

First, we wanted to assess whether the signals driving X-reactivation and meiosis are shared. Therefore, we cultured PGCLCs XGFP- in 3 different conditions, without retinoic acid to exclude external signals: (i) with somatic gonadal cells from E12.5 female embryos (ii) with mesonephric cells from E12.5 female embryos (iii) and with a combination of both gonadal and mesonephric cells. When observing the *Xrep* reporter signals, we observed that the condition including only the mesonephric cells was the condition with the highest X-reactivation by XGFP transgene re-expression. The reactivated cells appeared concentrated in defined regions suggesting an increased proliferation of those cells (Fig. 6a.ii)

Once we assessed that the signals from the mesonephros were sufficient for X-reactivation, we set out to determine whether the X-reactivated cells had undergone meiosis. We performed immunostaining of cryosections for DAZL, SYCP3 and XGFP and could not identify germ cells in the aggregate formed solely with mesonephric cells (Fig. 5c) while in the aggregates where the gonadal cells were present could successfully enter meiosis. Moreover, most of the meiotic cells were also X-reactivated. Taken together these results indicate that on the one hand, the mesonephros is releasing signals that can push a non-germ cell type into X-reactivation at the expense of meiotic entry. On the other hand, the gonadal niche signals are required for meiotic entry but can be dispensable for X-reactivation.

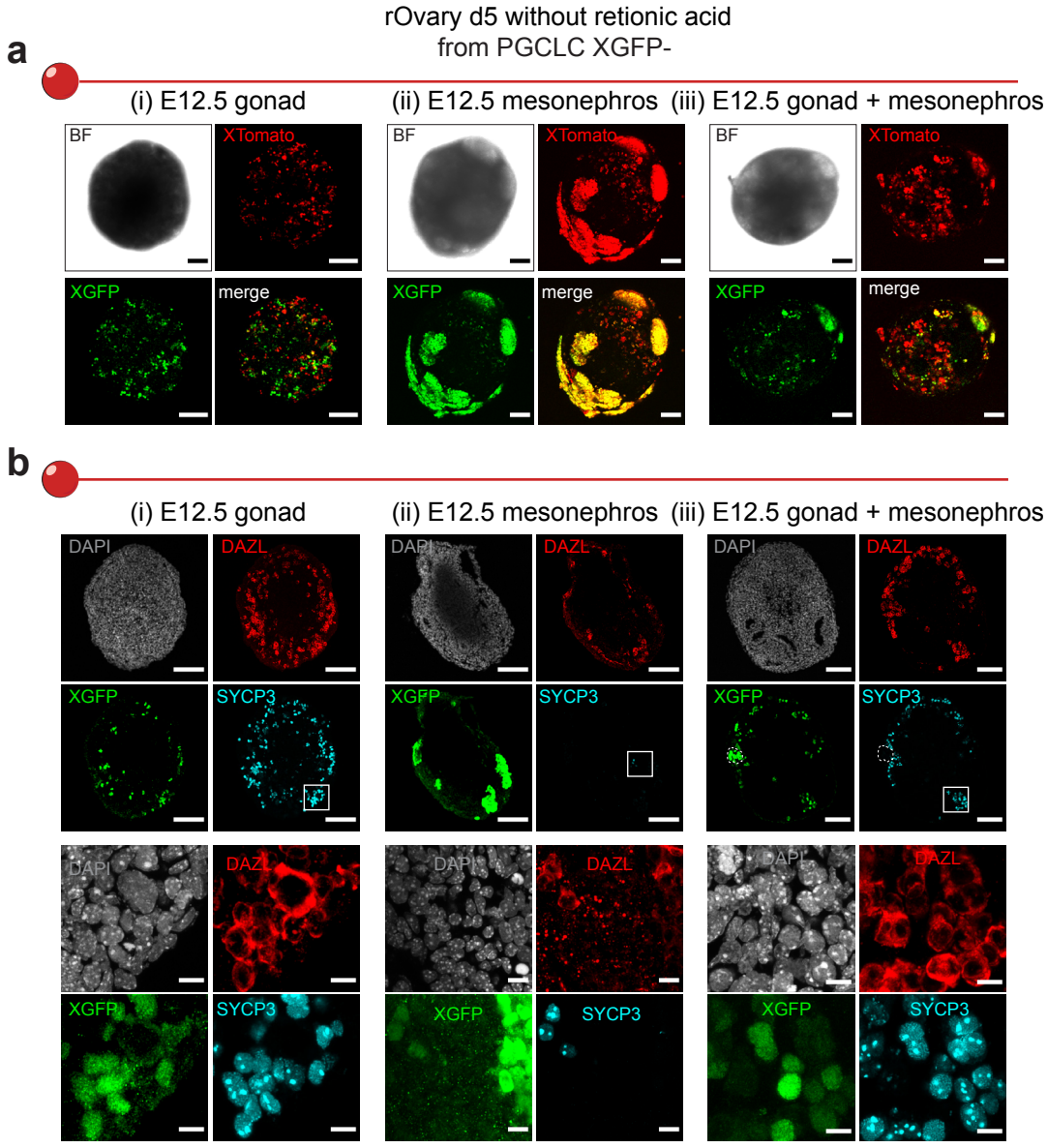

c

Meiotic cells SYCP3+
(n=1)

rOvary d5 without RA
from PGCLC XGFP-

gonad	meson.	gonad+ meson.
171	3	110

Figure 6. Uncoupling X-reactivation and meiosis
(a) Representative images of XGFP and XTomato reporters in the rOvaries aggregation day 5. Scale bar = 50 µm. BF = bright field. **(b)** Expression of DAZL (red), SYCP3 (cyan) and XGFP (green) in rOvaries cryosections. Cells were counterstained with DAPI (gray). White squares indicate the position of zoomed-in sections shown below. Full section scale bar = 100 µm, zoom section scale bar = 10 µm. **(c)** Table indicating the numbers of SYCP3+ cells per cryosection (n = 1). meson. = mesonephros.

DISCUSSION

PGCLCs come in two flavors: X-active and X-inactive

In this study, we describe a modified PGCLC induction protocol in combination with a tailor-made cell line for the induction of germ cells from ESCs with the aim of generating an *in vitro* model to study X-reactivation. Our adapted protocol first drives X-inactivation along ~10 days from the beginning of the induction, followed by the initiation of X-reactivation and meiosis. This approach allowed us to closely follow X-inactivation initiating in EpiLCs as they differentiate into PGCLCs, a process that was only poorly characterized.

Furthermore, as our protocol is based on the overexpression of germ cells specific transcription factors, there is no requirement for the addition of cytokines to recapitulate the germ cell fate. Whereas the majority of data available regarding *in vitro* PGCLC formation has been generated using the cytokine induction system (Hu et al. 2017; Hackett et al. 2018; Nagaoka et al. 2020; Hamada et al. 2020; Shimamoto et al. 2019), these studies were neither focusing on recapitulating the physiological X-status nor monitoring it and in fact, proved to be unsuitable to describe X-reactivation in PGCLCs. In our hands, the cytokine system did allow the expression of PGCLC surface markers but it impaired X-inactivation and led to a retention of the expression of naive pluripotency markers such as *Klf4* and a lack of upregulation of germ cell genes such as *Dnd1*. Two active X-chromosomes and the continuation of the pluripotency network have previously been related in ESCs culture systems (Schulz et al. 2014), however not in PGCLCs. Moreover, if the cytokines are affecting X-inactivation, they might potentially play a role in X-reactivation as well, opening up the opportunity to study the cytokine cocktail formed of BMP4, SCF, LIF and EGF as putative X-reactivation signals.

While we observed an increased number of X-inactive PGCLCs in our TF-based PGCLC induction system in combination with a prolonged period of EpiLC differentiation, we could still identify a minor population bearing two active X chromosomes in PGCLCs. This provided us with the opportunity to assess differences in terms of PGCLC X-status and gene expression, to ultimately relate X status and germ cell maturation. We found that X-active PGCLCs showed an aberrant expression

of late germ cells genes and meiotic genes. We could speculate that the genome-wide methylation levels of X-active PGCLCs were lower than those of X-inactive PGCLCs given that it is has been previously reported that genome-wide demethylation appears to trigger the transcription of late germ cell specific genes, such as *Ddx4*, *Dazl*, and *Sycp3 (Yanfeng Lin and Page 2005; Maatouk 2006; Toyooka et al. 2000)*.

X-inactivation reflects correct PGCLC specification

The first *in vivo* investigations regarding the X-status during epiblast development reported that by E6.5 all epiblast cells had undergone random X-inactivation (Rastan et al. 1980; Rastan 1982). However, a more complete *in vivo* study was missing. Recently, X dynamics *in vivo* have been ascertained during pre-gastrula development and revealed heterogeneity in the X-inactivation states (Mohammed et al. 2017) in contrast with the previously reported homogeneity. While previous studies have focussed on the X-status during epiblast development, little attention has been given to the dynamics of the X chromosome during the further transition of the epiblast into the germ cell lineage. The only available studies were performed *in vivo* and have been utilizing imagine techniques and small scale gene expression analysis (Chuva de Sousa Lopes et al. 2008; Sugimoto and Abe 2007).

We therefore wanted to assess X-linked gene activity at the scale of the entire X chromosome, during *in vitro* PGCLC differentiation. First, we wanted to initiate X-inactivation in EpiLCs. In all original protocols, EpiLCs were differentiated only for two days before PGCLC induction. Since it has been observed that female cells, carrying two X active chromosomes, take longer to exit pluripotency and therefore show a delay in differentiation (Schulz et al. 2014), it could explain the necessity to extend the duration of EpiLC differentiation from 2 to 4 days for the main X-inactivation markers to appear, while still allowing PGCLC specification.

In this study, we show that the EpiLC d4 we utilize to generate PGCLCS are heterogeneous: some EpiLCs bear an active X chromosome and naive pluripotency markers and one other portion starts to X inactivate, pointing to a significant asynchrony in X-inactivation among EpiLCs. Our findings are in line with *in vivo* single-cell datasets which describe the E6.5 epiblast as a heterogeneous tissue composed of cells that have completed random X-inactivation and cells that have not yet initiated X-inactivation. We therefore conclude that in our system PGCLC induction

initiates from a heterogeneous population of EpiLCs that has not completely undergone X-inactivation. However, genome-wide transcriptional profiling will be required for us to confirm the different identities of the EpiLC populations observed in our system.

As the X-inactivation route from EpiLCs continues into PGCLCs XGFP-, as expected, the number of inactive X-linked genes increased. Thanks to our system, we could explore the features defining the genes that did or did not X-inactivate. As presented in the results, the feature that appeared to be mainly influencing the timing of X-inactivation was the starting point of gene expression in ESCs. In addition, we found that while the X-inactivation machinery was inducing gene silencing, the levels of lncRNA *Xist* were unexpectedly not increasing. This could be due to the intrinsic robust pluripotency landscape that characterizes PGCLCs, which has been shown to completely suppress Xist expression (E. J. Sousa et al. 2018). Therefore, we could speculate that only regions that are either easily accessible or must be suppressed will be preferentially coated by Xist. Conversely, the genes that appear to have escaped X-inactivation, we could speculate that are either lagging behind in X-inactivation or that their repression has been prevented to allow further developmental processes.

X-inactivation followed by X-reactivation safeguards meiosis

The entry into meiotic prophase, together with the generation of offspring, are the gold standards to evaluate proper *in vitro* germ cell formation. Two *in vitro* methods currently exist to promote meiosis: one recreates the female gonadal niche using *in vivo* derived somatic gonadal cells, whereas the other relies on specialized stromal feeders and the addition of cytokines. We utilized both methodologies and induced meiosis from both X-active (XGFP+) and X-inactive (XGFP-) PGCLCs. We observed that when culturing PGCLCs using either method, XGFP- cells could enter meiosis more efficiently compared to XGFP+ cells. This difference in efficiency might be explained by the distinct transcriptional landscape of XGFP+ PGCLCs, characterized by the increased expression of late germ cell markers and meiotic genes. Taken together, these results indicate that XGFP+ PGCLCs are not *bona fide* germ cells but rather a byproduct of our culture system. This suggests that X-inactivation is essential for proper germ cell differentiation as by bypassing the X-inactivation step, cells might acquire an aberrantly advanced germ cell identity, which might be incompatible with the meiotic induction cues.

X-reactivation and meiosis: separated processes coordinated in time

Together with meiosis, X-reactivation is a hallmark of female PGC development and their associated global epigenetic reprogramming. It has been observed that by E14.5, *in vivo* PGCs have not completed X reactivation (Sugimoto and Abe 2007), while already having initiated meiosis. We have demonstrated that X-reactivation and meiosis occur concomitantly. In fact, our data shows extremely few X-inactive meiotic cells (<97%, which might rather be explained by X-loss). However, whether or not X-reactivation is a requirement for meiosis will need further mechanistic investigation.

It is widely believed that retinoic acid synthesized by the mesonephros and diffusing into the ovary, represents an essential paracrine trigger for meiotic entry (J. Bowles and Koopman 2007; Spiller and Bowles 2019). However, more recent findings showed that retinoic acid and its receptors can be dispensable for meiotic entry (Vernet et al. 2020; Chassot et al. 2020; Nagaoka et al. 2020).

In addition to these findings, we observed that upon aggregation of XGFP- PGCLCs with **mesonephric somatic cells**, PGCLCs could not enter meiosis, while maintaining their capability to reactivate the X and proliferate, possibly due to the lack of essential meiotic inducing cytokines from the gonadal niche. However, when aggregating PGCLCs with **gonadal cells only**, or with a combination of **gonadal cells and mesonephric cells,** we observed meiotic entry in both conditions. Nevertheless, while X-reactivation and meiosis were mostly observed together, the combination of mesonephric and gonadal cells created tubular structures and included a considerable amount of X-reactivated cells that did not undergo meiosis.

This indicates that the signals required for meiosis and X-reactivation are distinct.

Nevertheless, whether X-reactivation is directed by the mesonephric signals instructing a passive dilution of DNA methylation or whether PGCLCs had reverted to embryonic gonadal cells (EGCs) and therefore reprogrammed into an ES-like state, still remains unknown.

Furthermore, the excess of retinoic acid produced by the mesonephric cells, could create a supraphysiological concentration of retinoic acid, which has been recurrently emphasized to alter physiological processes (Mark, Ghyselinck, and Chambon 2009; Cunningham and Duester 2015), possibly causing the activation of a reprogramming cascade of PGCLCs into EGCs, compromising the oogenic programm. In agreement

with this, it has been previously reported *in vivo* that EGCs are able to reactivate the X. (Resnick et al. 1992; Stewart, Gadi, and Bhatt 1994).

Taken together, we observed that the different urogenital niches can provide distinct signals acting on proliferation, X-reactivation and meiosis, highlighting the complex and sensitive signaling network underlying germ cell maturation.

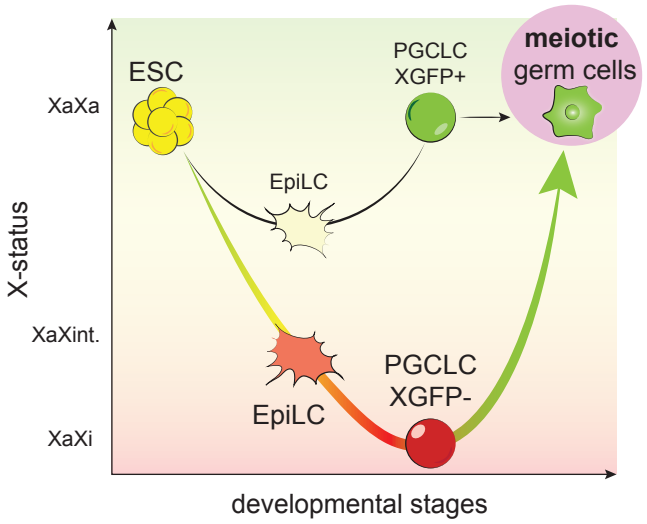

Figure Dis1. Working model of the interplay between X-status and germ cell specification
Graphical representation of the effects of X-status on germ cell developmental stages.

CONCLUSIONS

1. We created a tailor-made primordial germ cell-like cell induction system that facilitates the efficient generation of PGCLCs while simultaneously allowing the tracing of X chromosome dynamics during their specification.
2. PGCLCs are induced from a heterogeneous population of epiblast-like cells, with varying degrees of X-inactivation, which influences PGCLC differentiation downstream
3. While the majority of PGCLCs undergo X-inactivation, PGCLCs harboring two active X can be isolated.
4. However, even X-inactive PGCLCs do not undergo complete genic X-inactivation.
5. Maintenance of germ cell identity and meiotic potential is only preserved when PGCLCs undergo X-inactivation followed by X-reactivation.
6. Nevertheless X-reactivation can occur independently from meiosis as the combinatorial signals driving them seem to be distinct.
7. Taken together, these results show that X-inactivation during PGCLC formation, followed by X-reactivation, is essential to recapitulate the oogenic fate when proper conditions for meiotic entry are provided.

OUTLOOK

The X-inactivation/reactivation cycle in germ cells represents a complex and dynamic process influenced by a multitude of players. While some of the events characterizing the reactivation of the X chromosome have been explored, many are yet to be identified.

In the search for the optimal culture system to trace the X-chromosome while stimulating oogenesis, our system gave us valuable insights for the future development of even more powerful induction systems. First, additional reporters for either germ cell fate or meiosis should be implemented to readily isolate proper germ cells at different stages of differentiation. This will be an additional improvement since germ cells isolated via surface markers only were reported to lack 100% purity. Second, a FACS sorting step to isolate X-inactivating EpiLCs might increase the number of germ cells entering meiosis, potentially simplifying the downstream analysis. Third, an inducible system to facilitate the targeted degradation of known players of X-inactivation would allow the mechanistic elucidation of what has been, so far, only possible as correlations. Last, fully functional oocytes will have to be tested via offspring generation.

Taken together, although further improvements are still necessary to confer optimal experimental conditions, we constructed a reproducible system that will serve as a powerful tool to elucidate the complex dynamics of the chromosome during oogenesis in mammals.

METHODS

Cell culture

Embryonic stem cell culture: Serum condition

Embryonic Stem Cells (ESCs) were maintained and expanded on 0.2% gelatin-coated dishes in DMEM (Thermo Fisher Scientific, 31966021) supplemented with 10% Fetal Bovine Serum (FBS) (ES-qualified, Thermo Fisher Scientific, 16141079), 1,000 U/ml LIF (ORF Genetics, 01-A1140-0100), 1 mM Sodium Pyruvate (Thermo Fisher Scientific, 11360070), 1x MEM Non-Essential Amino Acids Solution (Thermo Fisher Scientific, 11140050), 50 U/ml penicillin/streptomycin (Ibian Tech, P06-07100) and 0.1 mM 2-mercaptoethanol (Thermo Fisher Scientific, 31350010). Cells were cultured at 37°C with 5% CO_2. Medium was changed every day and cells were passaged using 0.05% Trypsin-EDTA (Thermo Fisher Scientific, 25300054) and quenched 1:5 in DMEM supplemented with 10% FBS (Life Technologies, 10270106). Cells were monthly tested for mycoplasma contamination by PCR.

Embryonic stem cell culture: 2inhibitors (2i) condition

ESCs were cultured for 24h prior to the start of the primordial germ cell like cell induction in 2i/LIF medium. Briefly, a homemade version of the N2B27 medium was prepared based on previous reports (Ying et al. 2008) with additional modifications reported in (Katsuhiko Hayashi and Saitou 2013) containing two chemical inhibitors 0.4 µM PD032591 (Selleck Chemicals, S1036) and 3 µM CHIR99021 (SML1046, SML1046) together with 1,000 U/ml LIF (ORF Genetics, 01-A1140-0100). ESCs were seeded on a dish coated with 0.01% poly-L-ornithine (Sigma-Aldrich, P3655) and 500 ng/ml laminin (Corning, 354232).

XRep cell line generation

We used the female F2 ESC line EL16.7 TST, derived from a cross of *Mus musculus musculus* with *Mus musculus castaneus* (Ogawa, Sun, and Lee 2008). As a result, cells contain one X chromosome from *M.m musculus* (X^{mus}) and one from *M.m castaneus* (X^{cas}). Moreover, EL16.7 TST contains a truncation of Tsix on X^{mus} ($Tsix^{TST/+}$),

which abrogates *Tsix* expression and leads to the non-random inactivation of X^{mus} upon differentiation.

XGFP and XtdTomato dual color reporter

A GFP reporter construct (H. Wu et al. 2014) was targeted in the second exon of *Hprt* on X^{mus} as described in (Bauer et al. 2020). The same strategy was used to simultaneously target a tdTomato reporter construct in the second exon of *Hprt* on X^{cas} and a GFP reporter on X^{mus}. Briefly, $5x10^6$ EL16.7 TST ESCs were nucleofected with the AMAXA Mouse Embryonic Stem Cell Nucleofector Kit (LONZA, VPH-1001) using program A-30 with 1.6 µg each of GFP and tdTomato circularised targeting vectors and 5 µg single gRNA vector PX459 (5'-TATACCTAATCATTATGCCG-3') (Addgene, 48139, a gift from Feng Zhang). Homology arms flanking the target site were amplified from genomic DNA and cloned into pBluescript II SK(+) (Addgene, 212205) by restriction-enzyme based cloning and the cHS4-CAG-nlstdTomato-cHS4 and cHS4-CAG-nlsGFP-cHS4constructs, kindly provided by J. Nathans (H. Wu et al. 2014) were cloned between the two homology arms. 7.5 µM of RS-1 (Merck, 553510) was added to enhance homology-directed repair. To select for the homozygous disruption of *Hprt*, cells were grown in the presence of 10 µM 6-thioguanine (Sigma-Aldrich, A4882-250MG) for 6 days, and GFP+ / tdTomato+ cells were isolated by FACS using a BD Influx (BD Biosciences). Single clones were screened by Southern blot hybridization as described in (Bauer et al. 2020).

Rosa26 rtTA

1 µg of R26P-M2rtTA targeting vector (Addgene, 47381) and 5 µg of PX459 gRNA vector (5'-GACTCCAGTCTTTCTAGAAGA-3') were nucleofected with the AMAXA Mouse Embryonic Stem Cell Nucleofector Kit (LONZA, VPH-100) using program A-30 in the XRep. Cells were selected with 3 µg/ml puromycin (Ibian tech., ant-pr-1) for 5 days, with medium being changed daily. Clones were selected for rtTA expression gDNA was digested with EcoRV and then screened by Southern blot hybridization.

Transcription factors transfection and selection of clones

PB-TET vectors containing key germ cell factors Blimp1, Tfap2c and Prdm14 (Nakaki et al. 2013) were kindly given by F. Nakaki. The XRep cell line was generated by transfecting the R26rtTA XRep cell line under serum/LIF condition with 3 µg each of

PB-TET vectors, pPBCAG-hph and a PiggyBac Transposase vector using AMAXA Mouse Embryonic Stem Cell Nucleofector Kit (LONZA, VPH-1001). Transfected cells were selected with 200 μg/ml hygromycin B Gold (Ibian tech., ant-hg-1) for 10 days and genotyped with PCR for transgenes. The primer sequences for the genotype are shown in Table 1.

Copy number integration was estimated with Southern blotting. Briefly, 15 μg of genomic DNA were digested with BamHI. DNA fragments were electrophoresed in 0.8% agarose gel and transferred to an AMersham Hybond XL membrane (GE Healthcare, RPN303S). The b-geo probe was designed downstream of the BamHI site, generated by digesting the PB-TET-Avi-Blimp1 with CpoI/SmaI, labeled with dCTP [α-32P] (Perkin Elmer, NEG513H250UC) using High Prime (Roche, 11585592001), purified with illustra ProbeQuant G-50 Micro Column (GE Healthcare, 28903408) and hybridization performed in Church buffer. Radioisotope images were captured with a Phosphorimager Typhoon Trio.

Table 1. Primer sequences used in this study

Target Transcript	Forward (5'-3')	Reverse (5'-3')
Arbp	CAAAGCTGAAGCAAAGGAAGAG	AATTAAGCAGGCTGACTTGGTTG
Xist mus/cas	ATCATACTAAAGGCCACACAAAGAA**T/C**	ATTTGGATTGCAAGGTGGAT
Amot mus/cas	TTTGCTCCCACTTGGTCA**CA/AG**	GACACGTTTGGAGAGGGAAC
Prdx4 mus/cas	TGAGTCTTCAAGGTATACAC**TA/AG**	TGAAGTGGTAGCATGCTCTGTT
Prkx mus/cas	TGCAGAATGAGAAAGCAG**GC/CT**	CCACGATTACGCAGGTAGGT
Klf4	TGGTGCTTGGTGAGTTGTGG	GCTCCCCCGTTTGGTACCTT
Dnd1	GCTGCTCAAGTTCAGTACGCAC	GAAGTGCTGCTTTAGGTCTGGC
Zfp42 (Rex1)	CCCTCGACAGACTGACCCTAA	TCGGGGCTAATCTCACTTTCAT
Dnmt3b	CTCGCAAGGTGTGGGCTTTTGTAAC	CTGGGCATCTGTCATCTTTGCACC
Dnmt3l	CCAGGGCAGATTTCTTCCTAAGGTC	TGAGCTGCACAGAGGCATCC
Blimp1	AGCATGACCTGACATTGACACC	CTCAACACTCTCATGTAAGAGGC
Prdm14	ACAGCCAAGCAATTTGCACTAC	TTACCTGGCATTTTCATTGCTC
Tfap2c	GGGCTTTTCTCTCTTGGCTGGT	TCCACACGTCACCCACACAA
Avi-Blimp1	TGGTGCCTGTAAAGGTCAAAC	GGCGGAATTAGCTTATCGAC
3xFLAG-Prdm14	TCCTGGATCAAGAGGCTTTC	ACTAGCTAGAGCGGCCATCAC
V5-Tfap2c	ATTCCAGCAAGACGATGGAG	GGCGGAATTAGCTTATCGAC
rtTA	CTACCACCGATTCTATGCCCC	CGCTTTCGCACTTTAGCTGTT

Epiblast-like cell and primordial germ cell-like cell induction

XRep ESCs were induced into primordial germ cell-like cells (PGCLCs) as described previously (Katsuhiko Hayashi and Saitou 2013) with the following modifications: ESCs were thawed on 0.2% gelatin in serum/LIF and after 24h seeded at a density of 0.6 x10^5 cells/cm^2 in 2i/LIF medium on a dish coated with 0.01% poly-L-ornithine (Sigma-Aldrich, P3655) and 500 ng/ml laminin (Corning, 354232). 24h later, ESCs were dissociated with TrypLE Express for 5 mins at 37°C and induced into EpiLCs. After 48h, EpiLCs were split using TrypLE Express (Life Technologies 12604013) and re-seeded at 0.2 x 10^5 cells/cm^2 on 16.7 µg/ml human plasma fibronectin coated plates (Merck Millipore, FC010). After an additional 48h, EpiLCs were aggregated in U-bottom 96-well Lipidure-Coat plate (Thermo Fisher Scientific, 81100525) at 2,000 cells per aggregate in GK15 medium (GMEM (Life Technologies, 11710035), 15% KnockOut Serum Replacement (KSR) (Thermo Fisher, 10828028), 0.1 mM nonessential amino acids (NEAA) (Thermo Fisher Scientific, 11140050), 1 mM sodium pyruvate (Thermo Fisher Scientific, 11360), 2 mM GLutamax (Life Technologies, 35050061), 0.1 mM 2-mercaptoethanol (Thermo Fisher Scientific, 21985-023), and 100 U/ml penicillin and 0.1 mg/ml streptomycin (Thermo Fisher Scientific, 15140) with 1.5 µg/ml doxycycline (Tocris, 4090/50) for 5 days.

PGCLCs mitotic expansion

PGCLC mitotic expansion culture was performed as previously described (H. Ohta et al. 2017) with few modifications. Briefly, five days after PGCLC induction, SSEA1+/CD61+ PGCLCs were sorted by flow cytometry onto m220 feeder cells, which constitutively express a membrane-bound form of mouse Stem Cell Factor (Dolci et al. 1991; Majumdar et al. 1994) on 0.1% gelatin-coated optical bottom plates (Nunc, 165305). The expansion culture was maintained for a total of 9 days. The first 3 days in GMEM containing 100 ng/ml SCF, 10 µM forskolin (Sigma- Aldrich, F3917), 10 µM rolipram (Abcam, ab120029), 2.5% FBS (Capricorn Scientific, FBSES12B), 10% KSR, 0.1 mM NEAA, 1 mM sodium pyruvate, 2 mM GLutamax (Life Technologies, 35050061), 0.1 mM 2-bME, 100 U/ml penicillin, 0.1 mg/ml streptomycin and 100 nM all-trans Retinoic Acid (RA) (Enzo Life Sciences, BMLGR100).

PGCLCs meiosis induction

Meiosis was induced after 3 days of mitotic expansion culture as previously reported (Miyauchi et al. 2017; Miyauchi, Ohta, and Saitou 2018) by a combined treatment of 300 ng/ml BMP2 (R&D Systems, 355-BM) and 100 nM RA. Medium was replaced completely every two days until the end of the culture period.

rOvary reconstitution

5,000 sorted SSEA1+/CD61+ PGCLCs were mixed with 75,000 freshly thawed E12.5 female somatic gonadal cells (courtesy of the Hayashi Lab) and cultured in 1 well of a Lipidure-Coat plate at 37°C in a 5% CO_2 incubator for 2 days as described in (Katsuhiko Hayashi et al. 2017).

Oocyte *in vitro* differentiation (IVDi) culture

IVDi culture was performed as previously described (Katsuhiko Hayashi et al. 2017). Briefly, one single rOvary was placed in the middle of a 24-well Transwell-COL membrane (Corning, CLS3470-48EA) and cultured in alpha-MEM (Life Technologies, 12571063) with 0.15 mM ascorbic acid (Sigma-Aldrich, A7506), 2% FBS, 2 mM GLutamax (Life Technologies, 35050061), 0.1 mM 2-bME, 50 U/ml penicillin/streptomycin under normoxic condition (20% O_2 and 5% CO_2 at 37°C) for 11 days, changing IVDi medium every other day.

Fluorescence-activated cell sorting (FACS)

After 5 days of culture, PGCLC aggregates were dissociated using TrypLE Express (Thermo Fisher Scientific, 12604021) for 8 min at 37°C, with periodical tap-mixing. The reaction was quenched 1:5 with wash buffer DMEM/F12 (Thermo Fisher Scientific, 11320-082) containing 0.1% bovine serum albumin (BSA) fraction V (Thermo Fisher Scientific, 15260-037) and 30 mM HEPES (Gibco 15630-056) containing 0.1 mg/mL of DNAse I (Sigma-Aldrich, Sigma-Aldrich) . The cell suspension was centrifuged at 1200 rpm for 5 min, re-suspended in FACS buffer (0.1% BSA in PBS) and passed through a 70 µm cell strainer (Corning, 352350). Cell were stained with 1:100 SSEA1-eFluor 660 (Thermo Fisher Scientific, 50-8813-42) and 1:10 CD61-PE-Vio770 (Miltenyi Biotec, 130102627) for 1h at 4°C. Cells were washed thrice with FACS Buffer, stained with 1:1000 DAPI and then FACS sorted using a BD FACSAria IIsorp or a BD Influx. Double

positive population of PGCLC was collected in GK15 medium. Data was analysed with Flowjo (Tree Star) software.

Cell cycle analysis

Identification of G_1, S, G_2 cell cycle phases was based on DNA content and performed as described previously (Bonev et al. 2017) with minor modifications. Briefly, ESCs, EpiLC, PGCLCs were dissociated and quenched as described above. Cells were then fixed for 10 min at room temperature with freshly prepared 1% formaldehyde in PBS (Sigma-Aldrich, F8775-4X25ML) and the reaction then quenched by addition of 0.2M glycine (NZYTech, MB01401). $1x10^6$ cells/ml were permeabilized using 0.1% saponin (Sigma-Aldrich, 47036-50G-F). 10 µg/ml DAPI (Thermo Fisher Scientific, D1306) and 100 µg/ml RNase A (Thermo Fisher Scientific, EN0531) were added and samples incubated for 30 min at room temperature protected from light with slight agitation. After washing once with cold PBS, samples were resuspended in cold 0.5% BSA in PBS at a concentration of $1x10^6$ cells/ml and immediately FACS analyzed using a BD LSRFortessa.

Immunofluorescence

Immunofluorescence of PGCLCs bodies and rOvaries

Immunofluorescence analysis of PGCLC bodies or rOvaries was performed on cryosections prepared as follows: aggregates were fixed with 4% paraformaldehyde (PFA) (Electron Microscopy Science, 15713) in PBS at room temperature for 30 min, followed by three washes in PBS and submerged in serial concentrations of 10% and 30% of sucrose (Sigma-Aldrich, S0389) in PBS, 15 mins and overnight at 4°C respectively. The samples were embedded in OCT compound (Sakura Finetek, 4583), snap-frozen in liquid nitrogen, and cryo-sectioned at a thickness of 10 µm at -20°C on a cryostat (Leica, CM1850). The sections were placed on a coated glass slide (MAS-GP type A; Matsunami, S9901) and dried completely.

For immunostaining, the slides were blocked with PBS containing 10% normal goat serum (NGS) (Abcam, ab7481), 3% BSA (Sigma-Aldrich, A3311), and 0.2% Triton X-100 (Sigma-Aldrich, T9284) for 1 hr at room temperature, followed by incubation with the primary antibodies diluted in a 1:1 solution of blocking buffer to PBS with 0.2% Tween (PBST) (Sigma-Aldrich, P7949) overnight at room temperature. The slides were

washed three times with PBST, then incubated with the secondary antibodies diluted as the primary, with DAPI at 1 µg/ml for 1 hr at room temperature. Following three washes in PBST, the samples were mounted in VECTASHIELD with DAPI (Vector Laboratories, H1200) and observed under a Leica SP8 confocal microscope. All images were analyzed using Fiji/Image J software (Schindelin et al. 2012). All antibodies used in this study are listed in Table 2.

Table 2. Antibodies used in this study

Name	Description	Dilution	Company	Catalog#
Primary antibody				
anti-Sox2	Rabbit polyclonal	100x	Abcam	ab97959
anti-Tfap2 (6E4/4)	Mouse monoclonal	300x	Santa Cruz	SC12762
anti-cleaved PARP1	Rabbit monoclonal	100x	Abcam	ab32064
anti-Sycp3	Mouse monoclonal	100x	Abcam	ab97672
anti-γH2A.X S139	Rabbit polyclonal	100x	Abcam	ab11174
anti-Dazl	Rabbit polyclonal	200x	Abcam	ab34139
anti-GFP	Chicken polyclonal	500x	Abcam	ab13970
anti-RFP	Mouse monoclonal	100x	Rockland	200301379
Surface markers				
SSEA1-eFluor 660	Mouse monoclonal	50x	Thermos	50-8813-42
CD61-PE-Vio770	Hamster monoclonal	10x	Miltenyi Biotec	130-102-627
Secondary antibody				
Anti-chicken IgY	Goat polyclonal / Alexa488	500x	Life Technologies	A11039
Anti-rabbit IgG	Goat polyclonal / Alexa488	500x	Life Technologies	A11034
Anti-mouse IgG	Goat polyclonal / Alexa555	500x	Life Technologies	A21424
Anti-rabbit IgG	Donkey polyclonal/Alexa647	500x	Life Technologies	A31573

Immunofluorescence of cultured PGCLC-derived cells

Immunofluorescence analysis of cultured PGCLC-derived cells was performed as described in (Nagaoka et al. 2020). Briefly, PGCLCs were cultured on m220 feeder cells seeded on a 0.1% gelatin-coated plate used specifically for imaging (Nunc, 165305). PGCLC-derived cells were fixed at c5, c7 or c9 with 4% PFA (Electron Microscopy Science, 15713) in PBS at room temperature for 30 min, followed by three

washes in PBS. Fixed cells were blocked in PBS containing 10% NGS, 3% BSA, and 0.2% Triton X-100 for 1 hr, then incubated with the primary antibodies diluted in a 1:1 solution of blocking buffer to PBS with 0.2% Tween (PBST) at room temperature overnight. After three washes in PBST, cells were incubated with the secondary antibodies and DAPI at room temperature for 2 hr and washed three times in PBST. Finally, the well was filled with VECTASHIELD without DAPI (Vector laboratories, H1000). Immunostained samples were observed with a Leica SP8 confocal microscope.

Meiotic cell spreads from germ cells

Cultured PGCLC-derived cells were harvested by TrypLE Express at 37°C for 5 min, quenched with 1:1 TrypLE wash buffer (DMEM/F12 containing 0.1% BSA fraction V, 30 mM HEPES), filtered through a 70 μM strainer and centrifuged at 1200 rpm for 5 min. Cell pellets were dislodged by tapping and washed once in PBS. Cells were then treated with a hypotonic solution (30 mM Tris-HCl, 50 mM sucrose (Sigma, S0389), 17 mM trisodium citrate, 5 mM ethylenediaminetetraacetic acid (EDTA), 2.5 mM dithiothreitol (DTT) (Sigma, D0632), 0.5 mM phenylmethylsulfonylfluoride (PMSF) (Sigma, P7626), pH 8.2-8.4 at room temperature for 20 min. Cells were spun down 3 min at 1200 rpm, resuspended in 100 mM sucrose and the cell suspension distributed onto slides (Matsunami, S9901) covered with 1% PFA in H_2O (Electron Microscopy Science, 15713) with 0.2% Triton X-100 (pH 9.2-9.4). The slides were incubated at room temperature overnight in a humidified chamber. Finally, the slides were air-dried and washed with 0.5% Kodak Photo-Flo 200 (Kodak, B00K335F6S) for 2 min at room temperature. The spread slides were blocked in PBS containing 10% NGS, 1% BSA for 1 hr, then incubated with the primary antibodies diluted in a 1:1 solution of blocking buffer to PBS with 0.2% Tween (PBST) at room temperature overnight. After three washes in PBST, cells were incubated with the secondary antibodies and DAPI at room temperature for 2 hr, washed three times in PBST and mounted in VECTASHIELD mounting medium with DAPI (Vector Laboratories, h1200). Immunostained cells were observed under a Leica SP8 confocal microscope.

Immunofluorescence of IVDi tissues

Day 11 IVDi tissues were treated while still attached to the transwell member as follow: culture medium was carefully removed from the transwell and the whole membrane

was fixed in 4% PFA (Electron Microscopy Science, 15713) in PBS for 30 min at room temperature, washed twice with PBS and blocked overnight at room temperature in 10% NGS, 1% BSA, 0.2% Triton X-100. Primary antibodies were diluted in a 1:1 solution of blocking buffer to PBS with 0.2% Tween (PBST) and incubated overnight. After 3 washes with PBST, secondary antibodies and DAPI diluted as the primary, were incubated an additional overnight, washed thrice and the whole membrane mounted on VECTASHIELD with DAPI (Vector Laboratories, H1200). Immunostained tissues were observed under a Leica SP8 confocal microscope.

RNA-fluorescent *in situ* hybridization and immunofluorescence

Cells were fixed with 3% paraformaldehyde PFA (Electron Microscopy Science, 15713) for 10 min with 2 mM Ribonucleoside-Vanadyl Complex RVC (New England Biolabs, S1402S) at room temperature and then permeabilized for 5 min on ice in 0.5% Triton-X with 2mM RVC. Cells were then blocked in 3% BSA/PBS with 2mM RVC for 1h at room temperature, incubated with primary antibodies diluted in blocking solution with 2mM RVC overnight at 4°C. The secondary antibodies were diluted in blocking buffer and incubated 1h at room temperature. Cells were then again fixed in 3% PFA for 10 min at room temperature. Strand-specific RNA FISH was performed with fluorescently labeled oligonucleotides (IDT) as described previously (Del Rosario et al. 2017). Briefly, probe mix was prepared by mixing 10 ng/ml equimolar amounts of Cy5 labeled Xist probes BD384-Xist-Cy5-3' (5'-ATG ACT CTG GAA GTC AGT ATG GAG /3Cy5Sp/ -3'), BD417-5'Cy5-Xist-Cy5-3' (5'- /5Cy5/ATG GGC ACT GCA TTT TAG CAA TA /3Cy5Sp/ -3'), 0.5 µg/µL yeast t-RNA (Life Technologies, 15401029) and 20 mM RVC. Probe mix was pre annealed at 80°C for 10 min followed by 30 min at 37°C and hybridized in 25% formamide, 10% dextran sulfate, 2xSSC pH 7 at room temperature overnight. Slides were then washed in 25% formamide 2xSSC pH 7 at room temperature, followed by washes in 2xSSC pH 7 and then mounted with Vectashield (Vector Laboratories, H1200). Images were acquired using a Zeiss Cell Observer.

RNA extraction, cDNA synthesis and qPCR analysis

RNA was isolated using phenol-chloroform extraction (Sigma Aldrich, P2069) followed by ethanol precipitation and quantified by Nanodrop. cDNA was produced with a High-Capacity RNA-to-cDNA Kit (Thermo Fisher Scientific, 4387406) and was used for

qRT-PCR analysis in triplicate reactions with Power SYBR Green PCR Master Mix (Thermo Fisher Scientific, 4367659). The gene expression levels are presented as ΔΔCt normalized with the mean Ct values of one housekeeping gene, Arbp, in a normalization sample (ESCs). The primer sequences used this study are listed in Table 2.

mRNA-Seq analysis

RNA libraries were prepared using the TruSeq Stranded Total RNA Library Preparation Kit (Illumina, 20020596) followed by 125 bp paired-end sequencing on an Illumina HiSeq 2500. FastQ files that passed quality control were aligned to the mm10 reference genome containing CAST/EiJ and 129S1/SvImJ SNPs positions masked. The positions of all 36 mouse strains SNPs were downloaded from ftp://ftp-mouse.sanger.ac.uk/REL-1505-SNPs_Indels/mgp.v5.merged.snps_all.dbSNP142.vcf.gz.tbi.

From here, we generated a VCF file containing only the SNPs information for the strains of interest, CAST/EiJ and 29S1/SvImJ. Reads were then aligned using STAR (Dobin et al. 2013) implementing the WASP method (van de Geijn et al. 2015) for filtering of allele specific alignments. The generated bam files were used for counting reads using the HTseq tool (v0.6.1) (Anders, Pyl, and Huber 2015). All of the steps above were performed using a customized Nextflow pipeline (Di Tommaso et al. 2017). We obtained between $50*10^6$ and $75*10^6$ reads. Coherence between samples, time points and replicates was verified by principal component analysis (PCA). Batch effects in principal component analysis (PCA) were corrected using the R package limma (Ritchie et al. 2015). Differential expression analysis was performed using the R package DESeq2 (v1.16) (Love, Huber, and Anders 2014). Briefly, differentially expressed genes were called by comparing PGCLCs XGFP+ and PGCLCs XGFP- or PGCLCs XGFP+ to ESCs. The *DESeqDataSet* (dds) was generated considering the dataset in its entirety while the DEseq analysis was conducted on dataset filtered as follows: Read counts were **normalized** by library size using *estimateSizeFactors*, were **filtered** for having a mean across the samples >10 (a more stringent cut off than the sum across the samples >10) and poorly annotated genes on chromosomal patches were removed. The resulting 17089 genes were kept for downstream analysis. Log2 fold change was shrinked using the “normal” parameter.

We took a list of X-linked genes for which a clear distinction of A and B compartment could be observed in the published ESCs and overalayed it with the allelic ratio of our X-linked genes.

Gene Ontology enrichment analysis performed on top and bottom differentially expressed genes defined as FDR < 0.001 e log2 fold change > |1| using the Gorilla. Over-represented categories were simplified using Revigo (http://revigo.irb.hr/) using a similarity of 0.4 as threshold. As background, all identified genes were used.

SC RNA-seq analysis

Single cell RNA libraries were prepared using the SMARTseq V5 protocol (unpublished), followed by 75 bp paired-end sequencing on an Illumina HiSeq 2500.

BIBLIOGRAPHY

Adams, Ian R., and Anne McLaren. 2002. “Sexually Dimorphic Development of Mouse Primordial Germ Cells: Switching from Oogenesis to Spermatogenesis.” *Development* 129 (5): 1155–64.

Allers, T., and M. Lichten. 2001. “Differential Timing and Control of Noncrossover and Crossover Recombination during Meiosis.” *Cell* 106 (1): 47–57.

Ancelin, Katia, Ulrike C. Lange, Petra Hajkova, Robert Schneider, Andrew J. Bannister, Tony Kouzarides, and M. Azim Surani. 2006. “Blimp1 Associates with Prmt5 and Directs Histone Arginine Methylation in Mouse Germ Cells.” *Nature Cell Biology*. https://doi.org/10.1038/ncb1413.

Anders, Simon, Paul Theodor Pyl, and Wolfgang Huber. 2015. “HTSeq--a Python Framework to Work with High-Throughput Sequencing Data.” *Bioinformatics* 31 (2): 166–69.

Aramaki, Shinya, Katsuhiko Hayashi, Kazuki Kurimoto, Hiroshi Ohta, Yukihiro Yabuta, Hiroko Iwanari, Yasuhiro Mochizuki, et al. 2013. “A Mesodermal Factor, T, Specifies Mouse Germ Cell Fate by Directly Activating Germline Determinants.” *Developmental Cell*. https://doi.org/10.1016/j.devcel.2013.11.001.

Ara, Toshiaki, Yuri Nakamura, Takeshi Egawa, Tatsuki Sugiyama, Kuniya Abe, Tadamitsu Kishimoto, Yasuhisa Matsui, and Takashi Nagasawa. 2003. “Impaired Colonization of the Gonads by Primordial Germ Cells in Mice Lacking a Chemokine, Stromal Cell-Derived Factor-1 (SDF-1).” *Proceedings of the National Academy of Sciences of the United States of America* 100 (9): 5319–23.

Barakat, Tahsin Stefan, and Joost Gribnau. 2012. “X Chromosome Inactivation in the Cycle of Life.” *Development* 139 (12): 2085–89.

Bauer, Moritz, Enrique Vidal, Eduard Zorita, Stefan F. Pinter, Guillaume J. Filion, and Bernhard Payer. 2020. “Chromosome Compartments on the Inactive X Guide TAD Formation Independently of Transcription during X-Reactivation.” https://doi.org/10.1101/2020.07.02.177790.

Best, Diana, Daniela A. Sahlender, Norbert Walther, Andrew A. Peden, and Ian R. Adams. 2008. “Sdmg1 Is a Conserved Transmembrane Protein Associated with Germ Cell Sex Determination and Germline-Soma Interactions in Mice.” *Development* 135 (8): 1415–25.

Bonev, Boyan, Netta Mendelson Cohen, Quentin Szabo, Lauriane Fritsch, Giorgio L. Papadopoulos, Yaniv Lubling, Xiaole Xu, et al. 2017. “Multiscale 3D Genome Rewiring during Mouse Neural Development.” *Cell* 171 (3): 557–72.e24.

Borensztein, Maud, Laurène Syx, Katia Ancelin, Patricia Diabangouaya, Christel Picard, Tao Liu, Jun-Bin Liang, et al. 2017. “Xist-Dependent Imprinted X Inactivation and the Early Developmental Consequences of Its Failure.” *Nature Structural & Molecular Biology* 24 (3): 226–33.

Börner, G. Valentin, Nancy Kleckner, and Neil Hunter. 2004. “Crossover/noncrossover Differentiation, Synaptonemal Complex Formation, and Regulatory Surveillance at the Leptotene/zygotene Transition of Meiosis.” *Cell* 117 (1): 29–45.

Borsani, G., R. Tonlorenzi, M. C. Simmler, L. Dandolo, D. Arnaud, V. Capra, M. Grompe, et al. 1991. “Characterization of a Murine Gene Expressed from the Inactive X Chromosome.” *Nature* 351 (6324): 325–29.

Bostick, M., J. K. Kim, P-O Esteve, A. Clark, S. Pradhan, and S. E. Jacobsen. 2007.

"UHRF1 Plays a Role in Maintaining DNA Methylation in Mammalian Cells." *Science*. https://doi.org/10.1126/science.1147939.
Bowles, J., and P. Koopman. 2007. "Retinoic Acid, Meiosis and Germ Cell Fate in Mammals." *Development*. https://doi.org/10.1242/dev.001107.
Bowles, Josephine, Chun-Wei Feng, Cassy Spiller, Tara-Lynne Davidson, Andrew Jackson, and Peter Koopman. 2010. "FGF9 Suppresses Meiosis and Promotes Male Germ Cell Fate in Mice." *Developmental Cell* 19 (3): 440–49.
Bowles, Josephine, Deon Knight, Christopher Smith, Dagmar Wilhelm, Joy Richman, Satoru Mamiya, Kenta Yashiro, et al. 2006. "Retinoid Signaling Determines Germ Cell Fate in Mice." *Science* 312 (5773): 596–600.
Brockdorff, N., A. Ashworth, G. F. Kay, P. Cooper, S. Smith, V. M. McCabe, D. P. Norris, G. D. Penny, D. Patel, and S. Rastan. 1991. "Conservation of Position and Exclusive Expression of Mouse Xist from the Inactive X Chromosome." *Nature* 351 (6324): 329–31.
Brons, I. Gabrielle M., Lucy E. Smithers, Matthew W. B. Trotter, Peter Rugg-Gunn, Bowen Sun, Susana M. Chuva de Sousa Lopes, Sarah K. Howlett, et al. 2007. "Derivation of Pluripotent Epiblast Stem Cells from Mammalian Embryos." *Nature*. https://doi.org/10.1038/nature05950.
Byskov, A. G., and L. Saxén. 1976. "Induction of Meiosis in Fetal Mouse Testis in Vitro." *Developmental Biology* 52 (2): 193–200.
Chang, David H., Giorgio Cattoretti, and Kathryn L. Calame. 2002. "The Dynamic Expression Pattern of B Lymphocyte Induced Maturation Protein-1 (Blimp-1) during Mouse Embryonic Development." *Mechanisms of Development* 117 (1-2): 305–9.
Chassot, Anne-Amandine, Morgane Le Rolle, Geneviève Jolivet, Isabelle Stevant, Jean-Marie Guigonis, Fabio Da Silva, Serge Nef, et al. 2020. "Retinoic Acid Synthesis by ALDH1A Proteins Is Dispensable for Meiosis Initiation in the Mouse Fetal Ovary." *Science Advances* 6 (21): eaaz1261.
Cheng, Shangli, Yu Pei, Liqun He, Guangdun Peng, Björn Reinius, Patrick P. L. Tam, Naihe Jing, and Qiaolin Deng. 2019. "Single-Cell RNA-Seq Reveals Cellular Heterogeneity of Pluripotency Transition and X Chromosome Dynamics during Early Mouse Development." *Cell Reports*. https://doi.org/10.1016/j.celrep.2019.02.031.
Chiquoine, A. D. 1954. "The Identification, Origin, and Migration of the Primordial Germ Cells in the Mouse Embryo." *The Anatomical Record* 118 (2): 135–46.
Chuva de Sousa Lopes, Susana M., Katsuhiko Hayashi, Tanya C. Shovlin, Will Mifsud, M. Azim Surani, and Anne McLaren. 2008. "X Chromosome Activity in Mouse XX Primordial Germ Cells." *PLoS Genetics* 4 (2): e30.
Cunningham, Thomas J., and Gregg Duester. 2015. "Mechanisms of Retinoic Acid Signalling and Its Roles in Organ and Limb Development." *Nature Reviews. Molecular Cell Biology* 16 (2): 110–23.
Daxinger, Lucia, and Emma Whitelaw. 2012. "Understanding Transgenerational Epigenetic Inheritance via the Gametes in Mammals." *Nature Reviews Genetics*. https://doi.org/10.1038/nrg3188.
De Felici, M., S. Dolci, and M. Pesce. 1992. "Cellular and Molecular Aspects of Mouse Primordial Germ Cell Migration and Proliferation in Culture." *The International Journal of Developmental Biology* 36 (2): 205–13.
Del Rosario, Brian C., Amanda M. Del Rosario, Anthony Anselmo, Peggy I. Wang, Ruslan I. Sadreyev, and Jeannie T. Lee. 2017. "Genetic Intersection of Tsix and

Hedgehog Signaling during the Initiation of X-Chromosome Inactivation." *Developmental Cell* 43 (3): 359–71.e6.
Di Tommaso, Paolo, Maria Chatzou, Evan W. Floden, Pablo Prieto Barja, Emilio Palumbo, and Cedric Notredame. 2017. "Nextflow Enables Reproducible Computational Workflows." *Nature Biotechnology* 35 (4): 316–19.
Dobin, Alexander, Carrie A. Davis, Felix Schlesinger, Jorg Drenkow, Chris Zaleski, Sonali Jha, Philippe Batut, Mark Chaisson, and Thomas R. Gingeras. 2013. "STAR: Ultrafast Universal RNA-Seq Aligner." *Bioinformatics* 29 (1): 15–21.
Dolci, S., D. E. Williams, M. K. Ernst, J. L. Resnick, C. I. Brannan, L. F. Lock, S. D. Lyman, H. S. Boswell, and P. J. Donovan. 1991. "Requirement for Mast Cell Growth Factor for Primordial Germ Cell Survival in Culture." *Nature* 352 (6338): 809–11.
Donovan, P. J., D. Stott, L. A. Cairns, J. Heasman, and C. C. Wylie. 1986. "Migratory and Postmigratory Mouse Primordial Germ Cells Behave Differently in Culture." *Cell* 44 (6): 831–38.
Eggler, Aimee L., Ross B. Inman, and Michael M. Cox. 2002. "The Rad51-Dependent Pairing of Long DNA Substrates Is Stabilized by Replication Protein A." *The Journal of Biological Chemistry* 277 (42): 39280–88.
Eguizabal, Cristina, Tanya C. Shovlin, Gabriela Durcova-Hills, Azim Surani, and Anne McLaren. 2009. "Generation of Primordial Germ Cells from Pluripotent Stem Cells." *Differentiation; Research in Biological Diversity* 78 (2-3): 116–23.
Engreitz, Jesse M., Amy Pandya-Jones, Patrick McDonel, Alexander Shishkin, Klara Sirokman, Christine Surka, Sabah Kadri, et al. 2013. "The Xist lncRNA Exploits Three-Dimensional Genome Architecture to Spread across the X Chromosome." *Science* 341 (6147): 1237973.
Eppig, John J., Karen Wigglesworth, and Marilyn J. O'Brien. 1992. "Comparison of Embryonic Developmental Competence of Mouse Oocytes Grown with and without Serum." *Molecular Reproduction and Development*. https://doi.org/10.1002/mrd.1080320107.
Evans, E. P., C. E. Ford, and M. F. Lyon. 1977. "Direct Evidence of the Capacity of the XY Germ Cell in the Mouse to Become an Oocyte." *Nature* 267 (5610): 430–31.
Findlay, John K., Karla J. Hutt, Martha Hickey, and Richard A. Anderson. 2015. "How Is the Number of Primordial Follicles in the Ovarian Reserve Established?1." *Biology of Reproduction*. https://doi.org/10.1095/biolreprod.115.133652.
García-Castro, Martín I., Robert Anderson, Janet Heasman, and Christopher Wylie. 1997. "Interactions between Germ Cells and Extracellular Matrix Glycoproteins during Migration and Gonad Assembly in the Mouse Embryo." *Journal of Cell Biology*. https://doi.org/10.1083/jcb.138.2.471.
Gartler, S. M., M. Rivest, and R. E. Cole. 1980. "Cytological Evidence for an Inactive X Chromosome in Murine Oogonia." *Cytogenetics and Cell Genetics* 28 (3): 203–7.
Gehring, Mary, Jin Hoe Huh, Tzung-Fu Hsieh, Jon Penterman, Yeonhee Choi, John J. Harada, Robert B. Goldberg, and Robert L. Fischer. 2006. "DEMETER DNA Glycosylase Establishes MEDEA Polycomb Gene Self-Imprinting by Allele-Specific Demethylation." *Cell* 124 (3): 495–506.
Geijn, Bryce van de, Graham McVicker, Yoav Gilad, and Jonathan K. Pritchard. 2015. "WASP: Allele-Specific Software for Robust Molecular Quantitative Trait Locus Discovery." *Nature Methods* 12 (11): 1061–63.
Ginsburg, M., M. H. Snow, and A. McLaren. 1990. "Primordial Germ Cells in the Mouse Embryo during Gastrulation." *Development* 110 (2): 521–28.

Grabole, Nils, Julia Tischler, Jamie A. Hackett, Shinseog Kim, Fuchou Tang, Harry G. Leitch, Erna Magnúsdóttir, and M. Azim Surani. 2013. “Prdm14 Promotes Germline Fate and Naive Pluripotency by Repressing FGF Signalling and DNA Methylation.” *EMBO Reports* 14 (7): 629–37.

Gubbay, John, Jérôme Collignon, Peter Koopman, Blanche Capel, Androulla Economou, Andrea Münsterberg, Nigel Vivian, Peter Goodfellow, and Robin Lovell-Badge. 1990. “A Gene Mapping to the Sex-Determining Region of the Mouse Y Chromosome Is a Member of a Novel Family of Embryonically Expressed Genes.” *Nature*. https://doi.org/10.1038/346245a0.

Guibert, S., T. Forne, and M. Weber. 2012. “Global Profiling of DNA Methylation Erasure in Mouse Primordial Germ Cells.” *Genome Research*. https://doi.org/10.1101/gr.130997.111.

Guo, Ge, Jian Yang, Jennifer Nichols, John Simon Hall, Isobel Eyres, William Mansfield, and Austin Smith. 2009. “Klf4 Reverts Developmentally Programmed Restriction of Ground State Pluripotency.” *Development* 136 (7): 1063–69.

Gu, Y., C. Runyan, A. Shoemaker, A. Surani, and C. Wylie. 2009. “Steel Factor Controls Primordial Germ Cell Survival and Motility from the Time of Their Specification in the Allantois, and Provides a Continuous Niche throughout Their Migration.” *Development*. https://doi.org/10.1242/dev.030619.

Hackett, Jamie A., Yun Huang, Ufuk Günesdogan, Kristjan A. Gretarsson, Toshihiro Kobayashi, and M. Azim Surani. 2018. “Publisher Correction: Tracing the Transitions from Pluripotency to Germ Cell Fate with CRISPR Screening.” *Nature Communications* 9 (1): 5328.

Hadjantonakis, Anna-Katerina, Marina Gertsenstein, Masahito Ikawa, Masaru Okabe, and Andras Nagy. 1998. “Non-Invasive Sexing of Preimplantation Stage Mammalian Embryos.” *Nature Genetics*. https://doi.org/10.1038/893.

Hajkova, Petra, Katia Ancelin, Tanja Waldmann, Nicolas Lacoste, Ulrike C. Lange, Francesca Cesari, Caroline Lee, Genevieve Almouzni, Robert Schneider, and M. Azim Surani. 2008. “Chromatin Dynamics during Epigenetic Reprogramming in the Mouse Germ Line.” *Nature*. https://doi.org/10.1038/nature06714.

Hajkova, Petra, Sylvia Erhardt, Natasha Lane, Thomas Haaf, Osman El-Maarri, Wolf Reik, Jörn Walter, and M. Azim Surani. 2002. “Epigenetic Reprogramming in Mouse Primordial Germ Cells.” *Mechanisms of Development*. https://doi.org/10.1016/s0925-4773(02)00181-8.

Hajkova, P., S. J. Jeffries, C. Lee, N. Miller, S. P. Jackson, and M. A. Surani. 2010. “Genome-Wide Reprogramming in the Mouse Germ Line Entails the Base Excision Repair Pathway.” *Science*. https://doi.org/10.1126/science.1187945.

Hamada, Norio, Nobuhiko Hamazaki, So Shimamoto, Orie Hikabe, Go Nagamatsu, Yuki Takada, Kiyoko Kato, and Katsuhiko Hayashi. 2020. “Germ Cell-Intrinsic Effects of Sex Chromosomes on Early Oocyte Differentiation in Mice.” *PLoS Genetics* 16 (3): e1008676.

Hayashi, Katsuhiko, Orie Hikabe, Yayoi Obata, and Yuji Hirao. 2017. “Reconstitution of Mouse Oogenesis in a Dish from Pluripotent Stem Cells.” *Nature Protocols*. https://doi.org/10.1038/nprot.2017.070.

Hayashi, Katsuhiko, Takashi Kobayashi, Takashi Umino, Ryo Goitsuka, Yasuhisa Matsui, and Daisuke Kitamura. 2002. “SMAD1 Signaling Is Critical for Initial Commitment of Germ Cell Lineage from Mouse Epiblast.” *Mechanisms of Development* 118 (1-2): 99–109.

Hayashi, Katsuhiko, Sugako Ogushi, Kazuki Kurimoto, So Shimamoto, Hiroshi Ohta,

and Mitinori Saitou. 2012. “Offspring from Oocytes Derived from in Vitro Primordial Germ Cell-like Cells in Mice.” *Science* 338 (6109): 971–75.
Hayashi, Katsuhiko, Hiroshi Ohta, Kazuki Kurimoto, Shinya Aramaki, and Mitinori Saitou. 2011. “Reconstitution of the Mouse Germ Cell Specification Pathway in Culture by Pluripotent Stem Cells.” *Cell*. https://doi.org/10.1016/j.cell.2011.06.052.
Hayashi, Katsuhiko, and Mitinori Saitou. 2013. “Generation of Eggs from Mouse Embryonic Stem Cells and Induced Pluripotent Stem Cells.” *Nature Protocols*. https://doi.org/10.1038/nprot.2013.090.
Hayashi, Katsuhiko, and M. Azim Surani. 2009. “Self-Renewing Epiblast Stem Cells Exhibit Continual Delineation of Germ Cells with Epigenetic Reprogramming in Vitro.” *Development* 136 (21): 3549–56.
Hayashi, K., S. M. C. de Sousa Lopes, and M. A. Surani. 2007. “Germ Cell Specification in Mice.” *Science*. https://doi.org/10.1126/science.1137545.
Heikkilä, Minna, Renata Prunskaite, Florence Naillat, Petri Itäranta, Jussi Vuoristo, Juhani Leppäluoto, Hellevi Peltoketo, and Seppo Vainio. 2005. “The Partial Female to Male Sex Reversal in Wnt-4-Deficient Females Involves Induced Expression of Testosterone Biosynthetic Genes and Testosterone Production, and Depends on Androgen Action.” *Endocrinology* 146 (9): 4016–23.
He, Yu-Fei, Bin-Zhong Li, Zheng Li, Peng Liu, Yang Wang, Qingyu Tang, Jianping Ding, et al. 2011. “Tet-Mediated Formation of 5-Carboxylcytosine and Its Excision by TDG in Mammalian DNA.” *Science*. https://doi.org/10.1126/science.1210944.
Hikabe, Orie, Nobuhiko Hamazaki, Go Nagamatsu, Yayoi Obata, Yuji Hirao, Norio Hamada, So Shimamoto, et al. 2016. “Reconstitution in Vitro of the Entire Cycle of the Mouse Female Germ Line.” *Nature* 539 (7628): 299–303.
Hill, Peter W. S., Harry G. Leitch, Cristina E. Requena, Zhiyi Sun, Rachel Amouroux, Monica Roman-Trufero, Malgorzata Borkowska, et al. 2018. “Epigenetic Reprogramming Enables the Transition from Primordial Germ Cell to Gonocyte.” *Nature* 555 (7696): 392–96.
Hochedlinger, Konrad, Yasuhiro Yamada, Caroline Beard, and Rudolf Jaenisch. 2005. “Ectopic Expression of Oct-4 Blocks Progenitor-Cell Differentiation and Causes Dysplasia in Epithelial Tissues.” *Cell*. https://doi.org/10.1016/j.cell.2005.02.018.
Hübner, Karin, Guy Fuhrmann, Lane K. Christenson, James Kehler, Rolland Reinbold, Rabindranath De La Fuente, Jennifer Wood, Jerome F. Strauss 3rd, Michele Boiani, and Hans R. Schöler. 2003. “Derivation of Oocytes from Mouse Embryonic Stem Cells.” *Science* 300 (5623): 1251–56.
Hu, Deqing, Xin Gao, Kaixiang Cao, Marc A. Morgan, Gloria Mas, Edwin R. Smith, Andrew G. Volk, et al. 2017. “Not All H3K4 Methylations Are Created Equal: Mll2/COMPASS Dependency in Primordial Germ Cell Specification.” *Molecular Cell* 65 (3): 460–75.e6.
Hunter, N., and N. Kleckner. 2001. “The Single-End Invasion: An Asymmetric Intermediate at the Double-Strand Break to Double-Holliday Junction Transition of Meiotic Recombination.” *Cell* 106 (1): 59–70.
Huynh, Khanh D., and Jeannie T. Lee. 2003. “Inheritance of a Pre-Inactivated Paternal X Chromosome in Early Mouse Embryos.” *Nature* 426 (6968): 857–62.
Ito, Shinsuke, Li Shen, Qing Dai, Susan C. Wu, Leonard B. Collins, James A. Swenberg, Chuan He, and Yi Zhang. 2011. “Tet Proteins Can Convert 5-Methylcytosine to 5-Formylcytosine and 5-Carboxylcytosine.” *Science*. https://doi.org/10.1126/science.1210597.
Jameson, Samantha A., Anirudh Natarajan, Jonah Cool, Tony DeFalco, Danielle M.

Maatouk, Lindsey Mork, Steven C. Munger, and Blanche Capel. 2012. “Temporal Transcriptional Profiling of Somatic and Germ Cells Reveals Biased Lineage Priming of Sexual Fate in the Fetal Mouse Gonad.” *PLoS Genetics*. https://doi.org/10.1371/journal.pgen.1002575.

Kafri, T., M. Ariel, M. Brandeis, R. Shemer, L. Urven, J. McCarrey, H. Cedar, and A. Razin. 1992. “Developmental Pattern of Gene-Specific DNA Methylation in the Mouse Embryo and Germ Line.” *Genes & Development* 6 (5): 705–14.

Kagiwada, Saya, Kazuki Kurimoto, Takayuki Hirota, Masashi Yamaji, and Mitinori Saitou. 2013. “Replication-Coupled Passive DNA Demethylation for the Erasure of Genome Imprints in Mice.” *The EMBO Journal* 32 (3): 340–53.

Kawase, Eihachiro, Yasuaki Shirayoshi, Koichiro Hashimoto, and Norio Nakatsuji. 1996. “A Combination of Buffalo Rat Liver Cell-Conditioned Medium, Forskolin and Membrane-Bound Stem Cell Factor Stimulates Rapid Proliferation of Mouse Primordial Germ Cells in Vitro Similar to That in Vivo.” *Development, Growth and Differentiation*. https://doi.org/10.1046/j.1440-169x.1996.t01-2-00011.x.

Keeney, S., C. N. Giroux, and N. Kleckner. 1997. “Meiosis-Specific DNA Double-Strand Breaks Are Catalyzed by Spo11, a Member of a Widely Conserved Protein Family.” *Cell* 88 (3): 375–84.

Kimura, T. 2003. “Conditional Loss of PTEN Leads to Testicular Teratoma and Enhances Embryonic Germ Cell Production.” *Development*. https://doi.org/10.1242/dev.00392.

Kimura, T., M. Tomooka, N. Yamano, K. Murayama, S. Matoba, H. Umehara, Y. Kanai, and T. Nakano. 2008. “AKT Signaling Promotes Derivation of Embryonic Germ Cells from Primordial Germ Cells.” *Development*. https://doi.org/10.1242/dev.013474.

Kim, Yuna, Akio Kobayashi, Ryohei Sekido, Leo DiNapoli, Jennifer Brennan, Marie-Christine Chaboissier, Francis Poulat, Richard R. Behringer, Robin Lovell-Badge, and Blanche Capel. 2006. “Fgf9 and Wnt4 Act as Antagonistic Signals to Regulate Mammalian Sex Determination.” *PLoS Biology* 4 (6): e187.

Kohda, Takashi, Jiyoung Lee, Kimiko Inoue, Natumi Ogonuki, Noriko Wakisaka-Saito, Tomoko Kaneko-Ishino, Atsuo Ogura, and Fumitoshi Ishino. 2002. “Epigenetic Regulation in Mammalian Development and Dysfunction: The Effects of Somatic Cloning and Genomic Imprinting.” *International Congress Series*. https://doi.org/10.1016/s0531-5131(02)01138-x.

Kohlmaier, Alexander, Fabio Savarese, Monika Lachner, Joost Martens, Thomas Jenuwein, and Anton Wutz. 2004. “A Chromosomal Memory Triggered by Xist Regulates Histone Methylation in X Inactivation.” *PLoS Biology*. https://doi.org/10.1371/journal.pbio.0020171.

Koopman, P., J. Gubbay, N. Vivian, P. Goodfellow, and R. Lovell-Badge. 1991. “Male Development of Chromosomally Female Mice Transgenic for Sry.” *Nature* 351 (6322): 117–21.

Koubova, Jana, Douglas B. Menke, Qing Zhou, Blanche Capel, Michael D. Griswold, and David C. Page. 2006. “Retinoic Acid Regulates Sex-Specific Timing of Meiotic Initiation in Mice.” *Proceedings of the National Academy of Sciences of the United States of America* 103 (8): 2474–79.

Kratzer, P. G., and V. M. Chapman. 1981. “X Chromosome Reactivation in Oocytes of Mus Caroli.” *Proceedings of the National Academy of Sciences of the United States of America* 78 (5): 3093–97.

Kurimoto, K., Y. Yabuta, Y. Ohinata, M. Shigeta, K. Yamanaka, and M. Saitou. 2008.

"Complex Genome-Wide Transcription Dynamics Orchestrated by Blimp1 for the Specification of the Germ Cell Lineage in Mice." *Genes & Development*. https://doi.org/10.1101/gad.1649908.

Labosky, P. A., D. P. Barlow, and B. L. Hogan. 1994. "Mouse Embryonic Germ (EG) Cell Lines: Transmission through the Germline and Differences in the Methylation Imprint of Insulin-like Growth Factor 2 Receptor (Igf2r) Gene Compared with Embryonic Stem (ES) Cell Lines." *Development* 120 (11): 3197–3204.

Lane, Natasha, Wendy Dean, Sylvia Erhardt, Petra Hajkova, Azim Surani, J$\diamond$rn Walter, and Wolf Reik. 2003. "Resistance of IAPs to Methylation Reprogramming May Provide a Mechanism for Epigenetic Inheritance in the Mouse." *Genesis*. https://doi.org/10.1002/gene.10168.

Lawson, K. A., N. R. Dunn, B. A. Roelen, L. M. Zeinstra, A. M. Davis, C. V. Wright, J. P. Korving, and B. L. Hogan. 1999. "Bmp4 Is Required for the Generation of Primordial Germ Cells in the Mouse Embryo." *Genes & Development*.

Leitch, Harry G., Kate Blair, William Mansfield, Harold Ayetey, Peter Humphreys, Jennifer Nichols, M. Azim Surani, and Austin Smith. 2010. "Embryonic Germ Cells from Mice and Rats Exhibit Properties Consistent with a Generic Pluripotent Ground State." *Development* 137 (14): 2279–87.

Leitch, Harry G., Kirsten R. McEwen, Aleksandra Turp, Vesela Encheva, Tom Carroll, Nils Grabole, William Mansfield, et al. 2013. "Naive Pluripotency Is Associated with Global DNA Hypomethylation." *Nature Structural & Molecular Biology* 20 (3): 311–16.

Lieberman-Aiden, Erez, Nynke L. van Berkum, Louise Williams, Maxim Imakaev, Tobias Ragoczy, Agnes Telling, Ido Amit, et al. 2009. "Comprehensive Mapping of Long-Range Interactions Reveals Folding Principles of the Human Genome." *Science* 326 (5950): 289–93.

Lin, Yanfeng, and David C. Page. 2005. "Dazl Deficiency Leads to Embryonic Arrest of Germ Cell Development in XY C57BL/6 Mice." *Developmental Biology* 288 (2): 309–16.

Lin, Y., M. E. Gill, J. Koubova, and D. C. Page. 2008. "Germ Cell-Intrinsic and -Extrinsic Factors Govern Meiotic Initiation in Mouse Embryos." *Science*. https://doi.org/10.1126/science.1166340.

Love, Michael I., Wolfgang Huber, and Simon Anders. 2014. "Moderated Estimation of Fold Change and Dispersion for RNA-Seq Data with DESeq2." *Genome Biology* 15 (12): 550.

Luikenhuis, Sandra, Anton Wutz, and Rudolf Jaenisch. 2001. "Antisense Transcription through theXist Locus Mediates Tsix Function in Embryonic Stem Cells." *Molecular and Cellular Biology*. https://doi.org/10.1128/mcb.21.24.8512-8520.2001.

Maatouk, D. M. 2006. "DNA Methylation Is a Primary Mechanism for Silencing Postmigratory Primordial Germ Cell Genes in Both Germ Cell and Somatic Cell Lineages." *Development*. https://doi.org/10.1242/dev.02500.

Magnúsdóttir, Erna, Sabine Dietmann, Kazuhiro Murakami, Ufuk Günesdogan, Fuchou Tang, Siqin Bao, Evangelia Diamanti, Kaiqin Lao, Berthold Gottgens, and M. Azim Surani. 2013. "A Tripartite Transcription Factor Network Regulates Primordial Germ Cell Specification in Mice." *Nature Cell Biology* 15 (8): 905–15.

Magnúsdóttir, Erna, Astrid Gillich, Nils Grabole, and M. Azim Surani. 2012. "Combinatorial Control of Cell Fate and Reprogramming in the Mammalian Germline." *Current Opinion in Genetics & Development* 22 (5): 466–74.

Mahadevaiah, Shantha K., James M. A. Turner, Frédéric Baudat, Emmy P. Rogakou,

Peter de Boer, Josefa Blanco-Rodríguez, Maria Jasin, Scott Keeney, William M. Bonner, and Paul S. Burgoyne. 2001. “Recombinational DNA Double-Strand Breaks in Mice Precede Synapsis.” *Nature Genetics*. https://doi.org/10.1038/85830.

Majumdar, M. K., L. Feng, E. Medlock, D. Toksoz, and D. A. Williams. 1994. “Identification and Mutation of Primary and Secondary Proteolytic Cleavage Sites in Murine Stem Cell Factor cDNA Yields Biologically Active, Cell-Associated Protein.” *The Journal of Biological Chemistry* 269 (2): 1237–42.

Mak, Winifred, Tatyana B. Nesterova, Mariana de Napoles, Ruth Appanah, Shinya Yamanaka, Arie P. Otte, and Neil Brockdorff. 2004. “Reactivation of the Paternal X Chromosome in Early Mouse Embryos.” *Science* 303 (5658): 666–69.

Mallol, Anna, Maria Guirola, and Bernhard Payer. 2019. “PRDM14 Controls X-Chromosomal and Global Epigenetic Reprogramming of H3K27me3 in Migrating Mouse Primordial Germ Cells.” *Epigenetics & Chromatin* 12 (1): 38.

Mark, Manuel, Norbert B. Ghyselinck, and Pierre Chambon. 2009. “Function of Retinoic Acid Receptors during Embryonic Development.” *Nuclear Receptor Signaling*. https://doi.org/10.1621/nrs.07002.

Marks, Hendrik, Tüzer Kalkan, Roberta Menafra, Sergey Denissov, Kenneth Jones, Helmut Hofemeister, Jennifer Nichols, et al. 2012. “The Transcriptional and Epigenomic Foundations of Ground State Pluripotency.” *Cell* 149 (3): 590–604.

Marks, Hendrik, Hindrik H. D. Kerstens, Tahsin Stefan Barakat, Erik Splinter, René A. M. Dirks, Guido van Mierlo, Onkar Joshi, et al. 2015. “Dynamics of Gene Silencing during X Inactivation Using Allele-Specific RNA-Seq.” *Genome Biology* 16 (August): 149.

Matsui, Yasuhisa, Deniz Toksoz, Satomi Nishikawa, Shin-Ichi Nishikawa, David Williams, Krisztina Zsebo, and Brigid L. M. Hogan. 1991. “Effect of Steel Factor and Leukaemia Inhibitory Factor on Murine Primordial Germ Cells in Culture.” *Nature*. https://doi.org/10.1038/353750a0.

Matsui, Yasuhisa, Krisztina Zsebo, and Brigid L. M. Hogan. 1992. “Derivation of Pluripotential Embryonic Stem Cells from Murine Primordial Germ Cells in Culture.” *Cell*. https://doi.org/10.1016/0092-8674(92)90317-6.

McLaren, A. 1995. “Germ Cells and Germ Cell Sex.” *Philosophical Transactions of the Royal Society of London. Series B: Biological Sciences*. https://doi.org/10.1098/rstb.1995.0156.

McLaren, Anne. 2003. “Primordial Germ Cells in the Mouse.” *Developmental Biology*. https://doi.org/10.1016/s0012-1606(03)00214-8.

Menke, Douglas B., and David C. Page. 2002. “Sexually Dimorphic Gene Expression in the Developing Mouse Gonad.” *Gene Expression Patterns*. https://doi.org/10.1016/s1567-133x(02)00022-4.

Mittwoch, U. 1993. “Blastocysts Prepare for the Race to Be Male.” *Human Reproduction* 8 (10): 1550–55.

Miyauchi, Hidetaka, Hiroshi Ohta, So Nagaoka, Fumio Nakaki, Kotaro Sasaki, Katsuhiko Hayashi, Yukihiro Yabuta, Tomonori Nakamura, Takuya Yamamoto, and Mitinori Saitou. 2017. “Bone Morphogenetic Protein and Retinoic Acid Synergistically Specify Female Germ-Cell Fate in Mice.” *The EMBO Journal* 36 (21): 3100–3119.

Miyauchi, Hidetaka, Hiroshi Ohta, and Mitinori Saitou. 2018. “Induction of Fetal Primary Oocytes and the Meiotic Prophase from Mouse Pluripotent Stem Cells.” *Methods in Cell Biology* 144 (April): 409–29.

Mohammed, Hisham, Irene Hernando-Herraez, Aurora Savino, Antonio Scialdone, Iain Macaulay, Carla Mulas, Tamir Chandra, et al. 2017. “Single-Cell Landscape of Transcriptional Heterogeneity and Cell Fate Decisions during Mouse Early Gastrulation.” *Cell Reports* 20 (5): 1215–28.

Molyneaux, Kathleen A., Hélène Zinszner, Prabhat S. Kunwar, Kyle Schaible, Jürg Stebler, Mary Jean Sunshine, William O’Brien, et al. 2003. “The Chemokine SDF1/CXCL12 and Its Receptor CXCR4 Regulate Mouse Germ Cell Migration and Survival.” *Development* 130 (18): 4279–86.

Monk, M., M. Boubelik, and S. Lehnert. 1987. “Temporal and Regional Changes in DNA Methylation in the Embryonic, Extraembryonic and Germ Cell Lineages during Mouse Embryo Development.” *Development* 99 (3): 371–82.

Monk, M., and A. McLaren. 1981. “X-Chromosome Activity in Foetal Germ Cells of the Mouse.” *Journal of Embryology and Experimental Morphology* 63 (June): 75–84.

Morgan, Hugh D., Wendy Dean, Heather A. Coker, Wolf Reik, and Svend K. Petersen-Mahrt. 2004. “Activation-Induced Cytidine Deaminase Deaminates 5-Methylcytosine in DNA and Is Expressed in Pluripotent Tissues.” *Journal of Biological Chemistry*. https://doi.org/10.1074/jbc.m407695200.

Morohaku, Kanako, Yuji Hirao, and Yayoi Obata. 2017. “Development of Fertile Mouse Oocytes from Mitotic Germ Cells in Vitro.” *Nature Protocols* 12 (9): 1817–29.

Morohaku, Kanako, Ren Tanimoto, Keisuke Sasaki, Ryouka Kawahara-Miki, Tomohiro Kono, Katsuhiko Hayashi, Yuji Hirao, and Yayoi Obata. 2016. “Complete in Vitro Generation of Fertile Oocytes from Mouse Primordial Germ Cells.” *Proceedings of the National Academy of Sciences of the United States of America* 113 (32): 9021–26.

Murakami, Kazuhiro, Ufuk Günesdogan, Jan J. Zylicz, Walfred W. C. Tang, Roopsha Sengupta, Toshihiro Kobayashi, Shinseog Kim, Richard Butler, Sabine Dietmann, and M. Azim Surani. 2016. “NANOG Alone Induces Germ Cells in Primed Epiblast in Vitro by Activation of Enhancers.” *Nature* 529 (7586): 403–7.

Nagaoka, So I., Fumio Nakaki, Hidetaka Miyauchi, Yoshiaki Nosaka, Hiroshi Ohta, Yukihiro Yabuta, Kazuki Kurimoto, et al. 2020. “ZGLP1 Is a Determinant for the Oogenic Fate in Mice.” *Science* 367 (6482). https://doi.org/10.1126/science.aaw4115.

Nakaki, Fumio, Katsuhiko Hayashi, Hiroshi Ohta, Kazuki Kurimoto, Yukihiro Yabuta, and Mitinori Saitou. 2013. “Induction of Mouse Germ-Cell Fate by Transcription Factors in Vitro.” *Nature* 501 (7466): 222–26.

Nesterova, Tatyana B., Jacqueline E. Mermoud, Kathy Hilton, John Pehrson, M. Azim Surani, Anne McLaren, and Neil Brockdorff. 2002. “Xist Expression and macroH2A1.2 Localisation in Mouse Primordial and Pluripotent Embryonic Germ Cells.” *Differentiation; Research in Biological Diversity* 69 (4-5): 216–25.

Nichols, Jennifer, and Austin Smith. 2009. “Naive and Primed Pluripotent States.” *Cell Stem Cell*. https://doi.org/10.1016/j.stem.2009.05.015.

Odor, D. L., and R. J. Blandau. 1971. “Organ Cultures of Fetal Mouse Ovaries. I. Light Microscopic Structure.” *The American Journal of Anatomy* 131 (4): 387–414.

Ogawa, Yuya, Bryan K. Sun, and Jeannie T. Lee. 2008. “Intersection of the RNA Interference and X-Inactivation Pathways.” *Science* 320 (5881): 1336–41.

Ohhata, Tatsuya, and Anton Wutz. 2013. “Reactivation of the Inactive X Chromosome in Development and Reprogramming.” *Cellular and Molecular Life Sciences: CMLS* 70 (14): 2443–61.

Ohinata, Yasuhide, Hiroshi Ohta, Mayo Shigeta, Kaori Yamanaka, Teruhiko

Wakayama, and Mitinori Saitou. 2009. “A Signaling Principle for the Specification of the Germ Cell Lineage in Mice.” *Cell* 137 (3): 571–84.
Ohinata, Yasuhide, Bernhard Payer, Dónal O’Carroll, Katia Ancelin, Yukiko Ono, Mitsue Sano, Sheila C. Barton, et al. 2005. “Blimp1 Is a Critical Determinant of the Germ Cell Lineage in Mice.” *Nature* 436 (7048): 207–13.
Ohta, Hiroshi, Kazuki Kurimoto, Ikuhiro Okamoto, Tomonori Nakamura, Yukihiro Yabuta, Hidetaka Miyauchi, Takuya Yamamoto, et al. 2017. “In Vitro Expansion of Mouse Primordial Germ Cell-like Cells Recapitulates an Epigenetic Blank Slate.” *The EMBO Journal*. https://doi.org/10.15252/embj.201695862.
Ohta, Kohei, Yanling Lin, Nathanael Hogg, Miyuki Yamamoto, and Yukiko Yamazaki. 2010. “Direct Effects of Retinoic Acid on Entry of Fetal Male Germ Cells into Meiosis in Mice.” *Biology of Reproduction* 83 (6): 1056–63.
Okamoto, Ikuhiro, Arie P. Otte, C. David Allis, Danny Reinberg, and Edith Heard. 2004. “Epigenetic Dynamics of Imprinted X Inactivation during Early Mouse Development.” *Science* 303 (5658): 644–49.
Ooi, Steen K. T., and Timothy H. Bestor. 2008. “The Colorful History of Active DNA Demethylation.” *Cell*. https://doi.org/10.1016/j.cell.2008.06.009.
Panning, B., and R. Jaenisch. 1996. “DNA Hypomethylation Can Activate Xist Expression and Silence X-Linked Genes.” *Genes & Development* 10 (16): 1991–2002.
Parma, Pietro, Orietta Radi, Valerie Vidal, Marie Christine Chaboissier, Elena Dellambra, Stella Valentini, Liliana Guerra, Andreas Schedl, and Giovanna Camerino. 2006. “R-spondin1 Is Essential in Sex Determination, Skin Differentiation and Malignancy.” *Nature Genetics* 38 (11): 1304–9.
Payer, Bernhard. 2016. “Developmental Regulation of X-Chromosome Inactivation.” *Seminars in Cell & Developmental Biology*. https://doi.org/10.1016/j.semcdb.2016.04.014.
Payer, Bernhard, Michael Rosenberg, Masashi Yamaji, Yukihiro Yabuta, Michiyo Koyanagi-Aoi, Katsuhiko Hayashi, Shinya Yamanaka, Mitinori Saitou, and Jeannie T. Lee. 2013. “Tsix RNA and the Germline Factor, PRDM14, Link X Reactivation and Stem Cell Reprogramming.” *Molecular Cell* 52 (6): 805–18.
Penny, Graeme D., Graham F. Kay, Steven A. Sheardown, Sohaila Rastan, and Neil Brockdorff. 1996. “Requirement for Xist in X Chromosome Inactivation.” *Nature*. https://doi.org/10.1038/379131a0.
Pesce, M., M. G. Farrace, M. Piacentini, S. Dolci, and M. De Felici. 1993. “Stem Cell Factor and Leukemia Inhibitory Factor Promote Primordial Germ Cell Survival by Suppressing Programmed Cell Death (apoptosis).” *Development* 118 (4): 1089–94.
Plath, K. 2003. “Role of Histone H3 Lysine 27 Methylation in X Inactivation.” *Science*. https://doi.org/10.1126/science.1084274.
Popp, Christian, Wendy Dean, Suhua Feng, Shawn J. Cokus, Simon Andrews, Matteo Pellegrini, Steven E. Jacobsen, and Wolf Reik. 2010. “Genome-Wide Erasure of DNA Methylation in Mouse Primordial Germ Cells Is Affected by AID Deficiency.” *Nature*. https://doi.org/10.1038/nature08829.
Rastan, S. 1982. “Timing of X-Chromosome Inactivation in Postimplantation Mouse Embryos.” *Journal of Embryology and Experimental Morphology* 71 (October): 11–24.
Rastan, S., M. H. Kaufman, A. H. Handyside, and M. F. Lyon. 1980. “X-Chromosome Inactivation in Extra-Embryonic Membranes of Diploid Parthenogenetic Mouse

Embryos Demonstrated by Differential Staining." *Nature*. https://doi.org/10.1038/288172a0.
Reik, W., W. Dean, and J. Walter. 2001. "Epigenetic Reprogramming in Mammalian Development." *Science* 293 (5532): 1089–93.
Resnick, J. L., L. S. Bixler, L. Cheng, and P. J. Donovan. 1992. "Long-Term Proliferation of Mouse Primordial Germ Cells in Culture." *Nature* 359 (6395): 550–51.
Reynolds, Nicola, Brian Collier, Victoria Bingham, Nicola K. Gray, and Howard J. Cooke. 2007. "Translation of the Synaptonemal Complex Component Sycp3 Is Enhanced in Vivo by the Germ Cell Specific Regulator Dazl." *RNA* 13 (7): 974–81.
Richardson, Brian E., and Ruth Lehmann. 2010. "Mechanisms Guiding Primordial Germ Cell Migration: Strategies from Different Organisms." *Nature Reviews. Molecular Cell Biology* 11 (1): 37–49.
Ritchie, Matthew E., Belinda Phipson, Di Wu, Yifang Hu, Charity W. Law, Wei Shi, and Gordon K. Smyth. 2015. "Limma Powers Differential Expression Analyses for RNA-Sequencing and Microarray Studies." *Nucleic Acids Research* 43 (7): e47.
Rogers, M. B., B. A. Hosler, and L. J. Gudas. 1991. "Specific Expression of a Retinoic Acid-Regulated, Zinc-Finger Gene, Rex-1, in Preimplantation Embryos, Trophoblast and Spermatocytes." *Development* 113 (3): 815–24.
Saitou, M., S. Kagiwada, and K. Kurimoto. 2012. "Epigenetic Reprogramming in Mouse Pre-Implantation Development and Primordial Germ Cells." *Development*. https://doi.org/10.1242/dev.050849.
Schindelin, Johannes, Ignacio Arganda-Carreras, Erwin Frise, Verena Kaynig, Mark Longair, Tobias Pietzsch, Stephan Preibisch, et al. 2012. "Fiji: An Open-Source Platform for Biological-Image Analysis." *Nature Methods* 9 (7): 676–82.
Schmidt, Dirk, Catherine E. Ovitt, Katrin Anlag, Sandra Fehsenfeld, Lars Gredsted, Anna-Corina Treier, and Mathias Treier. 2004. "The Murine Winged-Helix Transcription Factor Foxl2 Is Required for Granulosa Cell Differentiation and Ovary Maintenance." *Development* 131 (4): 933–42.
Schulz, Edda G., Johannes Meisig, Tomonori Nakamura, Ikuhiro Okamoto, Anja Sieber, Christel Picard, Maud Borensztein, Mitinori Saitou, Nils Blüthgen, and Edith Heard. 2014. "The Two Active X Chromosomes in Female ESCs Block Exit from the Pluripotent State by Modulating the ESC Signaling Network." *Cell Stem Cell* 14 (2): 203–16.
Seki, Yoshiyuki, Katsuhiko Hayashi, Kunihiko Itoh, Michinao Mizugaki, Mitinori Saitou, and Yasuhisa Matsui. 2005. "Extensive and Orderly Reprogramming of Genome-Wide Chromatin Modifications Associated with Specification and Early Development of Germ Cells in Mice." *Developmental Biology* 278 (2): 440–58.
Seki, Yoshiyuki, Masashi Yamaji, Yukihiro Yabuta, Mitsue Sano, Mayo Shigeta, Yasuhisa Matsui, Yumiko Saga, Makoto Tachibana, Yoichi Shinkai, and Mitinori Saitou. 2007. "Cellular Dynamics Associated with the Genome-Wide Epigenetic Reprogramming in Migrating Primordial Germ Cells in Mice." *Development* 134 (14): 2627–38.
Sharif, Jafar, Masahiro Muto, Shin-Ichiro Takebayashi, Isao Suetake, Akihiro Iwamatsu, Takaho A. Endo, Jun Shinga, et al. 2007. "The SRA Protein Np95 Mediates Epigenetic Inheritance by Recruiting Dnmt1 to Methylated DNA." *Nature*. https://doi.org/10.1038/nature06397.
Shimamoto, So, Yohei Nishimura, Go Nagamatsu, Norio Hamada, Haruka Kita, Orie Hikabe, Nobuhiko Hamazaki, and Katsuhiko Hayashi. 2019. "Hypoxia Induces the

Dormant State in Oocytes through Expression of Foxo3." *Proceedings of the National Academy of Sciences*. https://doi.org/10.1073/pnas.1817223116.
Silva, Jose, Winifred Mak, Ilona Zvetkova, Ruth Appanah, Tatyana B. Nesterova, Zoe Webster, Antoine H. F. M. Peters, Thomas Jenuwein, Arie P. Otte, and Neil Brockdorff. 2003. "Establishment of Histone h3 Methylation on the Inactive X Chromosome Requires Transient Recruitment of Eed-Enx1 Polycomb Group Complexes." *Developmental Cell* 4 (4): 481–95.
Simon, Matthew D., Stefan F. Pinter, Rui Fang, Kavitha Sarma, Michael Rutenberg-Schoenberg, Sarah K. Bowman, Barry A. Kesner, Verena K. Maier, Robert E. Kingston, and Jeannie T. Lee. 2013. "High-Resolution Xist Binding Maps Reveal Two-Step Spreading during X-Chromosome Inactivation." *Nature* 504 (7480): 465–69.
Sousa, Elsa J., Hannah T. Stuart, Lawrence E. Bates, Mohammadmersad Ghorbani, Jennifer Nichols, Sabine Dietmann, and José C. R. Silva. 2018. "Exit from Naive Pluripotency Induces a Transient X Chromosome Inactivation-like State in Males." *Cell Stem Cell*. https://doi.org/10.1016/j.stem.2018.05.001.
Sousa, Lisa Barros de Andrade e., Lisa Barros de Andrade e Sousa, Iris Jonkers, Laurène Syx, Ilona Dunkel, Julie Chaumeil, Christel Picard, et al. 2019. "Kinetics of Xist-Induced Gene Silencing Can Be Predicted from Combinations of Epigenetic and Genomic Features." *Genome Research*. https://doi.org/10.1101/gr.245027.118.
Spiller, Cassy, and Josephine Bowles. 2019. "Sexually Dimorphic Germ Cell Identity in Mammals." *Current Topics in Developmental Biology* 134 (February): 253–88.
Spiller, Cassy, Peter Koopman, and Josephine Bowles. 2017. "Sex Determination in the Mammalian Germline." *Annual Review of Genetics* 51 (November): 265–85.
Stewart, C. L., I. Gadi, and H. Bhatt. 1994. "Stem Cells from Primordial Germ Cells Can Reenter the Germ Line." *Developmental Biology* 161 (2): 626–28.
Sugimoto, Michihiko, and Kuniya Abe. 2007. "X Chromosome Reactivation Initiates in Nascent Primordial Germ Cells in Mice." *PLoS Genetics* 3 (7): e116.
Sung, Patrick, Lumir Krejci, Stephen Van Komen, and Michael G. Sehorn. 2003. "Rad51 Recombinase and Recombination Mediators." *Journal of Biological Chemistry*. https://doi.org/10.1074/jbc.r300027200.
Szabo, P. E., and J. R. Mann. 1995. "Biallelic Expression of Imprinted Genes in the Mouse Germ Line: Implications for Erasure, Establishment, and Mechanisms of Genomic Imprinting." *Genes & Development*. https://doi.org/10.1101/gad.9.15.1857.
Tada, T., M. Tada, Kathy Hilton, Sheila C. Barton, Takashi Sado, Nobuo Takagi, and M. A. Surani. 1998. "Epigenotype Switching of Imprintable Loci in Embryonic Germ Cells." *Development Genes and Evolution*. https://doi.org/10.1007/s004270050146.
Tahiliani, M., K. P. Koh, Y. Shen, W. A. Pastor, H. Bandukwala, Y. Brudno, S. Agarwal, et al. 2009. "Conversion of 5-Methylcytosine to 5-Hydroxymethylcytosine in Mammalian DNA by MLL Partner TET1." *Science*. https://doi.org/10.1126/science.1170116.
Takagi, Nobuo, and Motomichi Sasaki. 1975. "Preferential Inactivation of the Paternally Derived X Chromosome in the Extraembryonic Membranes of the Mouse." *Nature*. https://doi.org/10.1038/256640a0.
Tam, P. P., and M. H. Snow. 1981. "Proliferation and Migration of Primordial Germ Cells during Compensatory Growth in Mouse Embryos." *Journal of Embryology*

and Experimental Morphology 64 (August): 133–47.
Tam, P. P., S. X. Zhou, and S. S. Tan. 1994. “X-Chromosome Activity of the Mouse Primordial Germ Cells Revealed by the Expression of an X-Linked lacZ Transgene.” *Development* 120 (10): 2925–32.
Tedesco, Marianna, Maria Giovanna Desimio, Francesca Gioia Klinger, Massimo De Felici, and Donatella Farini. 2013. “Minimal Concentrations of Retinoic Acid Induce Stimulation by Retinoic Acid 8 and Promote Entry into Meiosis in Isolated Pregonadal and Gonadal Mouse Primordial Germ Cells.” *Biology of Reproduction* 88 (6): 145.
Tesar, Paul J., Josh G. Chenoweth, Frances A. Brook, Timothy J. Davies, Edward P. Evans, David L. Mack, Richard L. Gardner, and Ronald D. G. McKay. 2007. “New Cell Lines from Mouse Epiblast Share Defining Features with Human Embryonic Stem Cells.” *Nature* 448 (7150): 196–99.
Toyooka, Y., N. Tsunekawa, Y. Takahashi, Y. Matsui, M. Satoh, and T. Noce. 2000. “Expression and Intracellular Localization of Mouse Vasa-Homologue Protein during Germ Cell Development.” *Mechanisms of Development* 93 (1-2): 139–49.
Vernet, Nadège, Diana Condrea, Chloé Mayere, Betty Féret, Muriel Klopfenstein, William Magnant, Violaine Alunni, et al. 2020. “Meiosis Occurs Normally in the Fetal Ovary of Mice Lacking All Retinoic Acid Receptors.” *Science Advances* 6 (21). https://doi.org/10.1126/sciadv.aaz1139.
Vincent, Stéphane D., N. Ray Dunn, Roger Sciammas, Miriam Shapiro-Shalef, Mark M. Davis, Kathryn Calame, Elizabeth K. Bikoff, and Elizabeth J. Robertson. 2005. “The Zinc Finger Transcriptional Repressor Blimp1/Prdm1 Is Dispensable for Early Axis Formation but Is Required for Specification of Primordial Germ Cells in the Mouse.” *Development* 132 (6): 1315–25.
Wang, Chen-Yu, Teddy Jégu, Hsueh-Ping Chu, Hyun Jung Oh, and Jeannie T. Lee. 2018. “SMCHD1 Merges Chromosome Compartments and Assists Formation of Super-Structures on the Inactive X.” *Cell* 174 (2): 406–21.e25.
Weber, Susanne, Dawid Eckert, Daniel Nettersheim, Ad J. M. Gillis, Sabine Schäfer, Peter Kuckenberg, Julia Ehlermann, et al. 2010. “Critical Function of AP-2 gamma/TCFAP2C in Mouse Embryonic Germ Cell Maintenance.” *Biology of Reproduction* 82 (1): 214–23.
Weinberger, Leehee, Muneef Ayyash, Noa Novershtern, and Jacob H. Hanna. 2016. “Dynamic Stem Cell States: Naive to Primed Pluripotency in Rodents and Humans.” *Nature Reviews. Molecular Cell Biology* 17 (3): 155–69.
Wu, Hao, Junjie Luo, Huimin Yu, Amir Rattner, Alisa Mo, Yanshu Wang, Philip M. Smallwood, Bracha Erlanger, Sarah J. Wheelan, and Jeremy Nathans. 2014. “Cellular Resolution Maps of X Chromosome Inactivation: Implications for Neural Development, Function, and Disease.” *Neuron* 81 (1): 103–19.
Wu, Susan C., and Yi Zhang. 2010. “Active DNA Demethylation: Many Roads Lead to Rome.” *Nature Reviews. Molecular Cell Biology* 11 (9): 607–20.
Yabuta, Yukihiro, Kazuki Kurimoto, Yasuhide Ohinata, Yoshiyuki Seki, and Mitinori Saitou. 2006. “Gene Expression Dynamics during Germline Specification in Mice Identified by Quantitative Single-Cell Gene Expression Profiling.” *Biology of Reproduction* 75 (5): 705–16.
Yamaguchi, Shinpei, Hironobu Kimura, Masako Tada, Norio Nakatsuji, and Takashi Tada. 2005. “Nanog Expression in Mouse Germ Cell Development.” *Gene Expression Patterns*. https://doi.org/10.1016/j.modgep.2005.03.001.
Yamaji, Masashi, Yoshiyuki Seki, Kazuki Kurimoto, Yukihiro Yabuta, Mihoko Yuasa,

Mayo Shigeta, Kaori Yamanaka, Yasuhide Ohinata, and Mitinori Saitou. 2008. “Critical Function of Prdm14 for the Establishment of the Germ Cell Lineage in Mice.” *Nature Genetics* 40 (8): 1016–22.

Ying, Qi-Long, Jason Wray, Jennifer Nichols, Laura Batlle-Morera, Bradley Doble, James Woodgett, Philip Cohen, and Austin Smith. 2008. “The Ground State of Embryonic Stem Cell Self-Renewal.” *Nature*. https://doi.org/10.1038/nature06968.

Yokobayashi, Shihori, Ching-Yeu Liang, Hubertus Kohler, Peter Nestorov, Zichuan Liu, Miguel Vidal, Maarten van Lohuizen, Tim C. Roloff, and Antoine H. F. M. Peters. 2013. “PRC1 Coordinates Timing of Sexual Differentiation of Female Primordial Germ Cells.” *Nature* 495 (7440): 236–40.

Zhang, Jingchao, Man Zhang, Dario Acampora, Matúš Vojtek, Detian Yuan, Antonio Simeone, and Ian Chambers. 2018. “OTX2 Restricts Entry to the Mouse Germline.” *Nature* 562 (7728): 595–99.

Zvetkova, Ilona, Anwyn Apedaile, Bernard Ramsahoye, Jacqueline E. Mermoud, Lucy A. Crompton, Rosalind John, Robert Feil, and Neil Brockdorff. 2005. “Global Hypomethylation of the Genome in XX Embryonic Stem Cells.” *Nature Genetics* 37 (11): 1274–79.

Żylicz, Jan Jakub, Aurélie Bousard, Kristina Žumer, Francois Dossin, Eusra Mohammad, Simão Teixeira da Rocha, Björn Schwalb, et al. 2019. “The Implication of Early Chromatin Changes in X Chromosome Inactivation.” *Cell*. https://doi.org/10.1016/j.cell.2018.11.041.